Analysis of Ice and Snow Thickness Data in the Beaufort Sea from April 2010 and August 2011 Surveys

I. K. Peterson, S. J. Prinsenberg, J. S. Holladay and L. Lalumiere

Ocean and Ecosystem Sciences Division
Maritimes Region
Fisheries and Oceans Canada

Bedford Institute of Oceanography
P.O. Box 1006
Dartmouth, Nova Scotia
Canada B2Y 4A2

2014

Canadian Technical Report of
Hydrography and Ocean Sciences 296

Fisheries and Oceans Canada | Pêches et Océans Canada

Canada

Canadian Technical Report of Hydrography and Ocean Sciences

Technical reports contain scientific and technical information of a type that represents a contribution to existing knowledge but which is not normally found in the primary literature. The subject matter is generally related to programs and interests of the Oceans and Science sectors of Fisheries and Oceans Canada.

Technical reports may be cited as full publications. The correct citation appears above the abstract of each report. Each report is abstracted in the data base *Aquatic Sciences and Fisheries Abstracts.*

Technical reports are produced regionally but are numbered nationally. Requests for individual reports will be filled by the issuing establishment listed on the front cover and title page.

Regional and headquarters establishments of Ocean Science and Surveys ceased publication of their various report series as of December 1981. A complete listing of these publications and the last number issued under each title are published in the *Canadian Journal of Fisheries and Aquatic Sciences*, Volume 38: Index to Publications 1981. The current series began with Report Number 1 in January 1982.

Rapport technique canadien sur l'hydrographie et les sciences océaniques

Les rapports techniques contiennent des renseignements scientifiques et techniques qui constituent une contribution aux connaissances actuelles mais que l'on ne trouve pas normalement dans les revues scientifiques. Le sujet est généralement rattaché aux programmes et intérêts des secteurs des Océans et des Sciences de Pêches et Océans Canada.

Les rapports techniques peuvent être cités comme des publications à part entière. Le titre exact figure au-dessus du résumé de chaque rapport. Les rapports techniques sont résumés dans la base de données *Résumés des sciences aquatiques et halieutiques*.

Les rapports techniques sont produits à l'échelon régional, mais numérotés à l'échelon national. Les demandes de rapports seront satisfaites par l'établissement auteur dont le nom figure sur la couverture et la page de titre.

Les établissements de l'ancien secteur des Sciences et Levés océaniques dans les régions et à l'administration centrale ont cessé de publier leurs diverses séries de rapports en décembre 1981. Vous trouverez dans l'index des publications du volume 38 du *Journal canadien des sciences halieutiques et aquatiques*, la liste de ces publications ainsi que le dernier numéro paru dans chaque catégorie. La nouvelle série a commencé avec la publication du rapport numéro 1 en janvier 1982.

Canadian Technical Report of
Hydrography and Ocean Sciences 296

2014

ANALYSIS OF ICE AND SNOW THICKNESS DATA IN THE BEAUFORT SEA FROM APRIL 2010 AND AUGUST 2011 SURVEYS

by

I. K. Peterson, S. J. Prinsenberg, J. S. Holladay[1]
and L. Lalumiere[2]

Ocean and Ecosystem Sciences Division
Maritimes Region
Fisheries and Oceans Canada
Bedford Institute of Oceanography
P.O. Box 1006
Dartmouth, N.S., B2Y 4A2

[1] Geosensors Inc., 66 Mann Ave.,
Toronto, Ontario, M4S 2Y3

[2] Sensors by Design Ltd., 100 Peevers Crescent,
Newmarket, Ontario, L3Y 7T1

Cat. No. Fs97-18/296E-PDF ISBN 978-1-100-23564-6 ISSN 1488-5417

Correct citation for this publication:

Peterson, I.K., S.J. Prinsenberg, J.S. Holladay and L. Lalumiere, 2014. Analysis of Ice and Snow Thickness Data in the Beaufort Sea from April 2010 and August 2011 Surveys. Can. Tech. Rep. Hydrogr. Ocean Sci. 296: v+76 pp.

TABLE OF CONTENTS

ABSTRACT

Peterson, I.K., S.J. Prinsenberg, J.S. Holladay and L. Lalumiere, 2014. Analysis of Ice and Snow Thickness Data in the Beaufort Sea from April 2010 and August 2011 Surveys. Can. Tech. Rep. Hydrogr. Ocean Sci. 296: v+76 pp.

Ice surveys were conducted in the Beaufort Sea using helicopter-mounted sensors to measure snow and first-year (FY) ice thickness in the southern Beaufort Sea (Mackenzie Delta) in April 2010, and to measure multi-year (MY) ice thickness in the eastern Beaufort Sea in August 2011. Thicknesses of low-salinity ice inferred from ground-penetrating radar (GPR) data in the Mackenzie Delta were in good agreement with drill-hole measurements. In the eastern Beaufort Sea, electromagnetic (EM) -derived MY ice thicknesses were in good agreement with drill-hole measurements of 6m ice, but underestimated thicknesses of 10 m ice by 17%. Modal (most frequently occurring) snow thicknesses in the Mackenzie Delta were higher in inshore areas than in offshore areas

RÉSUMÉ

Peterson, I.K., S.J. Prinsenberg, J.S. Holladay and L. Lalumiere, 2014. Analysis of Ice and Snow Thickness Data in the Beaufort Sea from April 2010 and August 2011 Surveys. Can. Tech. Rep. Hydrogr. Ocean Sci. 296: v+76 pp.

On a effectué des relevés des glaces dans la mer de Beaufort à l'aide de capteurs installés sur un hélicoptère pour mesurer l'épaisseur de la neige et des glaces de première année dans la partie sud de la mer de Beaufort (delta Mackenzie) en avril 2010, et pour mesurer l'épaisseur des glaces de plusieurs années dans la partie est de la mer de Beaufort en août 2011. Les épaisseurs des glaces de faible salinité déterminées à partir des données de géoradar dans le delta Mackenzie correspondaient bien aux mesures effectuées par forage. Dans la partie est de la mer de Beaufort, les épaisseurs des glaces de plusieurs années calculées avec des instruments électromagnétiques correspondaient bien aux mesures de 6 m de glace effectuées par forage, mais sous-estimaient les épaisseurs de 10 m de glace de 17 %. Les épaisseurs modales (les plus fréquentes) de la neige dans le delta Mackenzie étaient plus grandes dans les zones côtières que dans les zones extracôtières.

1.0 INTRODUCTION

Ice surveys were conducted in the Beaufort Sea using helicopter-mounted sensors from the Bedford Institute of Oceanography (BIO) to measure snow and first-year (FY) ice thickness in the southern Beaufort Sea (Mackenzie Delta) in April 2010 (Prinsenberg et al., 2010), and to measure multi-year (MY) ice thickness in the eastern Beaufort Sea in August 2011 (Prinsenberg et al., 2014). This report provides further analysis of the data.

During the surveys, an electromagnetic (EM) sensor mounted on the helicopter was used to collect ice thickness profiles along flight lines several tens of kilometres in length, and to collect information on the freshwater layer beneath the ice in the Mackenzie Delta. The helicopter was also equipped with a ground-penetrating radar (GPR, 1000 MHz) to measure snow thickness along the flight lines, as well as ice thickness in the freshwater region of the Mackenzie Delta, since the EM cannot distinguish between ice and freshwater. In 2010, on-ice measurements of ice thickness and snow thickness were acquired by augering holes through the ice along the flight path, and water temperature, salinity and conductivity were measured with a CTD (conductivity-temperature-depth) profiler. In 2011, some of the EM ice thickness profiles were collected along lines where on-ice measurements of MY ice thickness were acquired by the National Research Council (NRC) (Johnston, 2011).

For the spring 2010 survey, the GPR ice and snow thicknesses are described in Section 1, and comparisons of the EM data with CTD and GPR data are presented in Appendices 1 and 2 respectively. For the summer 2011 survey, analysis of the EM ice thickness data and comparison with satellite imagery are presented in Section 2.

2.0 SPRING 2010 ICE SURVEY

The ice survey in April 2010 was conducted out of Inuvik, Northwest Territories using a Bell 206L helicopter from Canadian Helicopters. EM and GPR profiles were collected with helicopter-borne sensors across the shelf offshore of the Mackenzie Delta in the Beaufort Sea (Fig. 1). Low-salinity water is found under the ice in spring near the Mackenzie Delta, because river runoff is trapped shoreward of a band of ridged ice parallel to the shore (stamukhi zone).

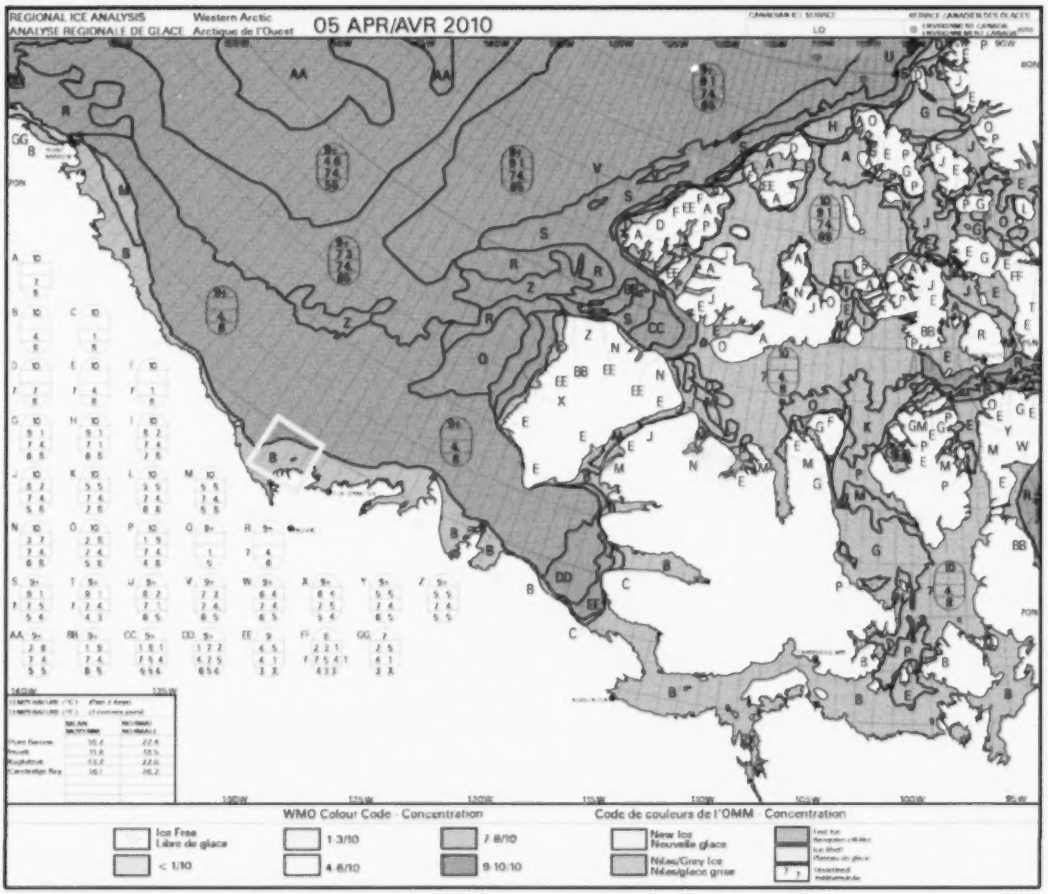

Fig. 1. Western Arctic ice chart for April 2010 produced by the Canadian Ice Service, showing location of RADARSAT image of the Mackenzie Delta region in Fig. 2 (green square).

On 01 April, EM and GPR data were collected along an L-shaped flight line which crossed the stamukhi zone (bright region between stations 46 and 47 in Fig. 2 at water depth of 10-14 m). Snow and ice thickness measurements were collected from drill-holes at 5 stations along the flight path on 08 April (Fig. 2), where water temperature, salinity and conductivity profiles were also collected with a CTD profiler. Plots of the CTD profiles (Prinsenberg et al., 2010) show that close to shore where water depths were less than 6 m, freshwater was present throughout the water column (stations 43 and 44). At stations 45 and 46, higher salinities were found at depth than at the surface. At station 45, the salinity was about 2 psu at the surface, increasing to 3 psu at depth. At station 46, just inside the stamukhi zone, the salinity was about 3 psu in the 7-m thick surface layer, and 20-23 psu in the lower layer. Beyond the stamukhi zone (station 47), the salinity was 30-32 psu throughout the water column.

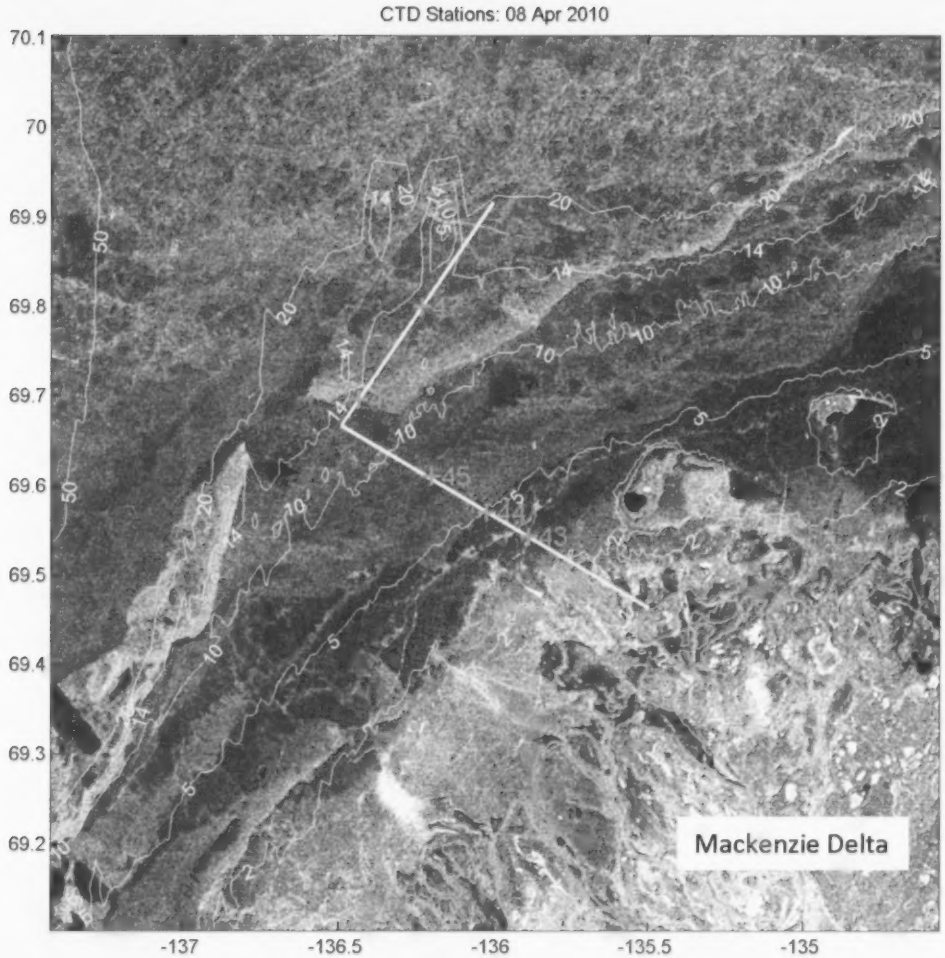

Fig. 2. Helicopter flight path (green line) and 5 on-ice stations (red crosses) overlaid on a RADARSAT-2 SAR image (~110 km x 110 km) of April 3 (RADARSAT-2 Data and Products © MacDonald, Dettwiler and Associates Ltd. (2010) - All Rights Reserved).

2.1 GPR SNOW AND ICE THICKNESS

2.1.1 Validation

GPR data were collected along the flight line in Fig. 2 on 01 April, and the echograms near the three stations closest to shore, 43, 44 and 45 (Fig. 2) are shown in Fig. 3. The traces (linear grey features) representing the air-snow and snow-ice interfaces are visible (top and middle traces), and the trace for the ice-water interface (bottom trace) is visible in areas where the ice surface is relatively smooth. However, farther offshore where salinities are higher, the ice-water

interface is not visible. The air-snow and snow-ice interfaces inferred automatically from the echograms are shown by the green and red lines respectively.

The snow and ice thicknesses measured at the on-ice stations are shown by the black arrows overlaid on the echogram. The centre arrows are plotted at the position along the flight line closest to the on-ice station, and the distance to the arrows on either side represents the off-line distance to the station (in scan line equivalents, see Appendix 1, Table 1). The thickness scale for the snow and ice layers is shown on the right, assuming dielectric constants of 1.5 and 3.2 for snow and ice respectively (Lalumiere, 2011).

The snow and ice thicknesses measured at the on-ice stations are in good agreement with the distances between the three interfaces on the echogram. Snow thicknesses were highest and most variable at the innermost station (43), where ice thickness was also variable. Ice thickness was higher at station 44 than farther offshore at station 45, probably because of earlier ice formation at station 44.

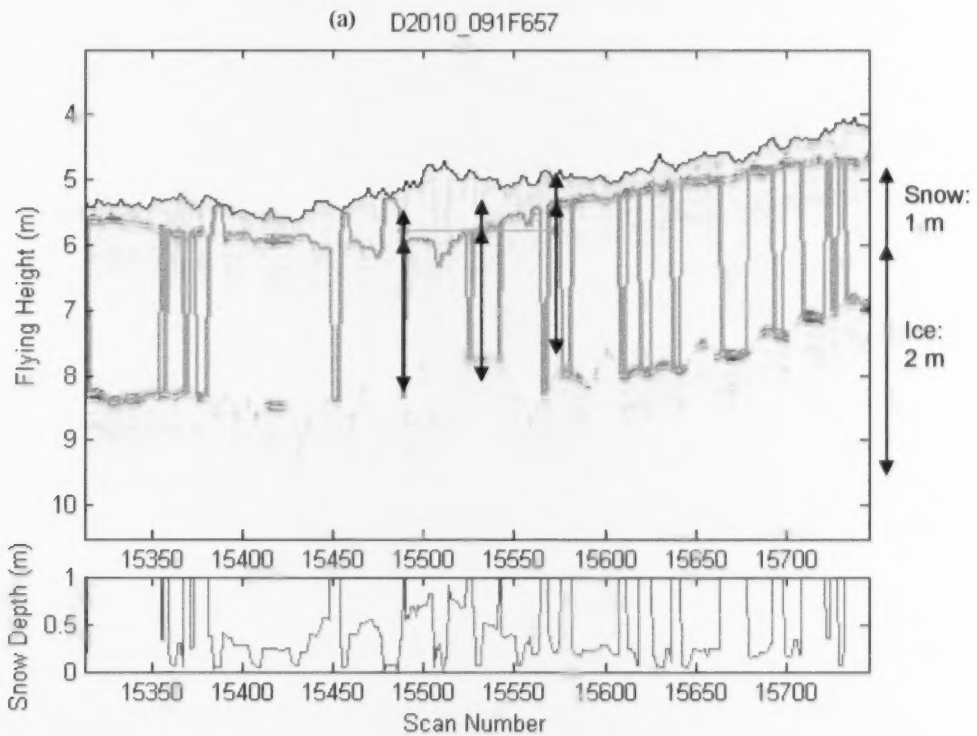

Fig. 3. GPR echogram and on-ice snow and ice thickness measurements at stations (a) 43, (b) 44 and (c) 45. The snow and ice thickness scale is shown on the right side of the plot.

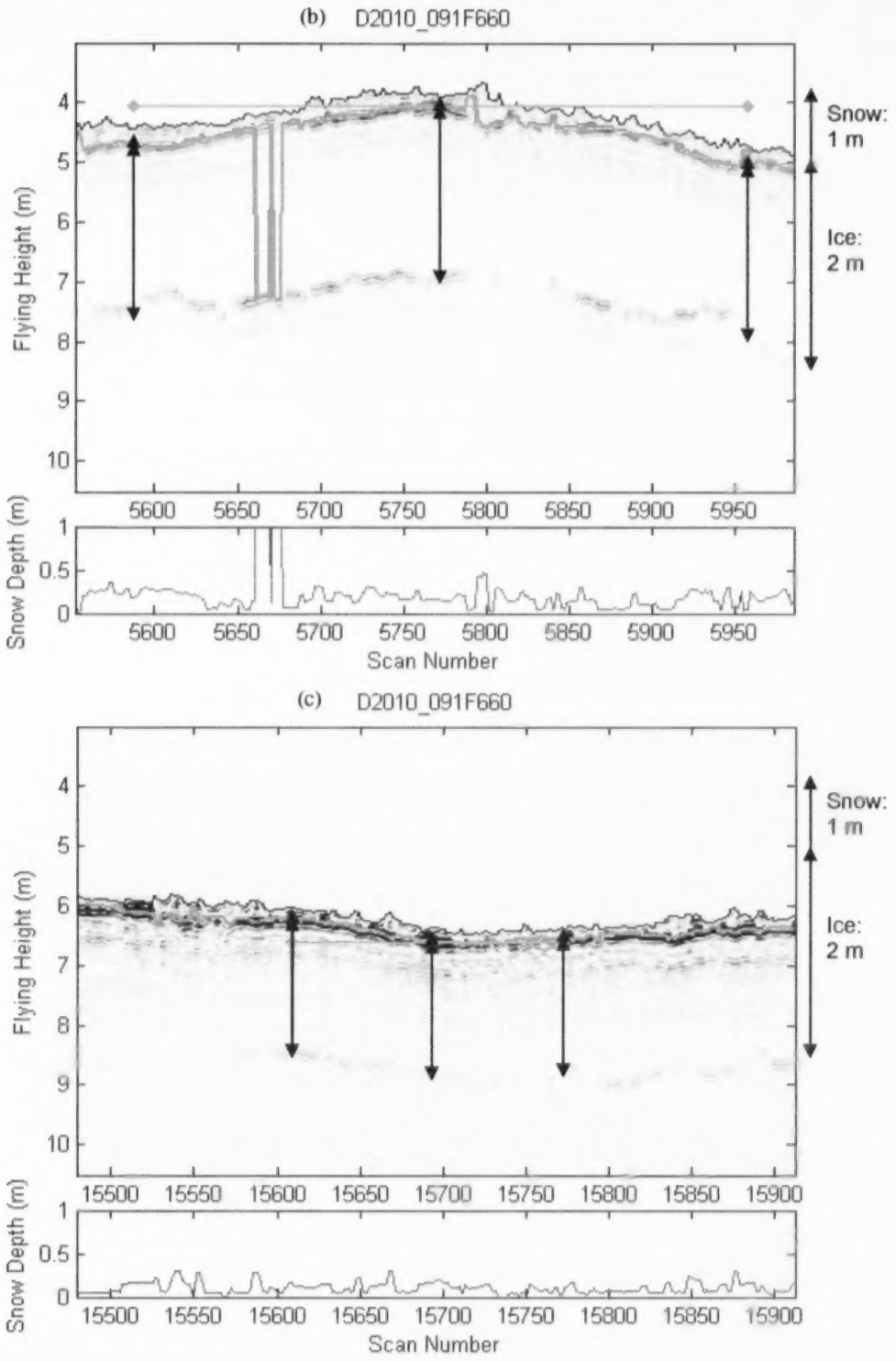

Fig. 3 (continued).

The snow depth computed from the inferred air-snow and snow-ice interfaces is shown in the lower panel of each plot. In areas where the ice-water echo is stronger than the snow-ice echo, the snow-ice echo is interpreted as the ice-water echo and the snow depth is over-estimated; the software was originally intended for use in high water-salinity areas where the ice-water interface is not detected.

2.1.2 Statistics

Modal snow thicknesses (i.e. most frequently occurring snow thicknesses) for individual flight lines were extracted from GPR data collected on 01-09 Apr 2010 by plotting the histogram of the snow thickness. The example in Figure 4 (Flight 646) shows the snow thickness time series in the top panel, the flight track in the bottom left panel, and the histogram in the bottom right panel. As in this example, the maximum value for the histogram usually corresponds to 0.05m, the thickness obtained when only one interface is detected. Therefore the modal snow thickness was extracted from thicknesses greater than 0.05m only.

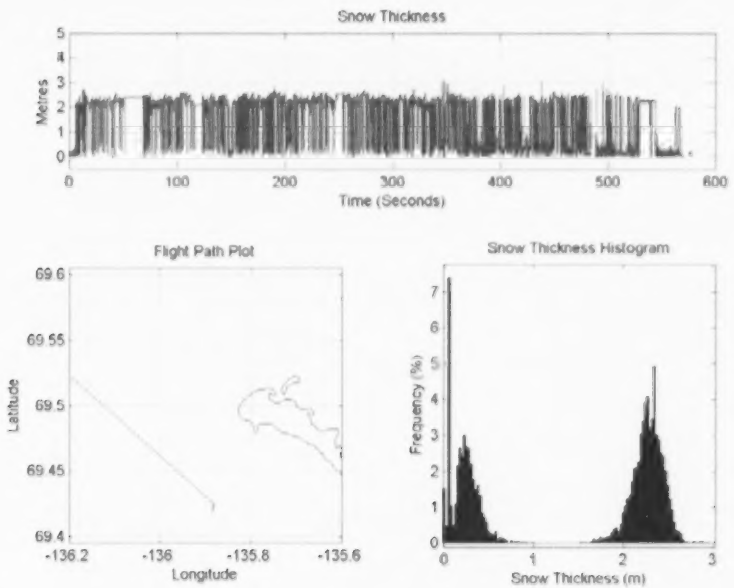

Fig. 4. Apparent snow thicknesses for Flight 646 on 01 April 2010. Values less than 1m represent snow thicknesses and values greater than 1m generally represent snow+ice thicknesses (scaled for snow thickness).

As mentioned previously, in the inshore region, there is a strong echo from the ice-water interface for smooth ice, and the present version of the GPR processing software often selects this interface instead of the snow-ice interface. As a result, the histogram is bimodal in the inshore region (Fig. 4), with one mode representing snow and the second mode representing snow-plus-ice. Thus an

estimate of modal ice thickness can be obtained by subtracting the modal snow thickness from the second mode and adjusting for the difference in the dielectric constant (Table 1). Improvements to the software would make it possible to estimate snow and ice thicknesses as separate quantities.

The modal snow and ice thicknesses are listed in Table 1, and next to the flight numbers for the maps in Figure 5. On the west side of the Mackenzie Delta (Fig. 5a, b and d) modal snow thicknesses are 0.15-0.38 m over the smooth ice inside the 5m bottom contour, about 0.08-0.15 m over the rough ice between the 5m contour and the stamukhi zone, and are 0.08-0.12 m beyond the stamukhi zone. On the east side of the Delta (Fig. 5c), modal snow thicknesses are about 0.2-0.3m to the south in Kittigazuit Bay, about 0.15m elsewhere south of 69.9°N, and 0.08m north of 69.9°N. Modal ice thicknesses are 1.2m to 1.7m, similar to those on the west side of the Delta.

Table 1. Modal snow and ice thicknesses from GPR data.

Date	Flight Line	Modal Snow thickness (m)	Modal Ice Thickness (m)
01 Apr	643	0.200	-
	644	0.325	1.23
	645	0.250	1.44
	646	0.225	1.45
	647	0.150	1.45
	649	0.150	-
	650	0.125	-
	651	0.075	-
	654	0.250	1.40
	655	0.225	1.34
	656	0.175	1.37
	657	0.250	1.44
	659	0.350	1.44
	660	0.150	1.47
	661	0.150	-

Date	Flight Line	Modal Snow thickness (m)	Modal Ice Thickness (m)
	663	0.125	-
	665	0.150	-
	666	0.125	-
	667	0.075	-
05 Apr	669	0.175	1.49
	670	0.275	1.42
	671	0.075	1.69
	672	0.075	-
05 Apr	673	0.075	-
	674	0.075	-
	676	0.100	-
	677	0.075	-
	679	0.250	1.44
	680	0.250	1.44
	681	0.375	1.42

Date	Flight Line	Modal Snow thickness (m)	Modal Ice Thickness (m)
	682	0.075	-
	683	0.150	-
	685	0.150	-
	686	0.075	-
	687	0.125	-
	688	0.075	-
	690	0.175	1.32
	691	0.350	1.37
	694	0.250	1.37
	695	0.225	1.28
	696	0.350	1.11
	697	0.275	1.22
08 Apr	699	0.250	1.23
	700	0.275	1.42

Date	Flight Line	Modal Snow thickness (m)	Modal Ice Thickness (m)
	701	0.225	1.45
	702	0.175	-
08 Apr	703	0.150	-
	704	0.075	-
	705	0.150	1.61
	706	0.150	1.64
	707	0.175	1.63
	709	0.150	-
	710	0.150	-
	711	0.150	-
	712	0.075	-
	713	0.075	-
09 Apr	719	0.075	-
	720	0.125	-

(a)

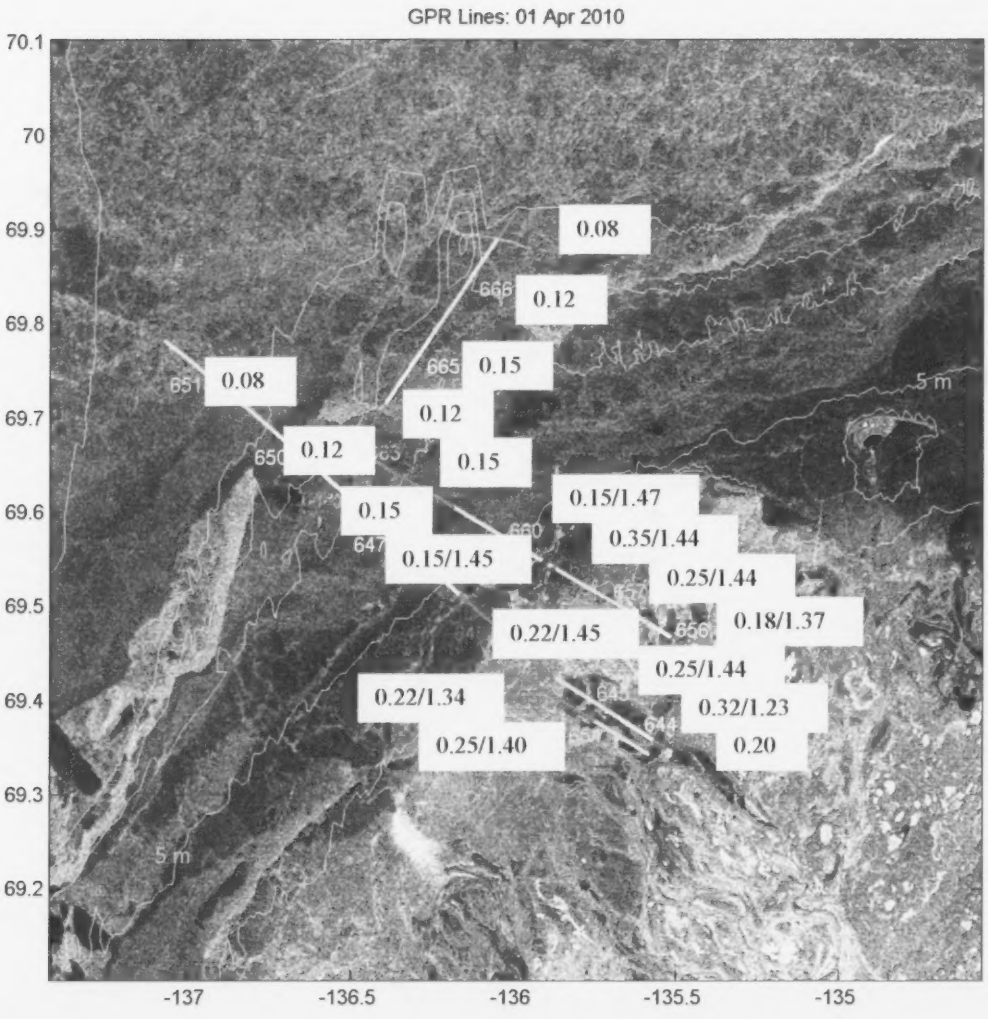

Fig. 5. RADARSAT image overlaid with GPR flight lines (coloured numbers) for (a) 1 April 2010, (b) 5 April, (c) 8 April and (d) 9 April 2010. The black numbers refer to the modal snow thickness for the flight line in metres, followed by the ice thickness if available.

(b)

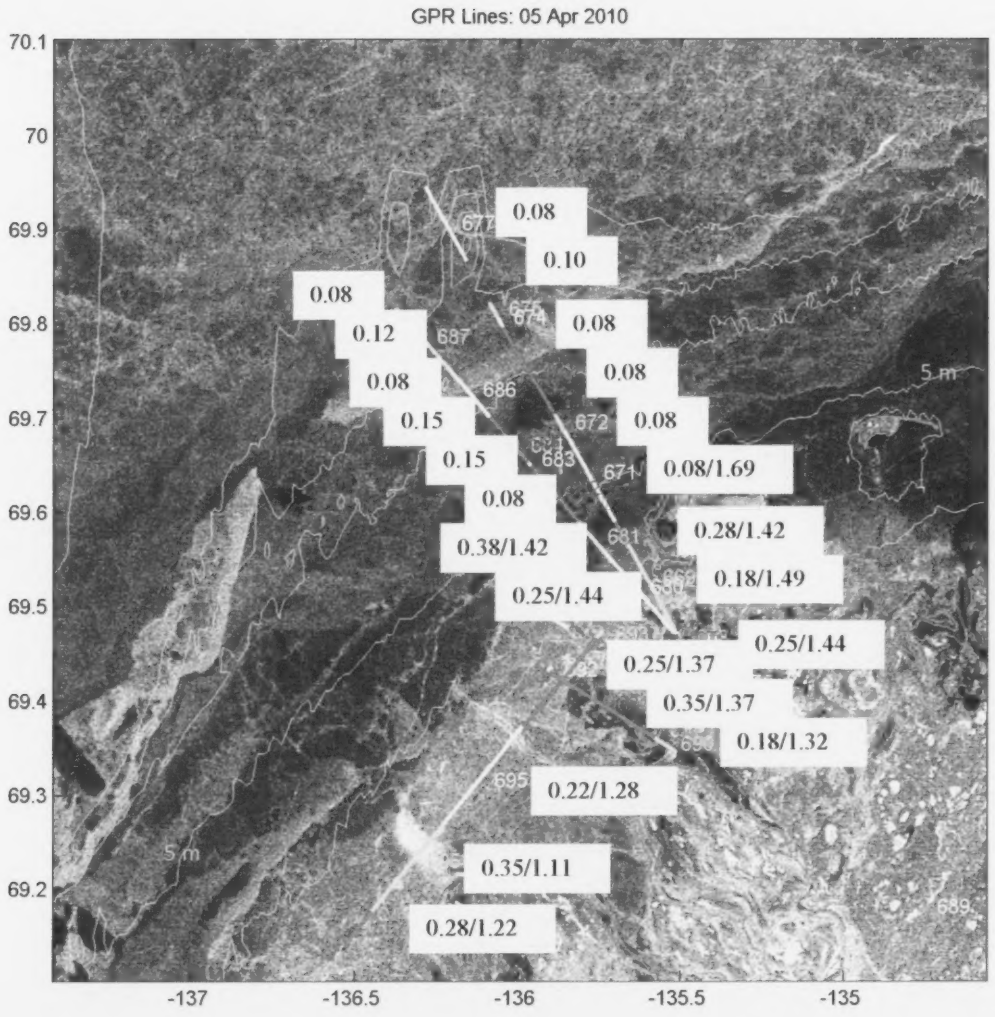
GPR Lines: 05 Apr 2010
70.1
70
69.9
69.8
69.7
69.6
69.5
69.4
69.3
69.2
-137
-136.5
-136
-135.5
-135
0.08
0.10
0.08
0.12
0.08
0.08
0.15
0.15
0.08
0.38/1.42
0.25/1.44
0.08
0.08
0.08
0.08/1.69
0.28/1.42
0.18/1.49
0.25/1.44
0.25/1.37
0.35/1.37
0.18/1.32
0.22/1.28
0.35/1.11
0.28/1.22
5 m
5 m
687
686
672
683
671
681
695
689

Fig. 5 (cont.)

(c)

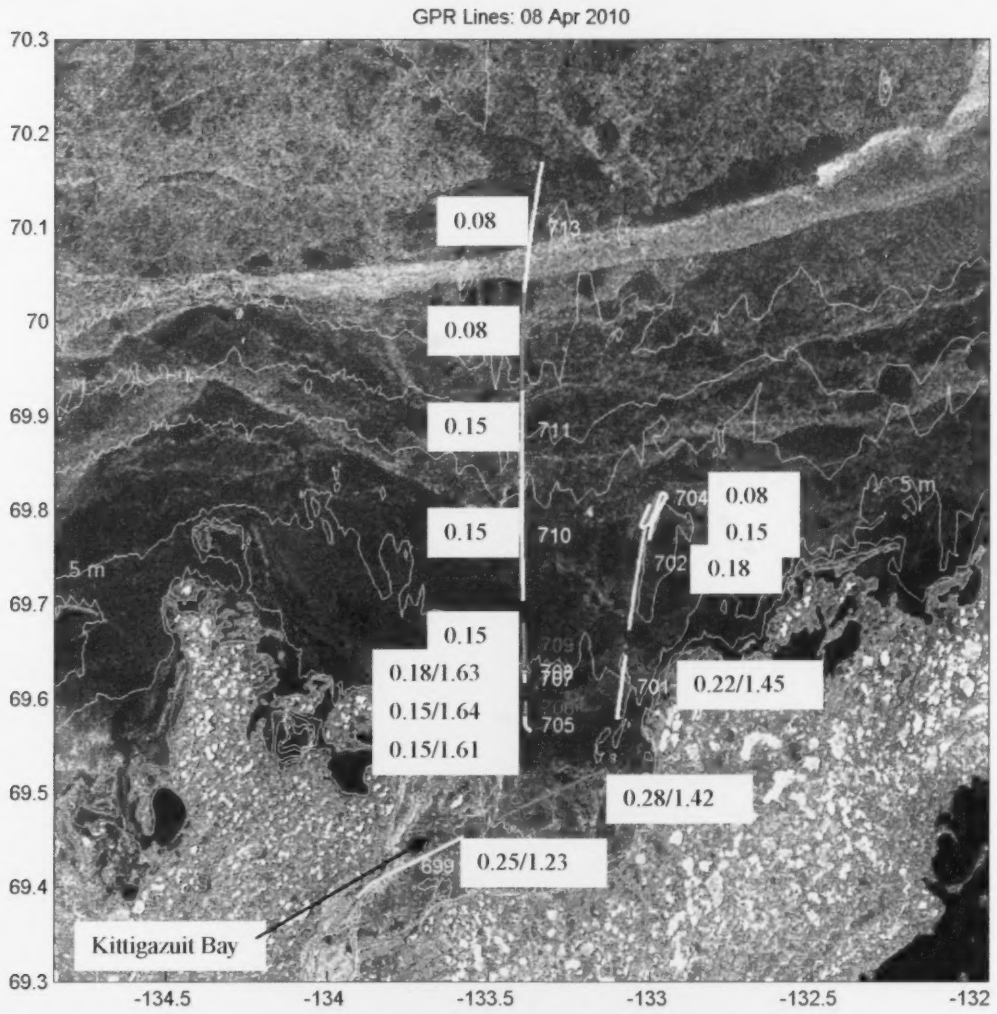
GPR Lines: 08 Apr 2010
70.3
70.2
70.1
70
69.9
69.8
69.7
69.6
69.5
69.4
69.3
-134.5
-134
-133.5
-133
-132.5
-132
0.08
0.08
0.15
0.15
0.15
0.18/1.63
0.15/1.64
0.15/1.61
0.08
0.15
0.18
0.22/1.45
0.28/1.42
0.25/1.23
713
711
710
704
702
709
707
701
705
699
5 m
5 m
Kittigazuit Bay

Fig. 5 (cont.)

(d)

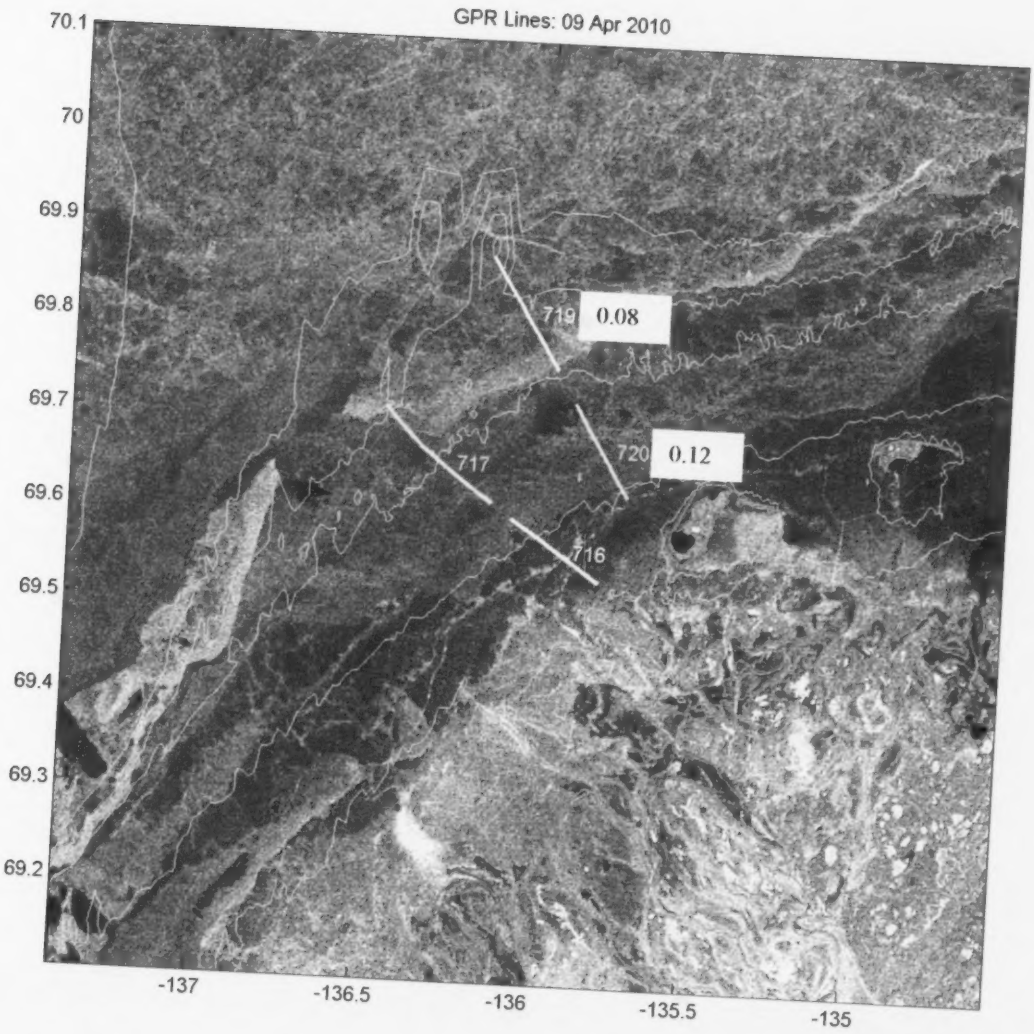
GPR Lines: 09 Apr 2010
70.1
70
69.9
69.8
69.7
69.6
69.5
69.4
69.3
69.2
719
0.08
717
720
0.12
716
-137
-136.5
-136
-135.5
-135

Fig. 5 (cont.)

2.2 EM DATA COMPARISONS WITH CTD AND GPR DATA

In Appendix 1, the EM data are compared with the on-ice measurements of snow thickness and ice thickness and CTD profiles of water conductivity, using 4 EM inversion models (three 2-layer and one 4-layer models). The EM models provide estimates of the thickness and conductivity for the various layers, as well as the model error. The models differ with respect to the settings of the layer conductivities, and whether they are fixed or free to vary. For the 2-layer models, the upper layer represents snow+ice+freshwater, while the lower layer represents seawater or sediments. Agreement between the layer thickness and conductivity from the EM models and from the on-ice measurements of snow thickness, ice thickness and water conductivity varied with location across the shelf.

In Appendix 2, EM and GPR data were compared and used together to interpret many conditions such as fresh or saline ice overlying fresh water or saline water, with frozen or unfrozen sediments.

3.0 SUMMER 2011 SURVEY

In the summer of 2011, a helicopter survey of multi-year ice was conducted in the Beaufort Sea west of Banks Island (Fig. 6) as part of a collaboration between the Centre of Earth Observation Science (CEOS) of the University of Manitoba, and Imperial Oil Limited (Prinsenberg et al., 2011). In addition, ice properties were measured directly through ice auger holes by the National Research Council as part of a Joint Industry Project. According to the ice chart produced by the Canadian Ice Service, ice concentrations were 50-70%, and the ice was 60-86% old ice and 14-40% thick first-year ice.

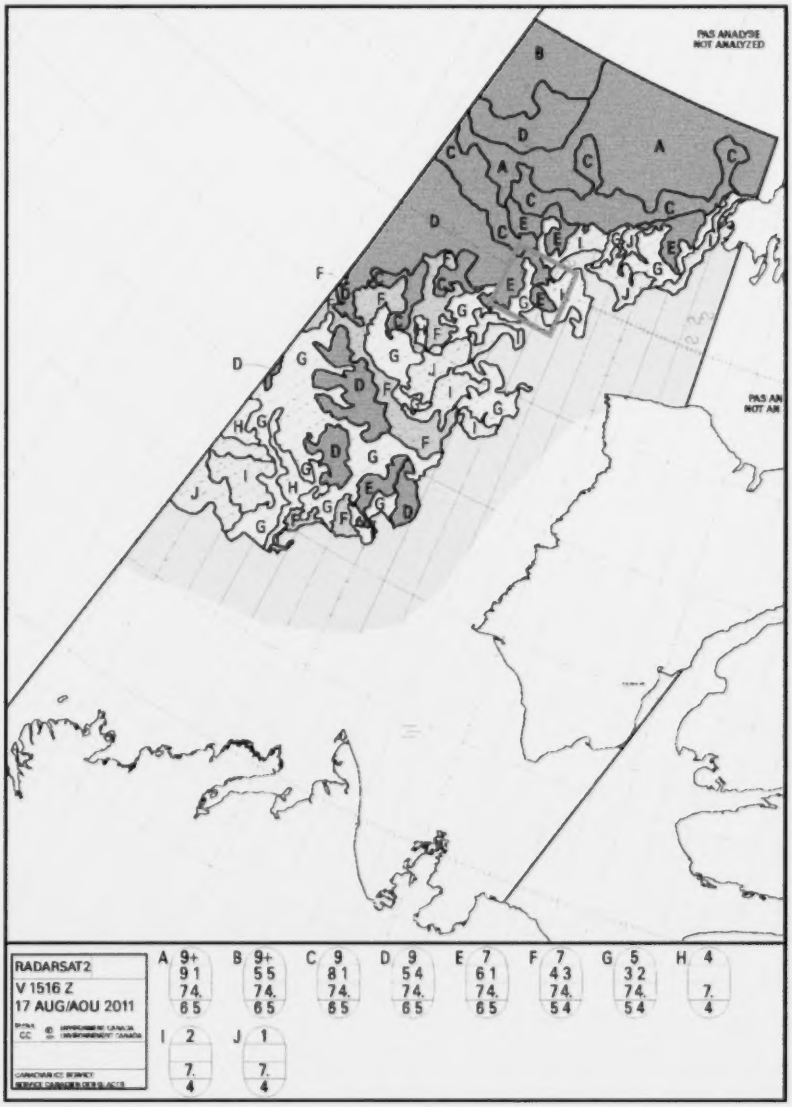

Fig. 6. Ice chart for 17 August 2011 produced by the Canadian Ice Service, showing location of MODIS image in Fig. 7.

At two sites, B1S1 (Box 1, Site 1) and B1S2 (Box 1, Site 2) (Fig. 7), EM ice thickness data were collected with the BIO helicopter sensors along a few short lines, where on-ice thickness and other ice property data were collected by NRC. B1S1, sampled on 16 August, was near the ice edge on a vast multiyear ice floe Fig. 8). Although this floe is referred to as multiyear, it was an aggregate of floes of different ages, some of which may have been second-year or even first-year. It contained leads and bottomless melt-ponds, which were likely first-year ice in the previous winter. B1S2, sampled on 18 August, was on a smaller floe 30 km to the northwest inside the ice edge. Near both sites, EM, GPR and video data were also collected along several lines of up to about 10 km in length in regional surveys.

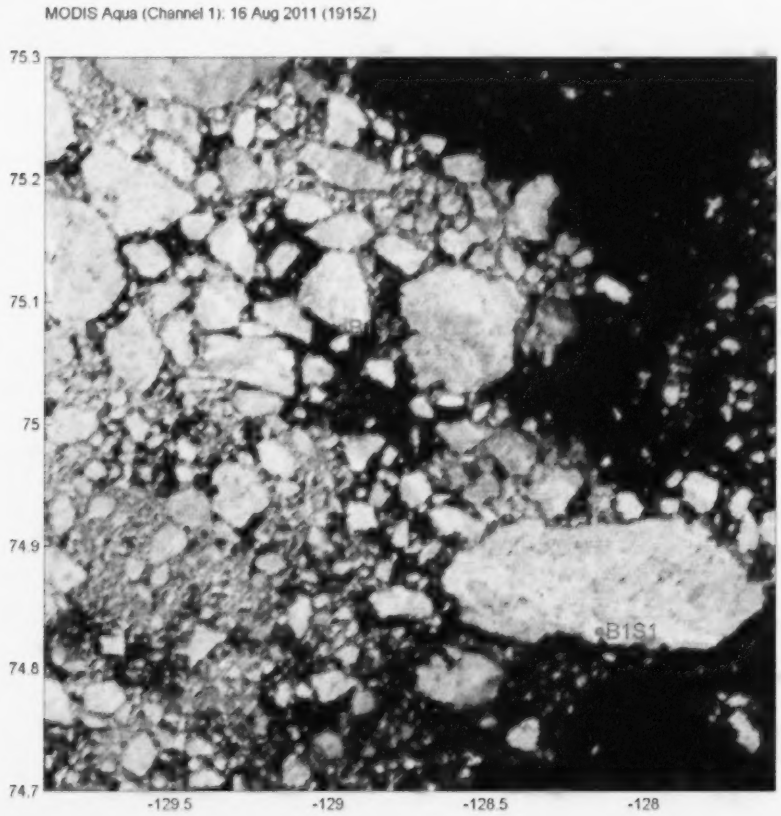

Fig. 7. MODIS image for 16 August 2011 showing the location of sites B1S1 and B1S2.

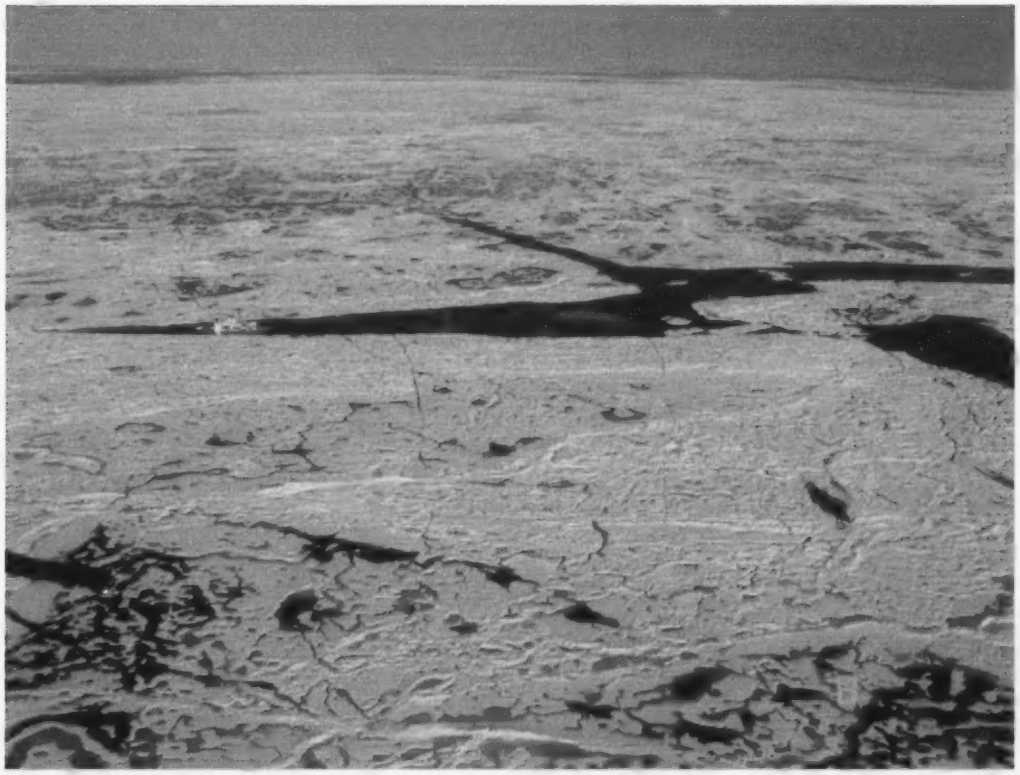

Fig. 8. Photograph of vast MY ice floe in the Beaufort Sea, consisting of areas of thick ridged MY ice (A) with blue-white melt-ponds on the ice surface, and areas of heavily-decayed ice (B) contain extensive melt ponds with dark thaw holes. The location of B1S1 (C) near the CCGS Amundsen, and the area of the regional survey (D) are also shown.

3.1 EM ICE THICKNESS VALIDATION

At the site B1S2 on 18 August, EM data were collected along lines in a chair-shaped configuration on Flight 11040 (Fig. 9), with the line parallel to the ship (the "chair-seat") flown several times. Figure 9 shows the flight paths (blue lines), drill-hole locations (black dots along blue lines), the EM ice thicknesses with real-time processing (green lines), and post-processing (red lines), and the drill-hole thicknesses (black lines). The scale for the ice thicknesses is 10m thickness per 50m distance. The real-time data are in good agreement with the post-processed data which have additional corrections for EM drift. However the repeatability is slightly better for the post-processed data. The EM thicknesses range from 5m to 10m, while the on-ice thicknesses are as high as 15m.

At the site B1S1 on 16 August, on-ice sampling was done along a similar pattern, but EM data were collected only along the line parallel to the ship, flown twice on Flights 11034 and 11037. The ice thickness and conductivity data from B1S1 are plotted in Figure 10. At B1S1, EM thicknesses range from 5m to 7m, and agreement with on-ice thicknesses is slightly better for post-processed data (red) than real-time data (green). The real-time thicknesses noted down in the field (blue) are also shown, and are close to those estimated from the data files. The ice conductivity (bottom panel) is greater than 0.015 S/m, and increases from left to right. The drill-holes on the right side contained pockets (indicated by asterisks), while most of the drill-holes on the left side did not contain pockets. "Pockets" are sea-water-filled voids that cause the drill auger to unexpectedly drop and can range from small (~10cm) to large (~0.5m, Johnston, personal communication).

For the site B1S2 on 18 August, Figure 11 (top panel) shows the real-time (green), post-processed (red) EM ice thicknesses, and drill-hole thicknesses (black) for line O (Transect 3), which was perpendicular to the ship. The ice conductivity (bottom panel) is less than 0.01 S/m, and only two of the drill-holes contained pockets. Figure 12 (top panel) shows the real-time (green), post-processed (red) EM ice thicknesses, and drill-hole thicknesses (black) for floe B1S2, line B, which was parallel (holes 1-10) and perpendicular (holes 10-20, Transect 3) to the ship. Fig. 12 shows results for both transects, made 90° to each other. As for line O on B1S2, the ice conductivity (bottom panel) is less than 0.01 S/m, and only two of the drill-holes contained pockets.

Figure 13 shows a scatter-plot of the EM ice thicknesses versus the drill-hole ice thicknesses. For B1S2 (blue markers), there are 2 outliers for which the drill-hole thickness is greater than 14 m. For the remaining B1S2 points, the correlation is 0.78 between the EM and drill-hole ice thicknesses; the regression line is shown in blue. For B1S1 (red markers), the relationship between the EM and drill-hole thicknesses is consistent with that for B1S2. The regression line indicates that there is good agreement of EM thicknesses with on-ice measurements of 6m, but on-ice measurements of 10m correspond to EM measurements of 8.3m. The underestimation of high ice thicknesses is probably due to the large footprint of the EM sensor (~30m), and to pockets of seawater that may be present in large ridge keels.

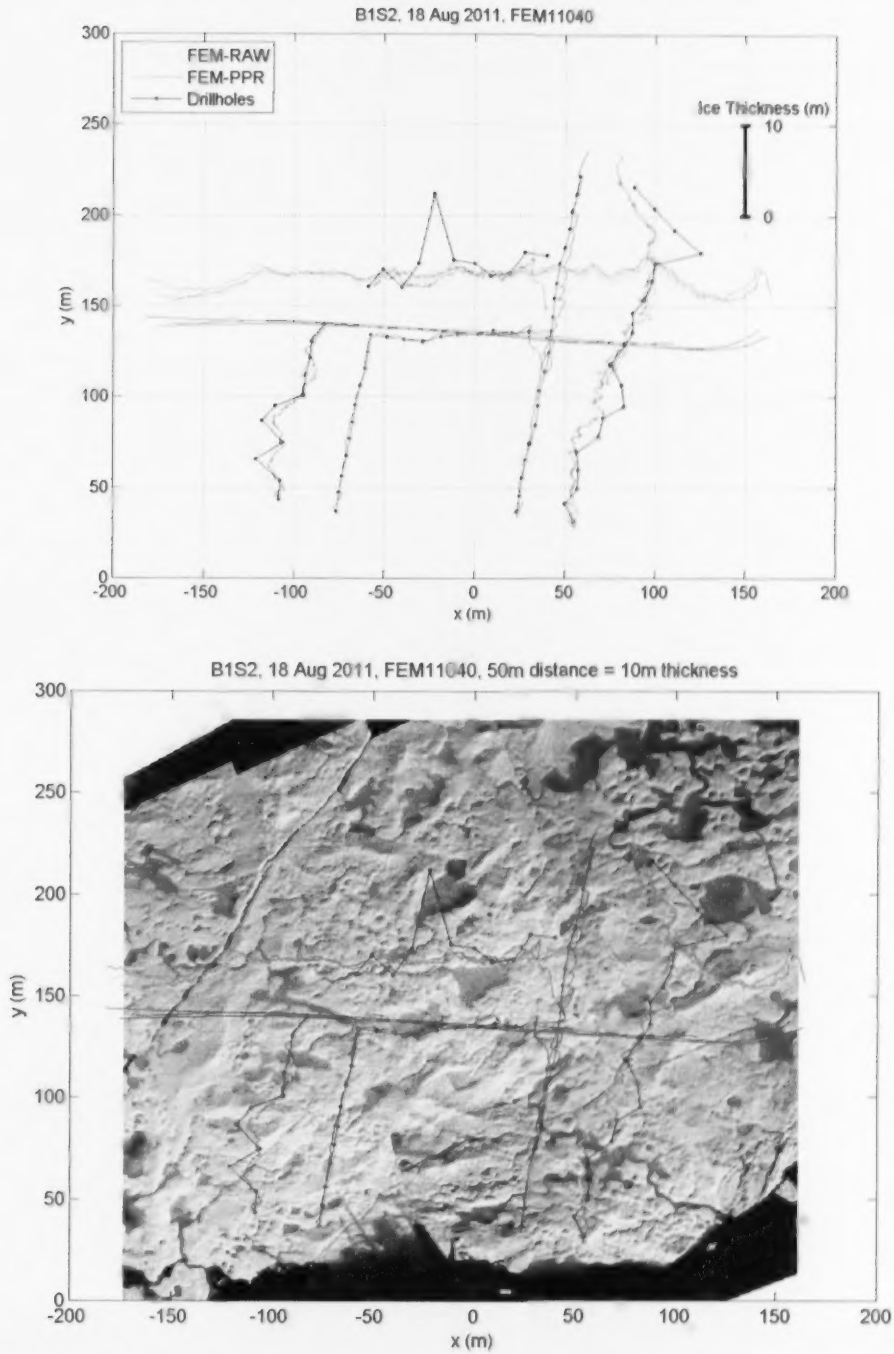

Fig. 9. Ice thickness at site B1S2 from EM real-time processing (green), EM post-processing (red), and drill-hole measurements by Michelle Johnston (NRC), relative to flight path (blue) and drill-hole sites (black dots on blue lines) (upper panel). Plot is overlaid on video data in lower panel.

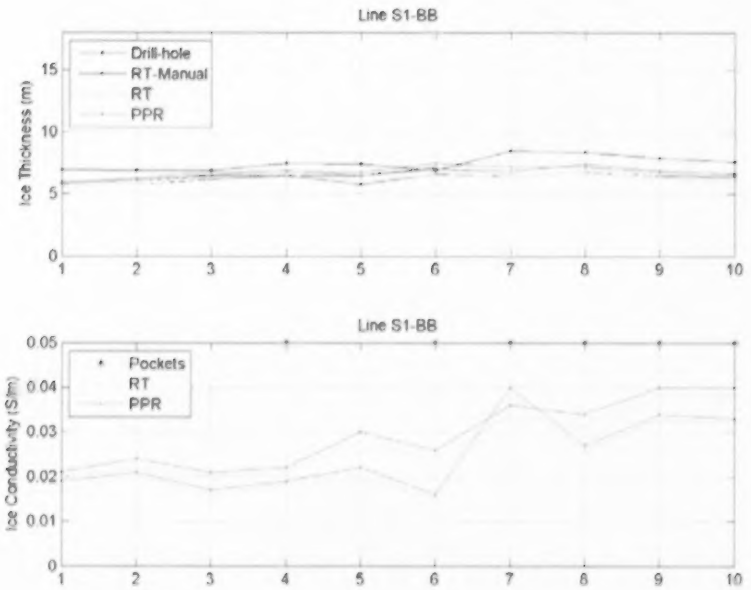

Fig. 10. EM and drill-hole ice thickness (top panel) and conductivity (bottom panel) for B1S1, line BB. S1-BB was surveyed twice (flights 11034 and 11037 on 16 Aug 2011). The holes are 10 m apart along the line.

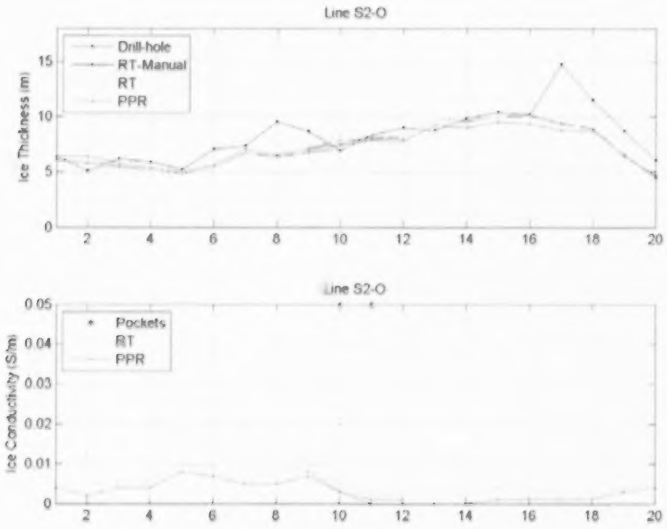

Fig. 11. EM and drill-hole ice thickness (top panel) and conductivity (bottom panel) for B1S2, line O. Both drill holes in which pockets occurred were located near a melt pond. The holes are 10 m apart along the line.

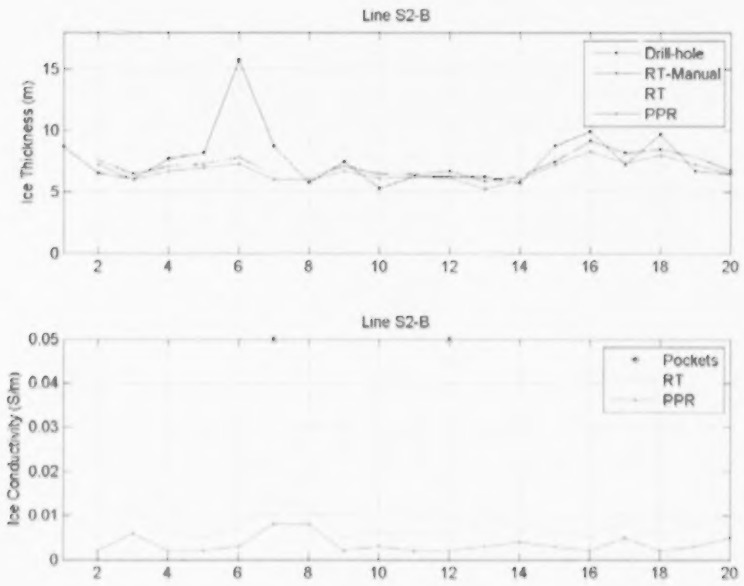

Fig. 12. EM and drill-hole ice thickness (top panel) and conductivity (bottom panel) for B1S2, line B. Holes 1-10 and 10-20 are on lines perpendicular to each other. The holes are 10 m apart along the lines.

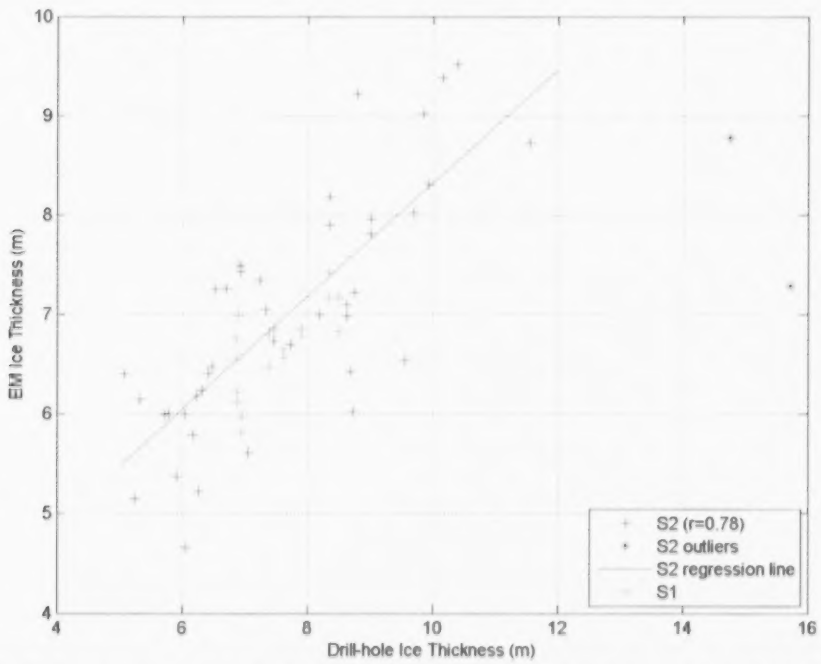

Fig. 13. EM versus drill-hole ice thickness for B1S2 (blue markers) and B1S1 (red markers). The regression line and correlation coefficient (r=0.78) are for B1S2 only without the 2 outliers.

3.2 REGIONAL SURVEY

On 16 August, EM profiles 10-15 km long were collected over the vast MY floe near B1S1 in a southeast-northwest direction. The apparent ice thicknesses (i.e. the upper layer thicknesses from a 2-layer EM model) are overlaid on a MODIS image from 16 August in Fig. 14, after adjusting the line positions for ice drift. High ice thicknesses (6-10m) are found near the southern edge of the floe and toward the northern part of the floe at 74.89°N, and correspond to high reflectance in the MODIS image. Elsewhere, the upper-layer thicknesses are generally uniform (~3m) and correspond to lower reflectance in the MODIS image. Between 74.89°N and the northern edge of the floe, thicknesses decrease to about 2m.

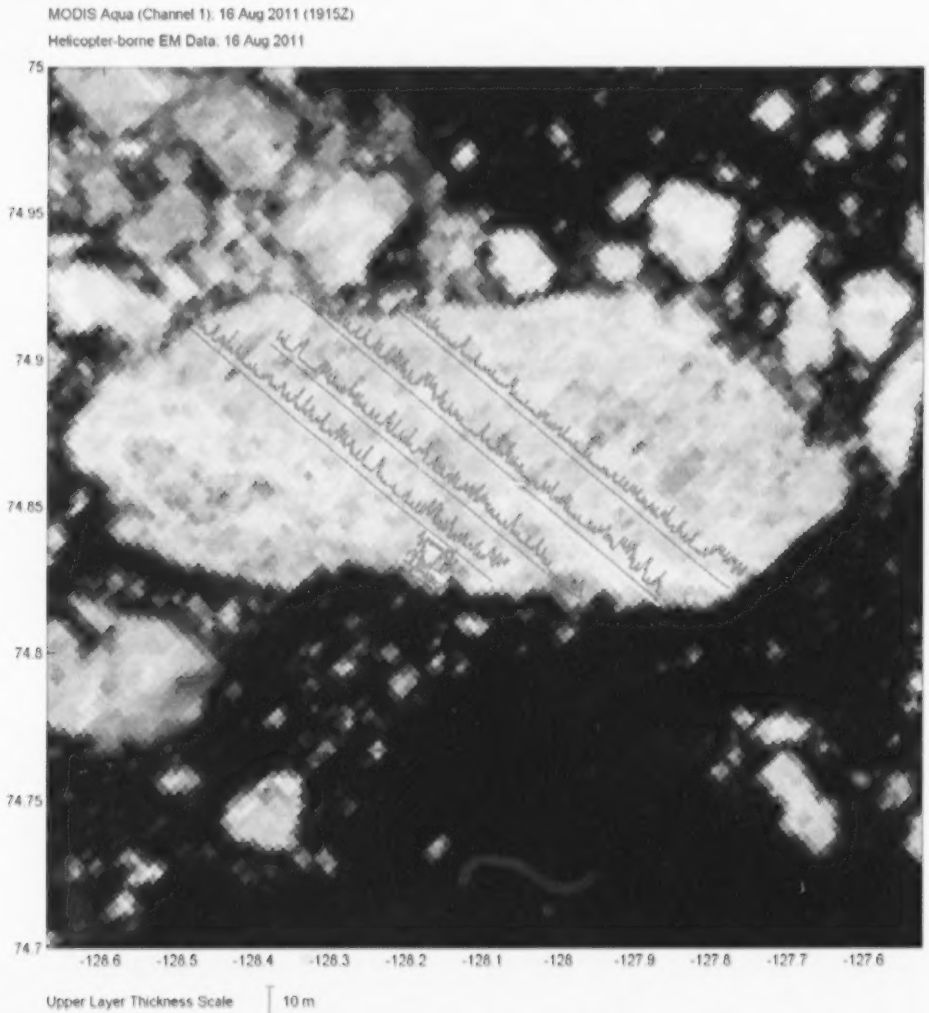

Fig. 14. MODIS image for 16 August 2011 overlaid with EM-derived upper layer thickness profiles collected on 16 August. The green line shows the position of the video mosaic in Fig. 18, and the flight direction for the four long EM profiles.

Histograms of the thicknesses for the four long lines across the floe are shown in Fig. 15 (a-d, from west to east). The modal thicknesses, (i.e. the most frequently occurring thicknesses) for lines a-d are 2.9m, 2.8m, 2.8m and 2.8m respectively.

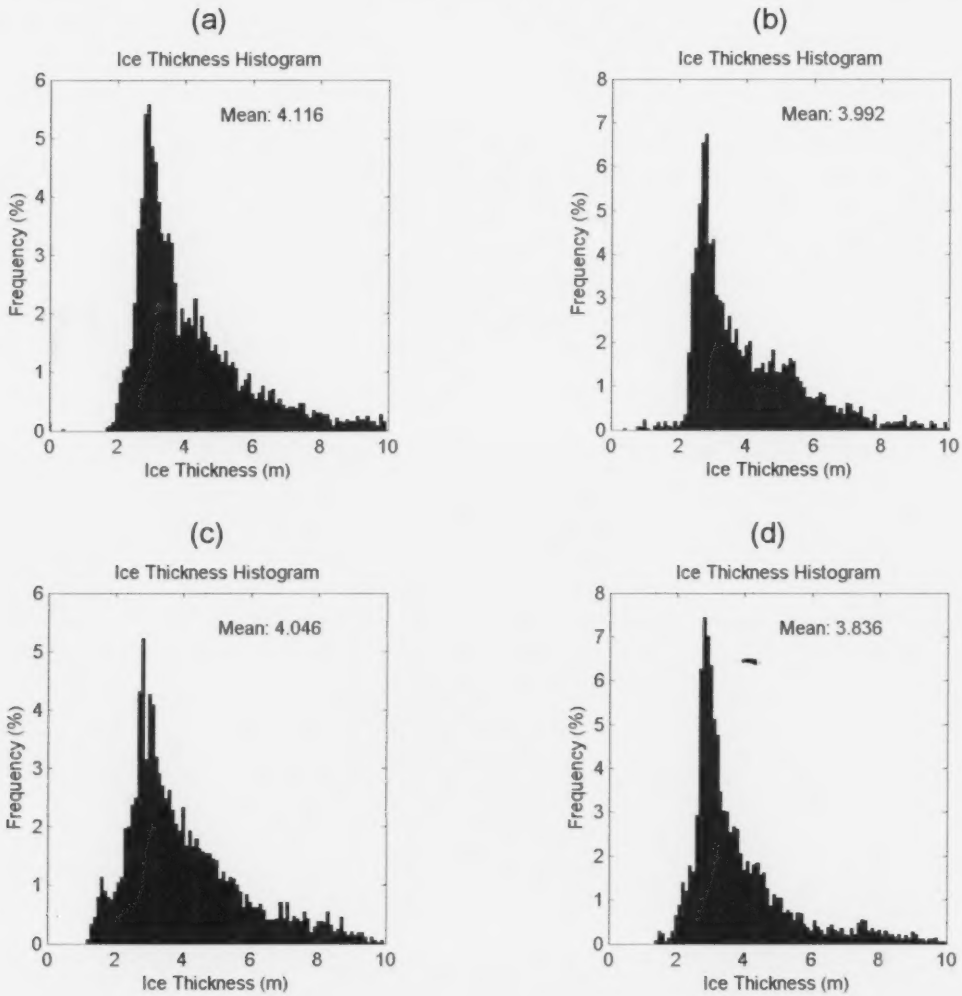

Fig. 15. Histograms for the four long flight lines in Fig.14 (from west to east).

Minimum thicknesses along the survey lines using a 50-point window (Fig. 16) show a similar pattern to that in Fig. 14. High minimum thicknesses are found near the southern edge of the floe and near 74.89°N. Between these two areas, the minimum thickness is very uniform at about 2.8m. Proceeding northward, the minimum thickness drops gradually from about 3m at 74.9°N to 2 m near the northern edge of the floe. Low minimum thicknesses are also found in areas close to the southern edge of the floe. The relatively uniform thicknesses in the areas of lower reflectance suggest that the apparent ice thickness represents both ice and a freshwater layer in the melt-ponds and under the thinner ice.

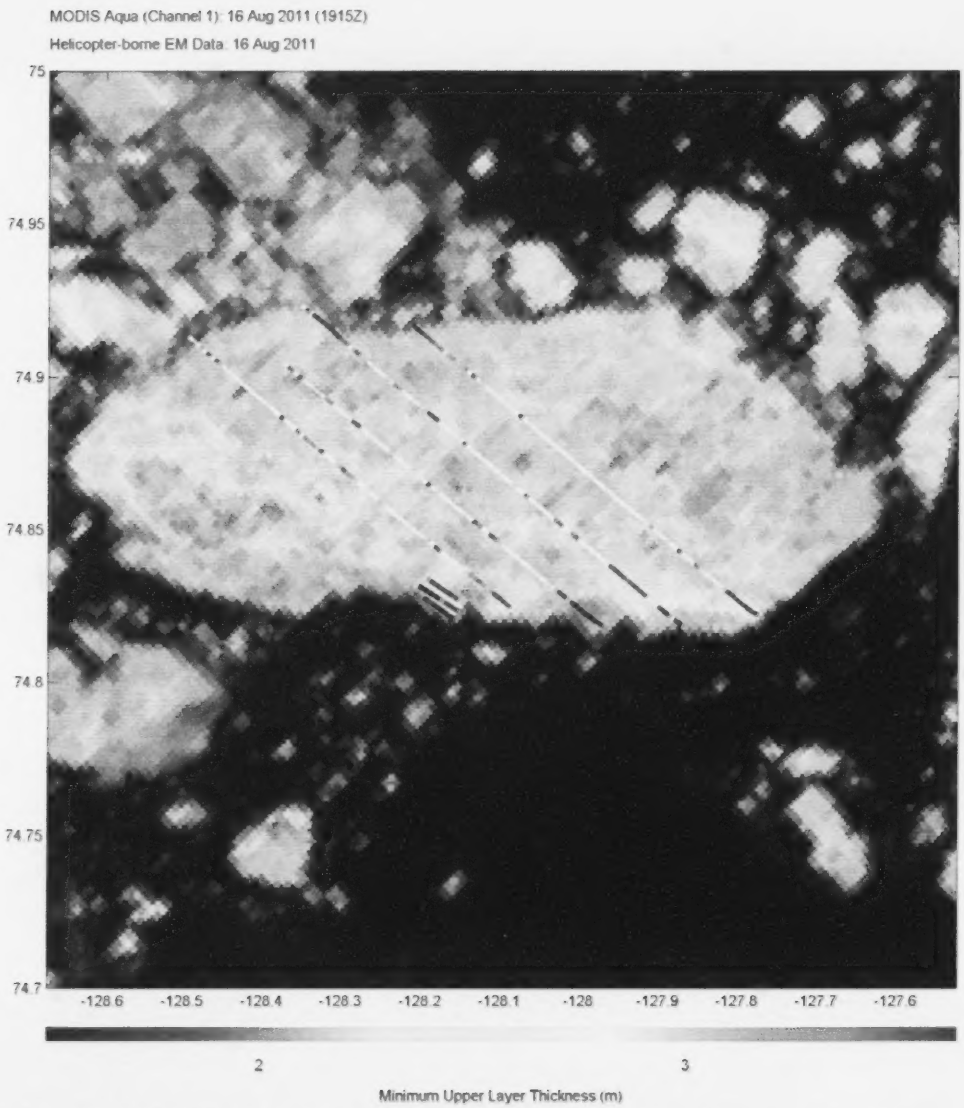

Fig. 16. MODIS image for 16 August 2011 overlaid with minimum upper layer thicknesses (using 50-point window).

On 19-20 August, long ice thickness profiles were collected near and to the west of B1S2, and over the vast floe near B1S1 in a north-south direction, and are overlaid on a MODIS image acquired on 20 August (Fig. 17). Thicknesses are more variable and there are higher values to the west near B1S2 than over the vast floe near B1S1.

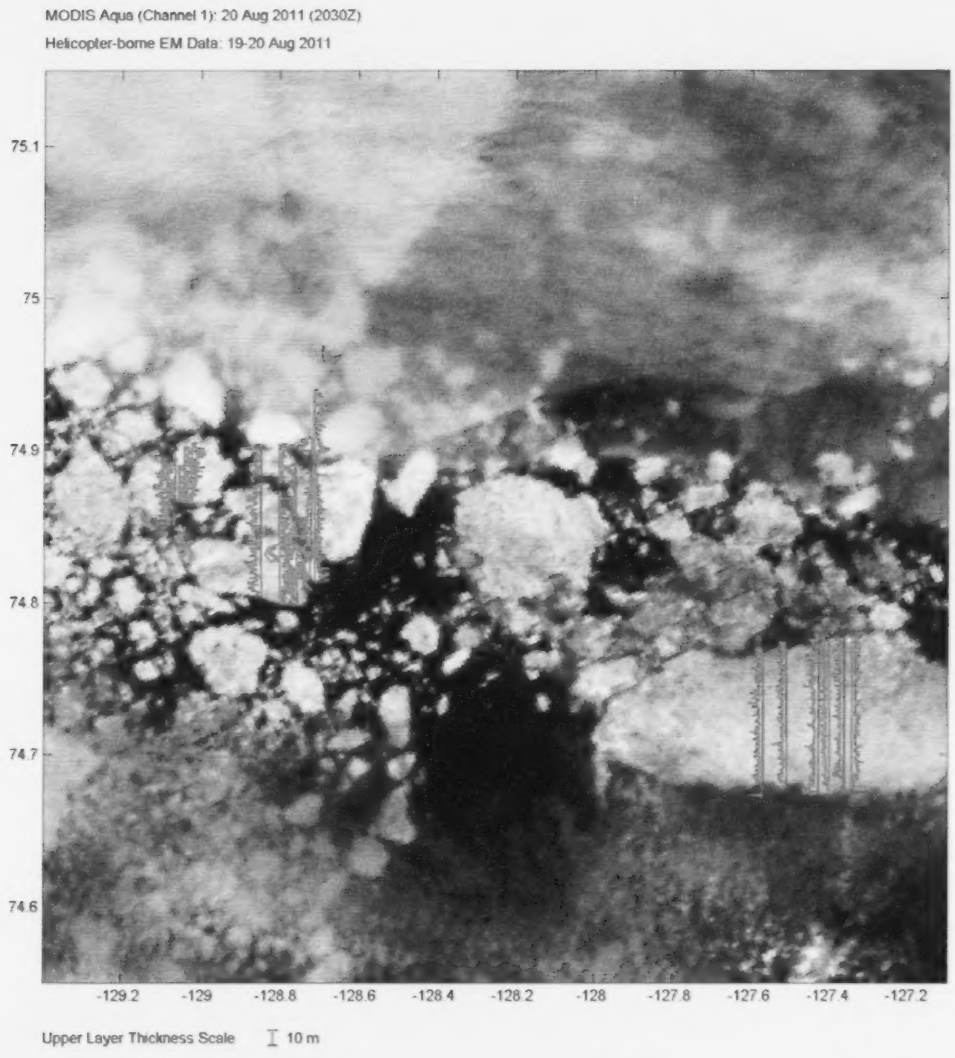

Fig. 17. MODIS image acquired on 20 August 2011 overlaid with EM-derived upper layer thickness profiles collected on 19-20 August.

Modal ice thicknesses (using a 50-point window) along the long flight lines are shown in Fig. 18. The modal thicknesses over the vast floe are generally about 2.5-3.0 m away from the floe edge. However modal thicknesses for the floes to the west are highly variable.

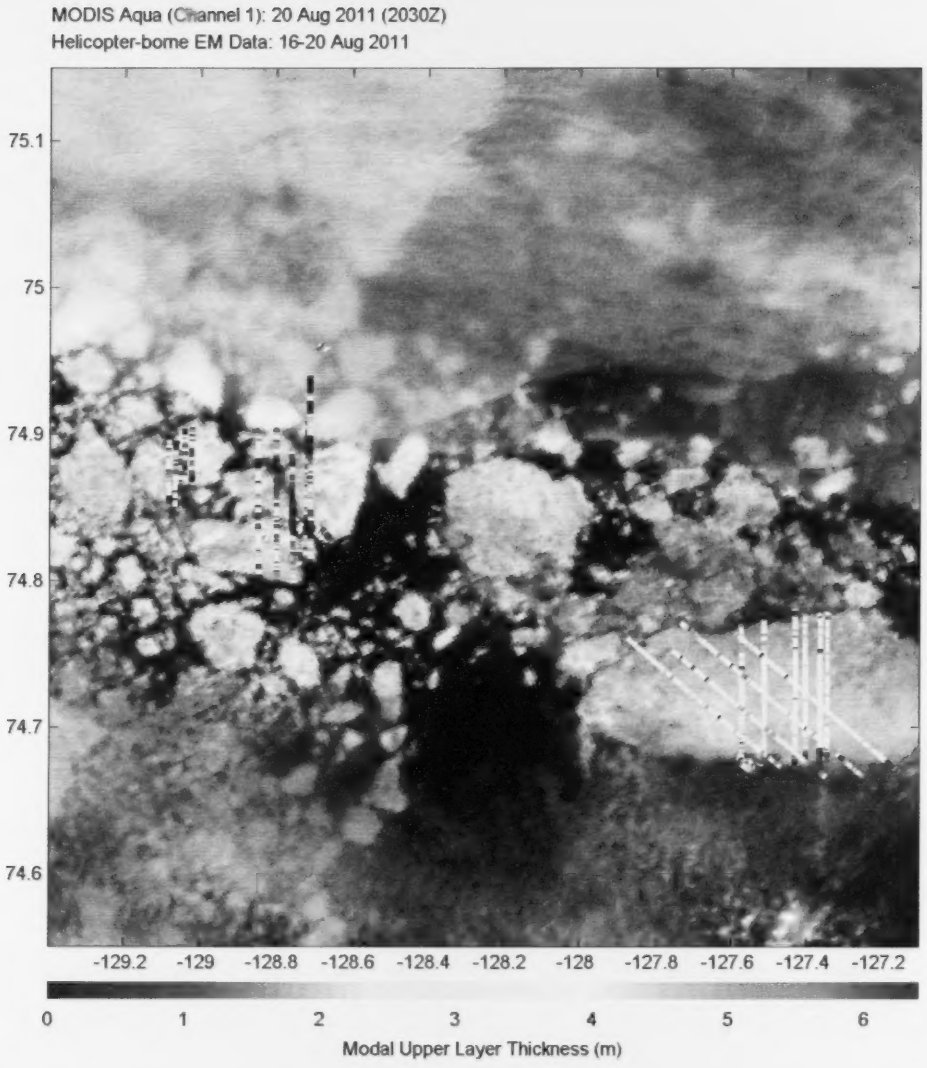

Fig. 18. MODIS image acquired on 20 August 2011 overlaid with modal EM-derived upper layer thicknesses collected on 16-20 August.

An example of a video mosaic from the southern section of the third long line (green line in Fig. 14) is shown in Fig. 19, plotted from the southern edge of the floe toward the northwest. High thicknesses from the southern half of the section (Fig. 14) correspond to ridged MY ice, while low thicknesses near the end of the section correspond to heavily-decayed ice.

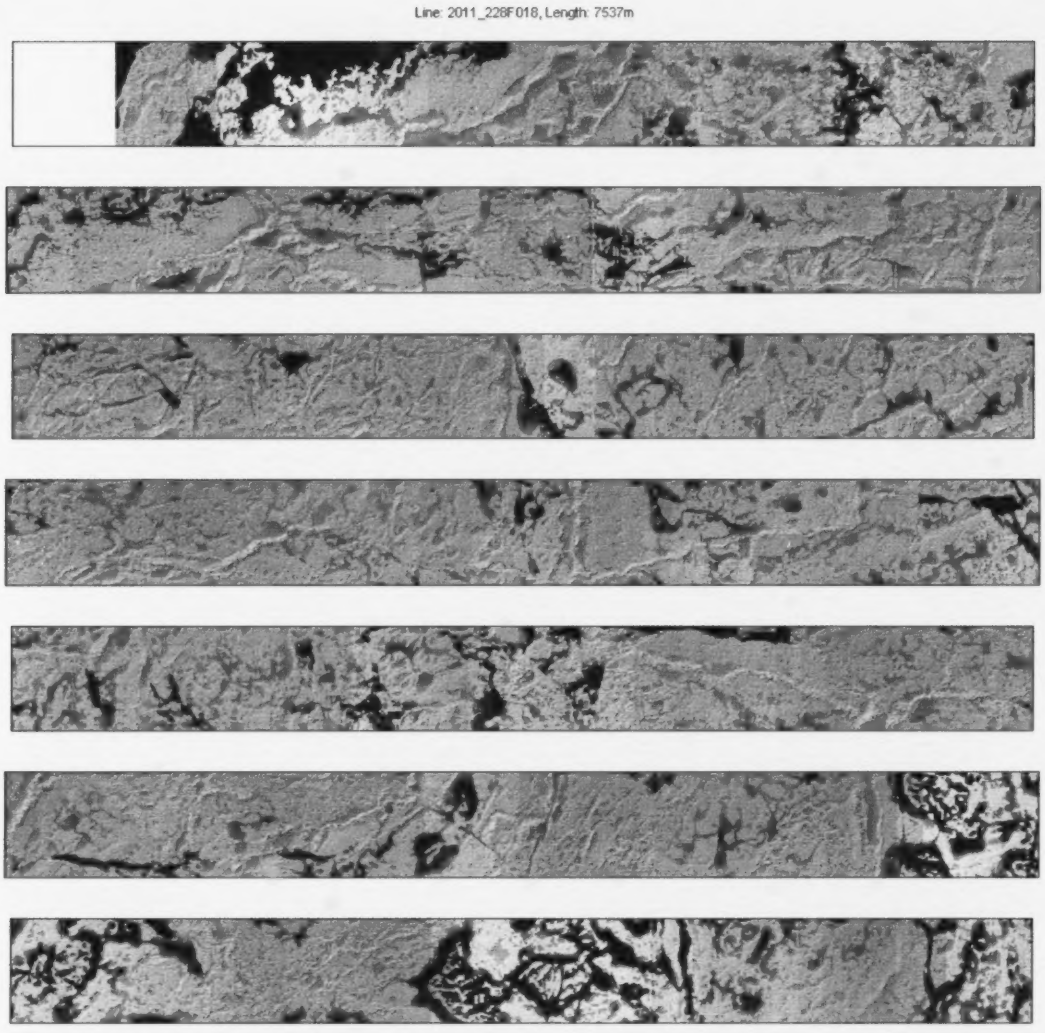

Fig. 19. Example of video mosaic collected on 16 August 2011 along green line in Fig. 14, and displayed from south-east to north-west.

Upper layer thickness profiles were also overlaid on RADARSAT-2 synthetic aperture radar (SAR) images (Fine Quad-pol) for HH (horizontal transmit, horizontal receive) and HV (horizontal transmit, vertical receive) polarizations (Fig. 20). For the HH polarization, backscatter is generally higher in the northeastern part of the floe than to the southwest. High thicknesses (6-10m) often correspond to areas of high backscatter such as near 74.88°N, and lower thicknesses (2-3m) often correspond to areas of moderate backscatter. However, there is less consistency in the relationship between thickness and image tone in the SAR image than the MODIS image, such as near the southern end of the westernmost long line. The backscatter in the HV image shows a similar pattern to that in the HH image. However there are areas of high backscatter near the southern edge of the floe in the HV image, but not the HH image.

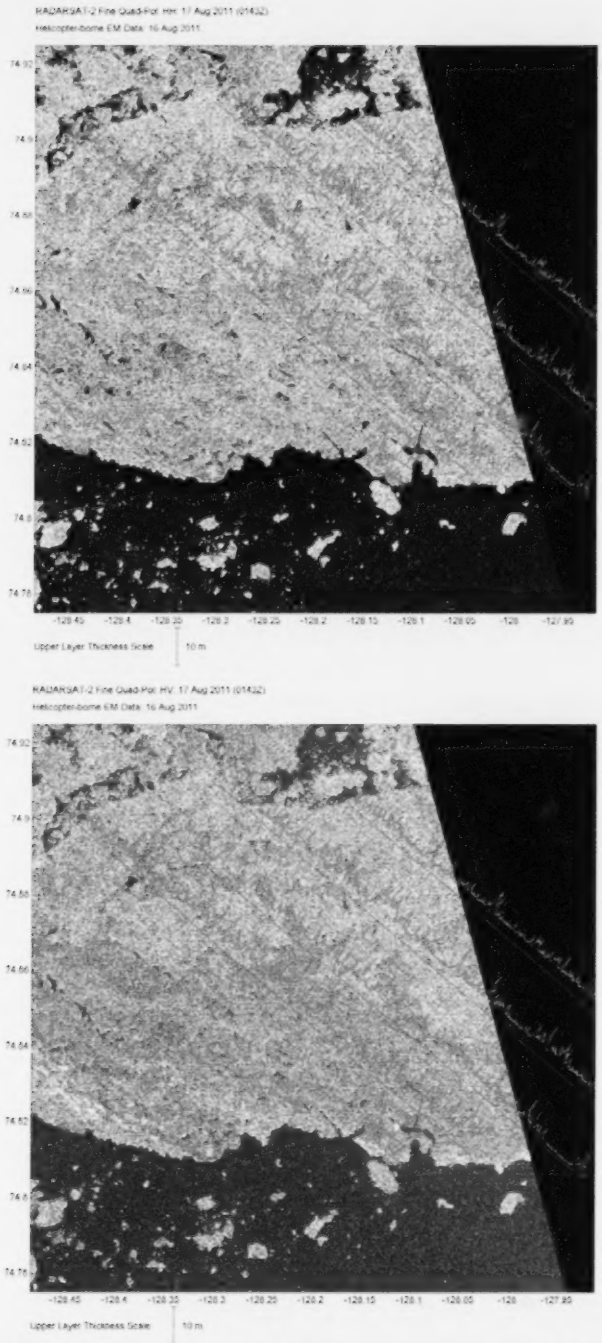

Fig. 20. RADARSAT-2 fine quad-pol (a) HH image and (b) HV image for 17 August 2011 overlaid with EM-derived upper layer thickness profiles. (RADARSAT-2 Data and Products © MacDonald, Dettwiler and Associates Ltd. (2011)- All Rights Reserved. RADARSAT is an official mark of the Canadian Space Agency).

4.0 CONCLUSIONS

In spring 2010 near the Mackenzie Delta, ice and snow thickness data were collected with helicopter-borne EM and GPR sensors near the Mackenzie Delta Ice thicknesses inferred from the GPR data in areas of low water salinity were in good agreement with drill-hole measurements. Modal snow thicknesses were higher in inshore areas than in offshore areas, where the ice formed later in the winter season. Snow+ice+freshwater layer thicknesses and conductivities were estimated from the EM data using three 2-layer and one 4-layer models; agreement between model results and on-ice measurements collected with a CTD profiler varied with location across the shelf. EM and GPR data were compared and used together to interpret many conditions such as fresh or saline ice overlying fresh water or saline water, with frozen or unfrozen sediments.

In summer 2011 in the eastern Beaufort Sea, EM ice thickness data collected at two ice measurement sites were in good agreement with drill-hole measurements collected by NRC of 6m ice, but underestimated thicknesses of 10 m ice by 17%. This is roughly consistent with Johnston and Haas (2009) who found airborne EM towed at an altitude of 15m (1) provides a reasonable estimate of the average thickness of deformed multi-year ice when the ice is less than about 10 m thick (2) provides no information about ice thicknesses in excess of 12m.

For a vast multi-year ice floe near the ice edge, ice thicknesses were higher in areas with few melt ponds and high reflectance in MODIS imagery, and were lower with a minimum thickness of about 3m in areas of heavily-decayed ice with many melt-ponds. The uniform minimum thickness suggests that a freshwater layer was present in the melt-ponds and below the thinner ice. Ice thickness measurements collected farther inside the ice edge were highly variable.

5.0 ACKNOWLEDGMENTS

We thank Michelle Johnston and Jim Hamilton for reviewing the manuscript. This work was supported by the Canadian Program of Energy Research Development (PERD), the Environmental Science and Research Fund (ESRF) and the Canadian Space Agency GRIP programs. In addition, the logistical costs of the helicopter sea ice survey of 2011 were supported by David Barber (Chief Scientist) of the University of Manitoba (UM) through a sea ice survey contract between the Centre of Earth Observation Science (CEOS) of the UM and Imperial Oil Ltd. The two sea ice surveys were successful in part due to the excellent field support by Canadian Helicopters personnel stationed at Inuvik and Canadian Coast Guard personnel stationed on the CCGS Amundsen. In particular the CHC pilots Corey Arsenault and Jory Bott and the CCG pilot Robert Pelletier and Engineer Eddy Perron are thanked for their continued assistance with the field work. We also thank Michelle Johnston (NRC) for providing the drill-hole ice thickness data for 2011. We acknowledge the use of MODIS data

products from the Land Atmosphere Near-real time Capability for EOS (LANCE) system operated by the NASA/GSFC/Earth Science Data and Information System (ESDIS) with funding provided by NASA/HQ.

6.0 REFERENCES

Johnston, M., 2011. Field measurements on multi-year ice in the Beaufort Sea, August 2011, Technical Report, CHC-TR-083, National Research Council Canada.

Johnston, M. and C. Haas (2011) Validating Helicopter-based EM (HEM) Thicknesses over Very Thick Multi-year Ice. Proceedings 21st International Conference on Port and Ocean Engineering under Arctic Conditions, POAC'11, 10 to 14 July 2011, Montreal, Canada, paper POAC11-32, 11 p.

Lalumiere, L., 2011. GPR Capabilities for Ice Thickness Sampling of Low Salinity Ice and for Detecting Oil-In-Ice. Can. Contract. Rep. Hydrogr. Ocean Sci. 56: iv+ 36pp.

Prinsenberg, S.J., I.K. Peterson, J.S. Holladay and L. Lalumiere, 2010. Helicopter-borne sensors monitoring the pack ice properties of Mackenzie Delta April 2010 Sea Ice Survey. Can Tech. Rep. Hydrogr. Ocean Sci. 267: viii+62pp.

Prinsenberg, Simon, Ingrid Peterson and Scott Holladay, 2011. IOL helicopter survey report 2011, Survey period Aug. 11-25, Internal report.

Appendix 1: Comparison of CTD and EM Data, April 2010

By: Scott Holladay, Geosensors Inc.

The Observed Data:

Two subsets of the FEM00009 IcePic dataset, acquired on April 1, 2010, were analyzed. Survey conditions were typically very good for the IcePic flights in the 2010 survey, and for this dataset in particular. The data in the file were also divided into segments to permit more detailed but rapid analysis of individual portions of the dataset. These segments, labelled S02, S04, ... S10 and corresponding to Segments 1, 2, ... 5 of the flight file, were separated by high-altitude backgrounds, and were acquired in such a way that the final portion of one segment was overlapped with the starting portion of the next.

Table 1: Mackenzie Delta 2010 on-ice station data (April 8, 2010) (from Prinsenberg et al., 2010, amended by JSH to include decimal degrees and UTM Zone 08 W coordinates and minimum distance in metres to FEM10009 survey track).

	Stn. 43	Stn. 44	Stn. 45	Stn. 46	Stn. 47	Stn. 48
Latitude (° N)	69 32.58 69.5430	69 34.20 69.5700	69 36.60 69.6100	69 41.76 69.6960	69 48.00 69.8000	69 34.41 69.5735
Longitude (° W)	135 53.04 -135.8840	136 1.20 -136.0200	136 12.00 - 136.2000	136 26.04 - 136.4340	136 13.80 -136.2300	136 01.57 -136.0262
UTM Easting	465520	460266	453342	444470	452602	460031
UTM Northing	7715160	7718253	7722840	7732624	7744047	7718648
Time (MDT)	15:35	16:10	15:20	14:50	14:04	15:56
Snow thickness (m)	.29,.27, .30,.35	.08,.02, .01,.11	.15,.12,.12, .10,.08,.08	.05	.10,.08, .09	0.00
Ice thickness (m)	1.28	1.69	1.3,1.3	.90,.91	1.11	
Freeboard (m)	-0.005	0.17	0.08	--	0.11	
Water depth (m)	4.1	5.8	8.6	14.2	15.5	
Salinity (snow bottom)	14,14	12,12	15,15	18,18	16,16	
Salinity (0-5cm)	5,5	5,5	9,9	6,6	15,15	2,2
Salinity (50cm)	0,0	2,2	2,2	3,2,3	6,6	
Salinity (100cm)	2,2	0,0	2,2	2,2	14,14	
Salinity (subice water)	0	---	0	3	30	
CTD cast	53	54	51	49	48	
Min dist. to FEM10009	13	155	69	25	31	

Table 2: CTD ground truth data used for plot annotation.

St	utmx	utmy	ST	IC	IT	WC1	WT1	WC2	WT2
43	465520	7715160	.302	.001	1.28	.001	2.82	0	0
44	460266	7718253	.055	.001	1.69	.018	4.11	0	0
45	453342	7722840	.108	.001	1.30	.079	5.2	.26	.4
46	444470	7732624	.05	.001	.905	.39	6.69	1.9	6.1
47	452602	7744047	.08	.02	1.11	2.45	7.0	2.52	8.5

In this table, utmx and utmy are Zone 8 UTM coordinates computed from observed positions, ST is snow thickness, IC is ice conductivity (estimated from observed salinity in chips), IT is ice thickness in m, WCn and WTn are sub-ice water layer "n" conductivities and thicknesses in S/m.

Overview of Inversion Results:

The laser altitude and EM data were inverted using multiple models in order to work out the best parameterisation scheme for the complicated conductivity layering observed in this area, as seen in the CTD profiles and resulting ground truth models shown above. The first subset was the four quadrature data channels usually used for real-time inversion and for in-field post-processing, due to their high degree of baseline stability. The second set comprised all four inphase and quadrature data channels. The data were carefully baselined, using baseline picks where the aircraft was flying straight and level at high altitude, to minimize EM drift effects before starting the inversion process. The model parameters in the two 2-layer models were chosen for their ability to approximately fit data for Segments 1 and 2; neither are matches for the normal offshore model used for real-time inversion by the system. Model 17 was developed to approximate conditions along the full length of the FEM10009 dataset.

IcePic Real-Time Starting Parameter Values

Layer #	Conductivity	Free	Thickness	Free
1	0.01 S/m	Y	1.0m	Y
2	2.5 S/m	N		

Model 2L_2Free Starting Parameter Values

Layer #	Conductivity	Free	Thickness	Free
1	0.0001 S/m	Y	1.0m	Y
2	0.30 S/m	N		

Model 2Allfree Starting Parameter Values

Layer #	Conductivity	Free	Thickness	Free
1	0.0001 S/m	Y	1.0m	Y
2	0.01 S/m	Y		

Model 17 Starting Parameter Values

Layer #	Conductivity	Free	Thickness	Free
1	0.01 S/m	N	4.5m	Y
2	0.20 S/m	Y	2.0m	Y
3	0.60 S/m	Y	1.0m	Y
4	0.20 S/m	N		

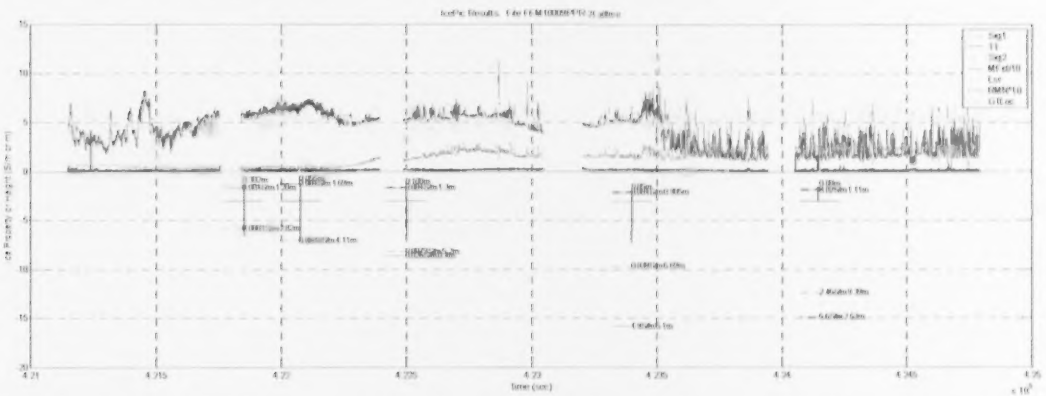

Real-time inverted 2-layer model (two free parameters Sig1 and T1, Sig2 fixed at 2.5 S/m), 4 QD data. The estimated ice thickness includes the freshwater layer in the inshore portion of the profile, but matches the observed ice thickness in the last segment, where seawater is present immediately below the ice.

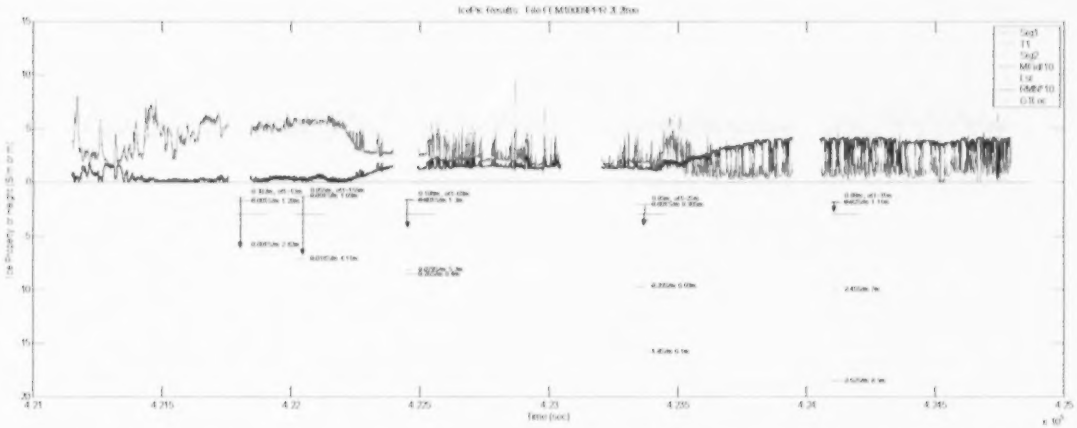

Inverted with 2 layers, two free parameters Sig1 and T1 (Sig2 fixed at 0.3 S/m), 4 QD data. Model fitting error is shown by the black trace, and increases as more saline water is present below the ice

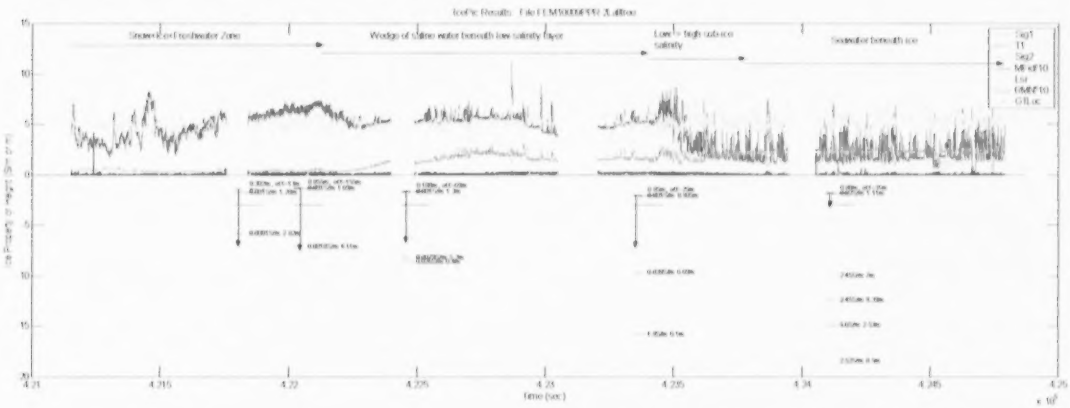

Inverted with 2 layers, three free parameters, 4 QD data. The "apparent" lower layer conductivity is shown by the dashed red trace. Note that the fitting error peaks in the transition between the freshwater and saltwater zones, and is low for the entire profile. CTD results are shown with text and horizontal lines.

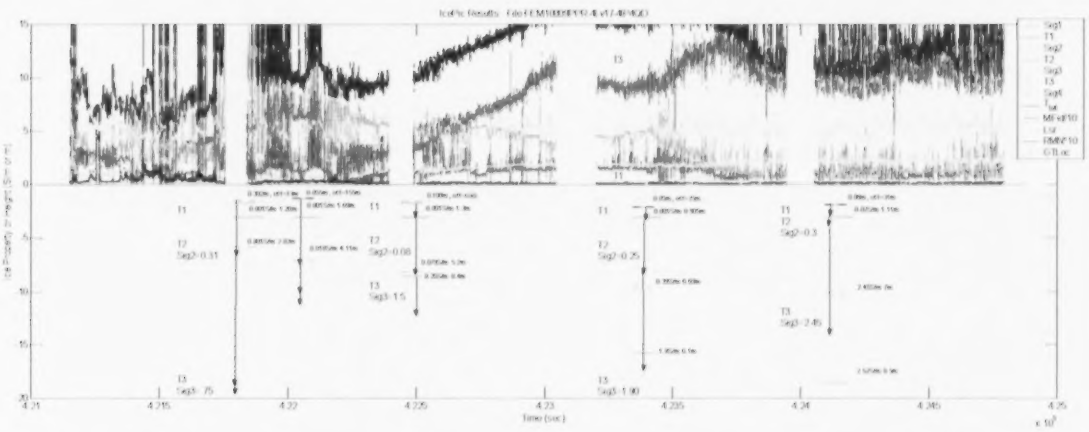

Inverted with Model 17, 4 layers, five free parameters, using all eight IP and QD data.

CTD sites 43 and 44 at the inshore (left) end of the line match the ice plus freshwater thickness quite well, particularly at site 43, for all models. The two-layer models do not offer any insight into saline sub-ice water thickness, but the second one does show where the sub-ice water trends into seawater.

The 2 layer models are useful in that they are rapid and robust to calculate, can be inverted using only the low-drift quadrature data, and yield stable results that are meaningful as long as their limitations are understood. The degree to which the parameters of such simple models can fit the observed data in these models, especially the second, is surprisingly high. The low fitting error in the three-free-parameter example above shows how well this can be done, at least for the quadrature data components. The misfit (black trace) in the two-layer, two-free-parameter model, which is similar to the real-time inversion model but includes a fixed lower layer conductivity of 0.3 S/m, is fairly high for most of the profile.

In the shallow, freshwater zone, the upper layer thickness corresponds to the snow+ice+freshwater thickness, and the lower layer conductivity represents a weighted average of conductivities of the sediment layers. In the offshore zone, the lower layer's conductivity approaches that of seawater, and the upper layer thickness corresponds to the observed ice+snow thickness, plus a thin layer of low-salinity sub-ice water where present. In the intermediate zone, the presence of a substantial thickness of low-salinity water below the ice which is itself underlain by saline water is shown by the combination of a large upper layer thickness T1 (blue trace) that considerably exceeds the observed ice thickness, and a fairly high conductivity Sig2 (red dashed) for the second layer.

The four-layer Model 17 inversion, performed using all observed data as inputs, yielded the best fits for most of the profile, though Segment 1 was actually somewhat better fit by the second model. Model 17 separated the effects of the shallow (low-salinity) and deep (higher-salinity) sub-ice water quite well. The key

downside of the much more complicated 4 layer model is that there are zones where the free parameters display parameter equivalence, resulting in oscillation in the inverted model where small data errors or model inadequacies cause parameters to flip back and forth, sometimes with compensating swings in other parameters. This is a typical outcome in inversion theory: seeking more resolution, particularly in more parameters, without introducing sufficient constraints on those parameters, increases uncertainty in most or all of the parameters being fitted. A more complicated multi-pass inversion process employing constraints (e.g. parameter smoothness) could be used to limit or eliminate many of these effects, but this was not practical within the present project.

Segment by Segment Results

Segment 1:

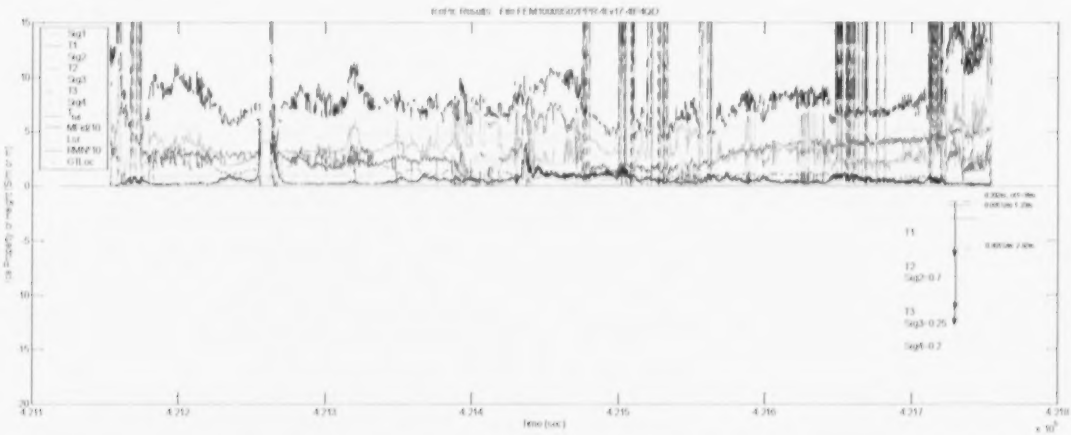

Segment 1 four-layer model. In this freshwater dominated regime, T1 corresponds to snow+ice+freshwater.

Model 17, which is summarized above, appears to have a sufficient degree of flexibility to accommodate the different ice/freshwater/seawater/bottom sediment conditions encountered in FEM10009. In this model, the upper layer has a relatively low fixed conductivity and a variable thickness with a large starting value. The middle two layers are relatively conductive at 0.2 and 0.6 S/m, with small starting thicknesses of 2 and 1m—all four of these parameters are free. The final layer's conductivity is fairly low at 0.2 S/m and fixed. It is possible that this model will not work well in areas where ice-bonded, deeply frozen sediments are present.

The main set of profiles shown above were generated using a "reset" mode of the inversion program, where the starting values of the model were used for every data point. This approach tends to bias the resulting inversion results towards the starting models, but increases processing time and can sometimes

increase inverted model instability. The second profile shown above for Segment 2 used the "no-reset" mode. There is usually little difference between the results from the two modes where all parameters being fit are well-resolved, but when parameter equivalence is a factor, the no-reset mode tends to stay locked into one state (which may be randomly determined by noise) of the pair of equivalent parameters. This is visible in the Segment 2 no-reset example near the middle of the profile: the green Sig3 trace locks into a rather large value in the no-reset example, whereas the reset example obtains a lower, oscillatory, more physically reasonable range of values to represent the saline sub-ice water layer.

Segment 1:

In Segment 1, where freshwater ice overlies freshwater and bathymetry values are small, the first conductive layer is expected to correspond to unfrozen sediments. This segment includes a narrow zone at its inshore end of what have been interpreted as ice-bonded frozen sediments where a gravel bar is present at fiducial 421469 sec. In the image extract below, the layer 1 thickness (T1) estimates from an earlier two-layer inversion are shown in red, along with the yellow outline of Garry Island. The gravel bar is picked out in yellow at left-centre of the extract, just above a dark patch in the processed polarimetric SAR underlay that indicates ice-bonded frozen sediments; a substantial "hump" is present in the T1 values at this point.

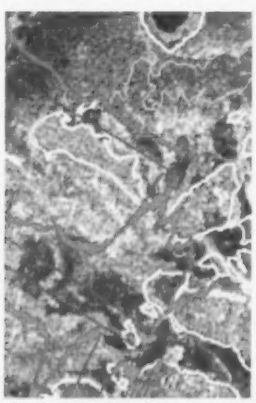

Extract from 2-layer model T1 plot overlaying processed polarimetric SAR data.

In the Model 17 Segment 1 profile above, the gravel bar location corresponds to the thickening to about 7.5m in the blue T1 trace. The character of the T1 trace becomes smoother and gradually increasing after this point in the profile. Two other sharp dips in the EM response Much thinner T1 values with thick T2 and Sig2 values of 3-5 S/m inshore of the gravel bar may indicate the presence of zones of saline water trapped behind the bar(s). This can be understood better by looking at a plot that includes fitted EM responses.

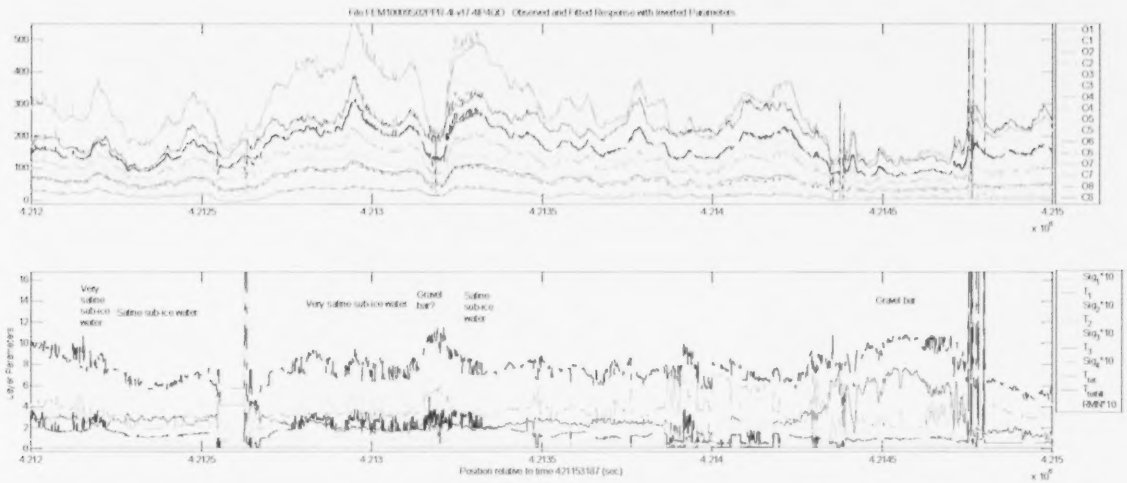

Fitted data plotted with inverted parameters for central portion of Segment 1, showing zones of low and high EM response corresponding to gravel bar(s) and apparent areas of highly saline sub-ice water. Note that in this figure, Sig3 and Sig4 are not *10 as indicated in the legend—their values are shown in S/m.

There is a substantial difference in the inverted parameters for the main gravel bar near 4.2145E8 millisec, compared to the narrower feature near 4.2132E8: T1 peaks and is 3 times larger than T2 in the former, while T2 peaks in the latter at almost 3 times the amplitude of T1. Values of Sig2 and Sig3 are roughly constant in the former, but dip relative to neighbouring values in the latter. Thus, the main gravel bar seems to exhibit a lower-conductivity signature, particularly in its shallower area, than the narrower feature. This is consistent with the presence of substantial frozen sediment below the main gravel bar and much less sediment freezing at the narrower feature due to its more limited exposure at the surface.

Segment 1 would benefit from further analysis and an examination of the results from the second pass over this line on April 9, but the results to date are reasonably consistent with the interpretation of data from the 2004 survey along this line obtained during CASES.

Segment 2:

This segment covers part of the transition from fresh water conditions to more saline conditions.

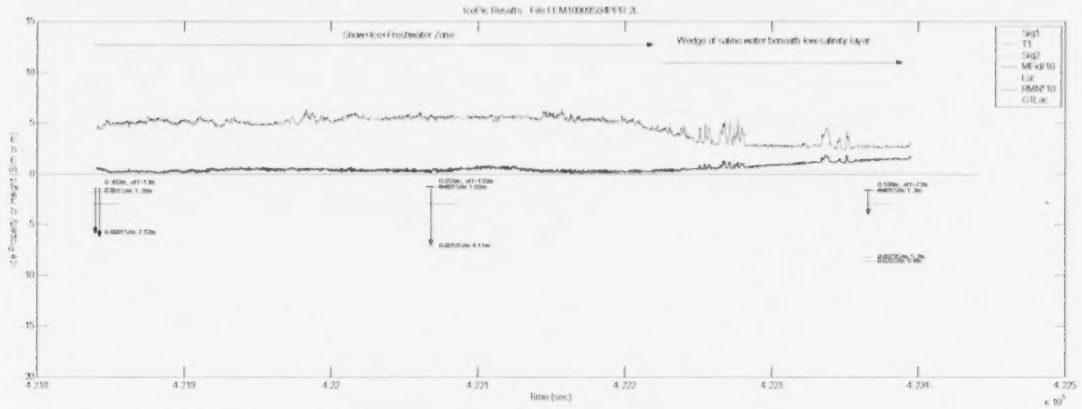

Second segment of FEM10009, inverted with 2 layers 2 free parameters

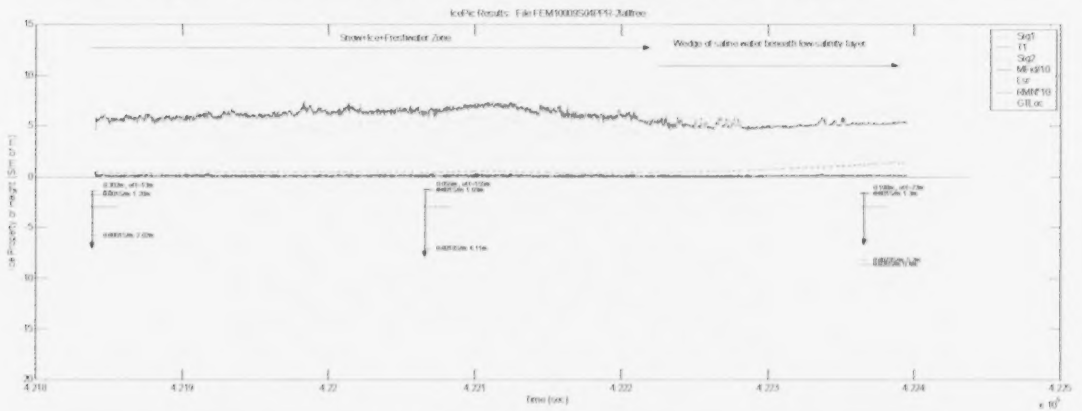

Second segment of FEM10009, inverted with 2 layers 3 free parameters. Allowing Sig2 to vary sharply improves the misfit in the second half of the model. The observed variation is a substantial increase at the middle and in the last third of the segment. The results are consistent with results for the entire flight.

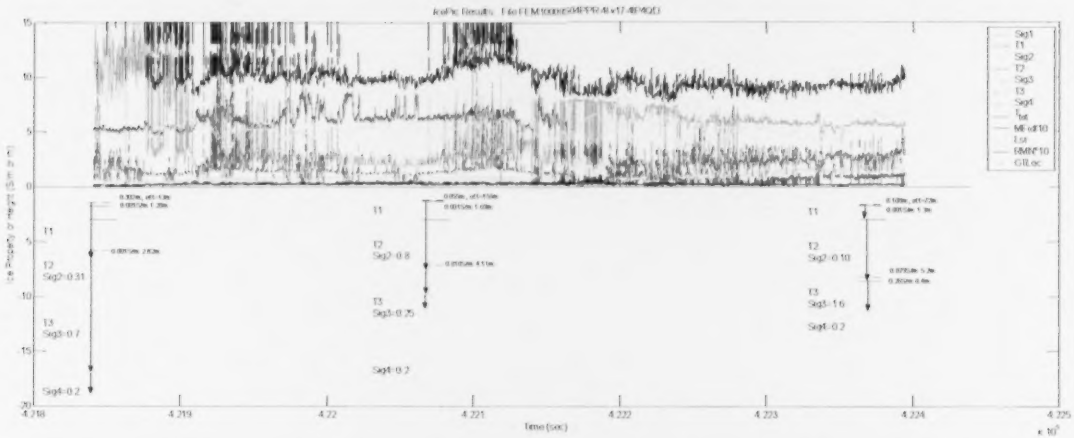

Segment 2 4 layer Model 17. At inshore end, T1 = snow+ice+freshwater, while offshore, T1 = snow+ice and T2 =brackish sub-ice water. Sig3 and T3 exceed CTD-measured saline water conductivity and thickness— this is not surprising at ~9m total depth.

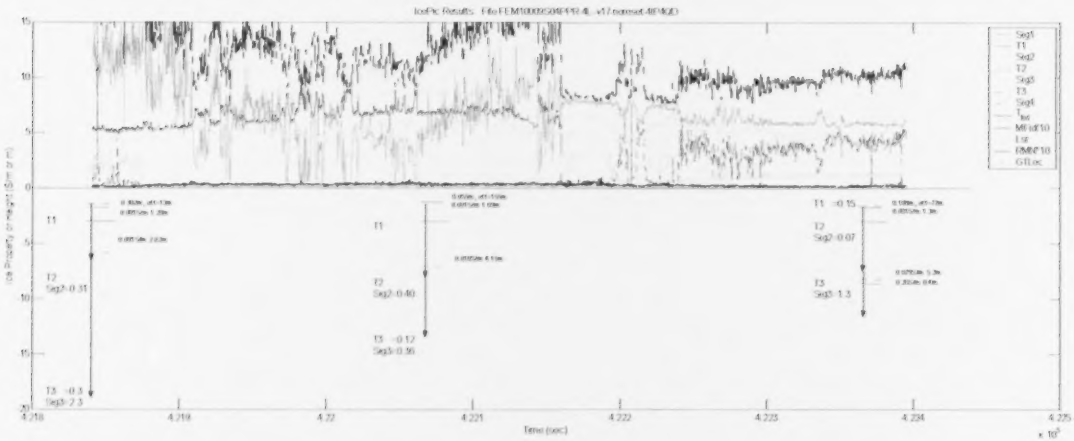

Segment 2 inverted with "reset" option turned off. Thicknesses and conductivities are often comparable and oscillation is reduced, but where parameters equivalence is present, parameters may become locked into one of the equivalent states, causing a bias that is different from that seen in the "reset" inverted model. This effect is visible in T2 for the middle third of the profile, and for the first half or more in T3—these differences also affected the total thickness profile in black.

The following plots show data fit quality along this segment for Models 2L, 2Lallfree and 17.

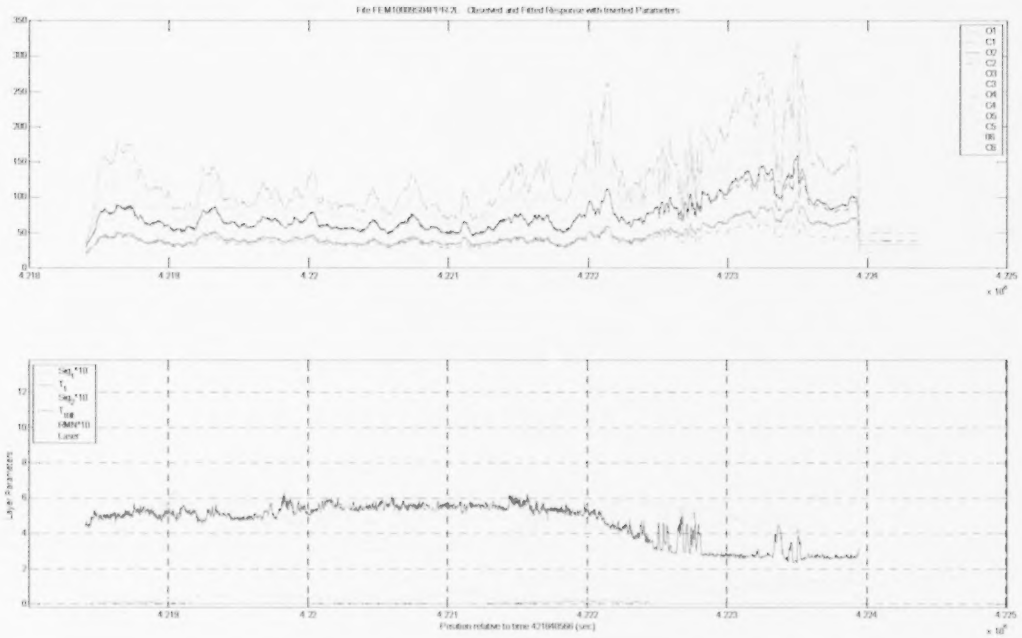

Observed and calculated responses for 2L 2-parameter free model obtained from quadrature responses, ie QD1,QD2,QD3,QD4. Misfits are visible as sections where the dotted line of a given colour does not coincide with the solid line of that colour. For example, misfits in the three lower frequencies (red, blue, green) are visible at the right end of this segment, while the highest frequency is fit fairly well.

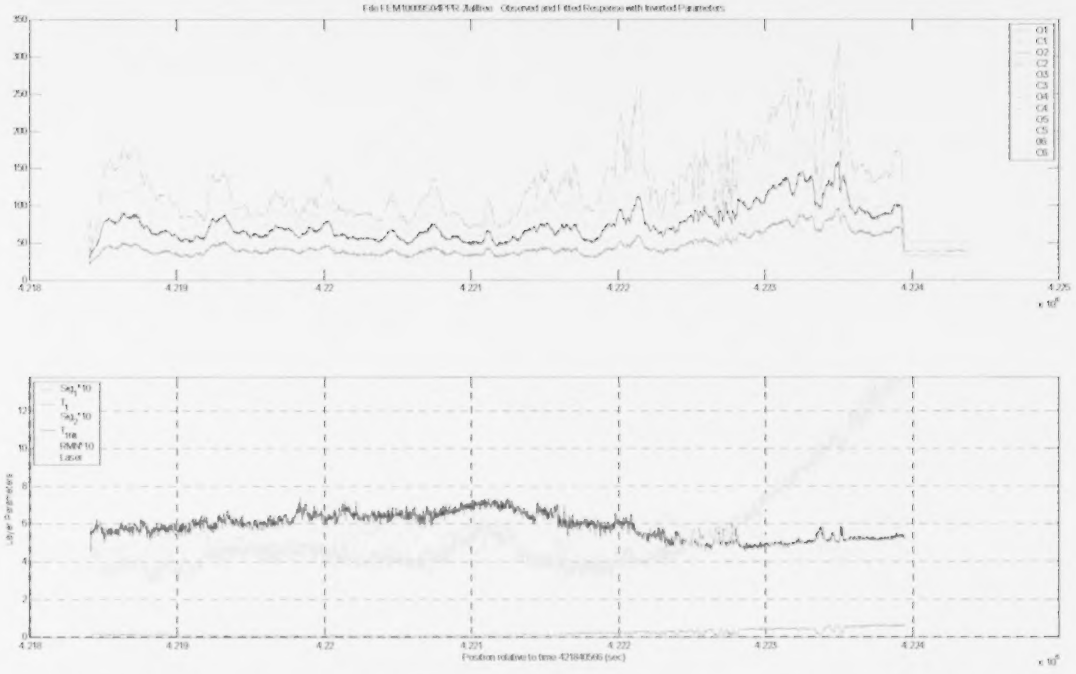

Observed and calculated responses for 2L all-parameters-free model obtained from quadrature responses. For the middle and in the last third of the segment, the lowest three frequencies' fits were improved.

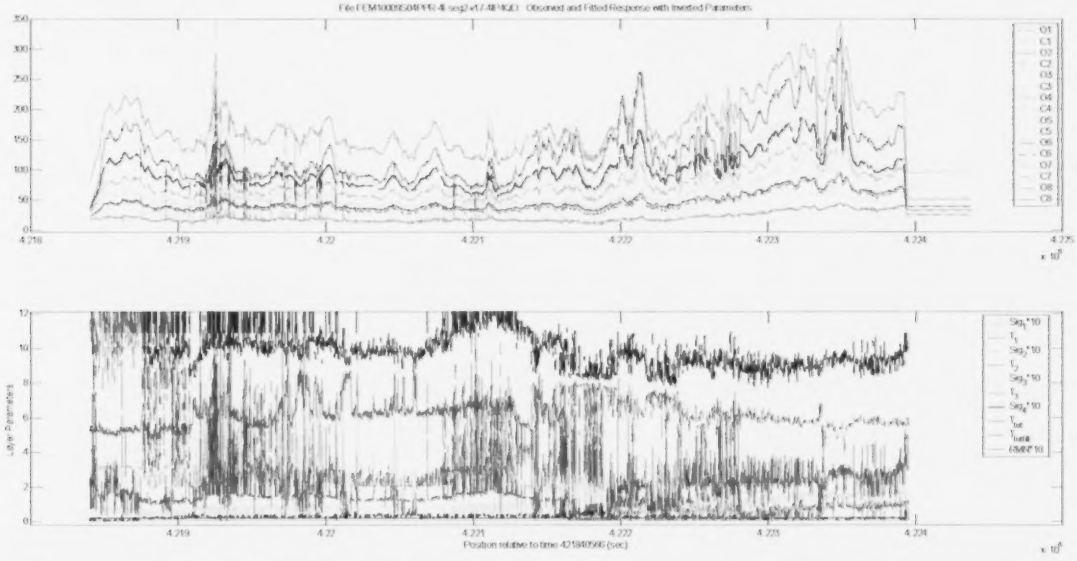

Segment 2, Model 17 data fits and model parameters. More input data were used, and most were fit well. The parameter colours were changed in some cases to make it easier to read the complicated lower panel.

Segment 3:

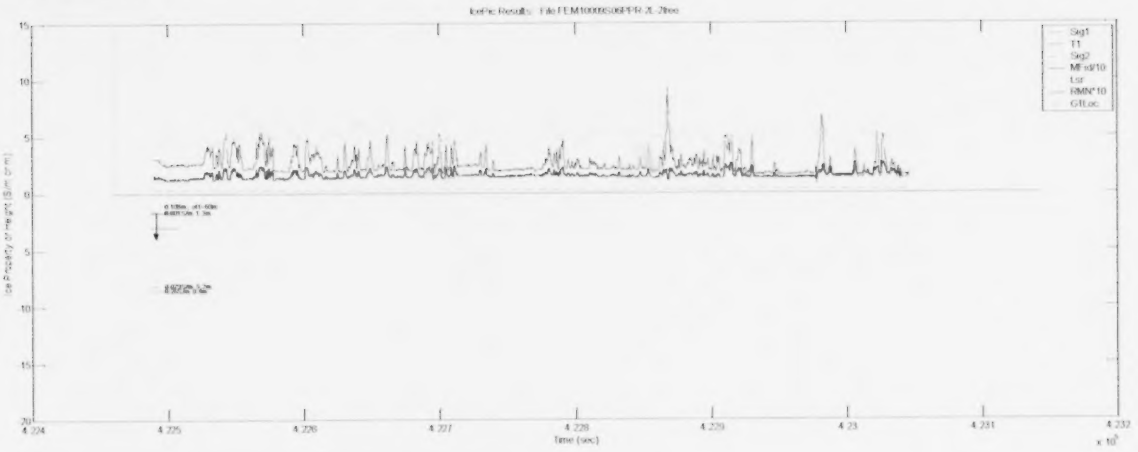

Segment 3, 2 layers, two free parameters

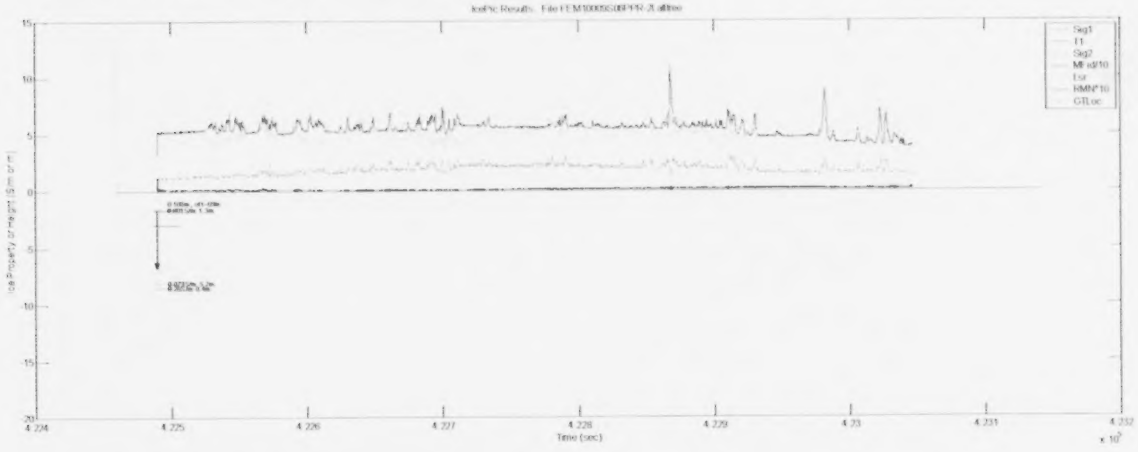

Segment 3, 2 layers, all parameters free

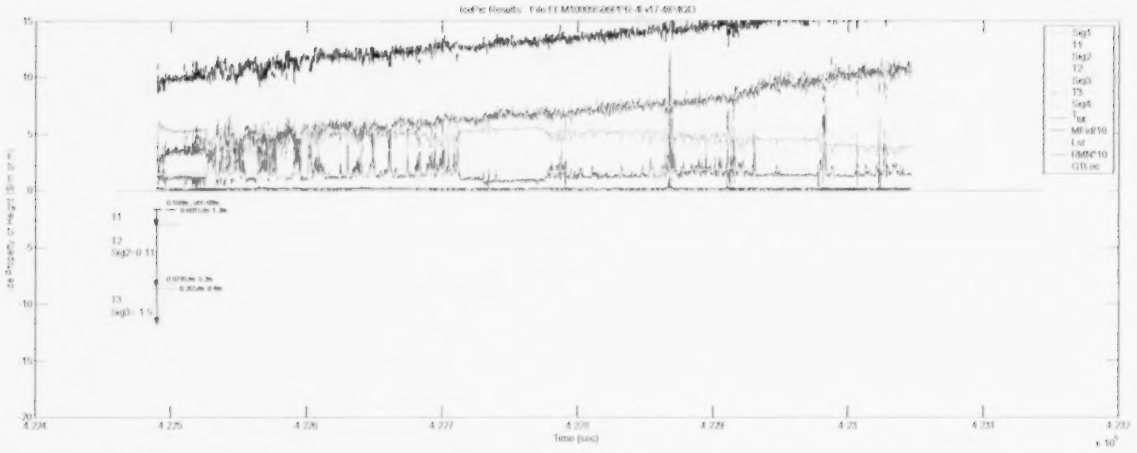

Segment 3, Model 17. The T1, T2 and T3 estimates are shown as solid blue, magenta and dotted blue traces. T1 and T2 match the ice thickness and top CTD Site 45 layer well, and Sig2 is a reasonable match for the sub-ice water conductivity.

Segment 4:

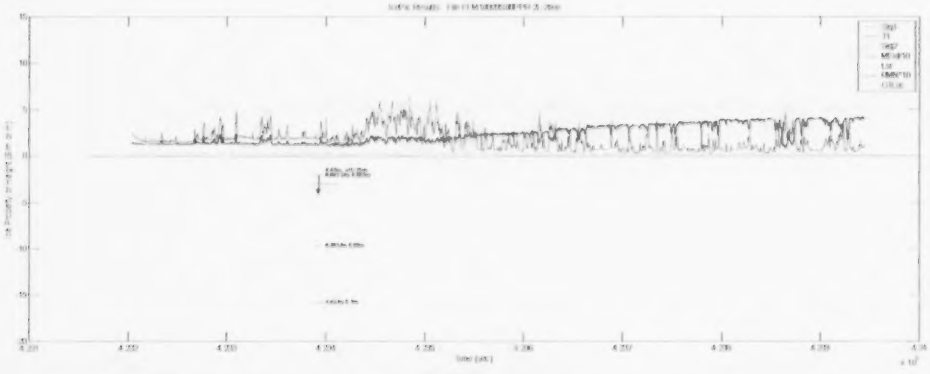

Segment 4, 2 layers, 2 free. T1 is not a very good match to the ice thickness.

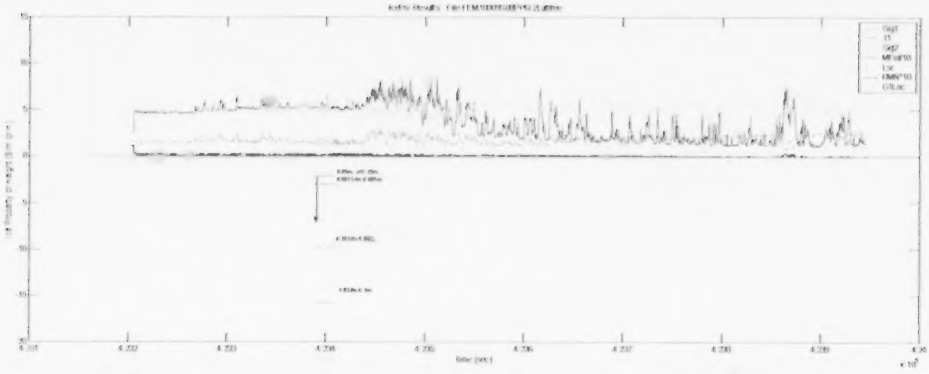

Segment 4, 2 layers, all parameters free: here the large T1 and elevated Sig1 values suggests a thick brackish sub-ice water layer.

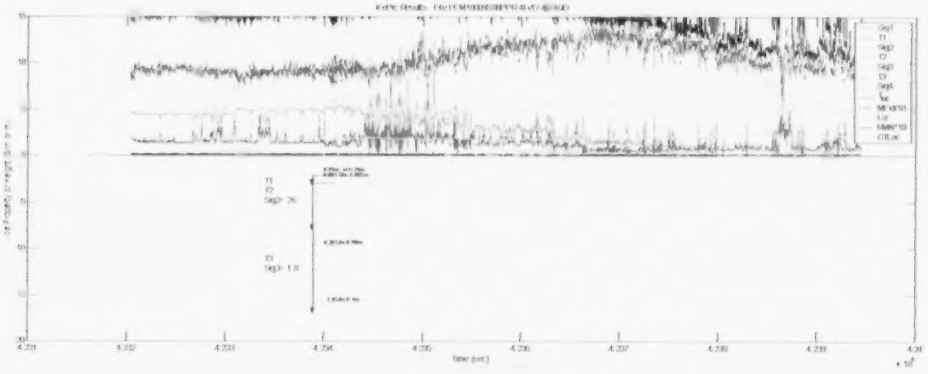

Segment 4, Model 17. The sub-ice brackish water layer (and ice thickness) thins rapidly in the middle of this segment, deeper water trends toward normal seawater salinity.

Segment 5:

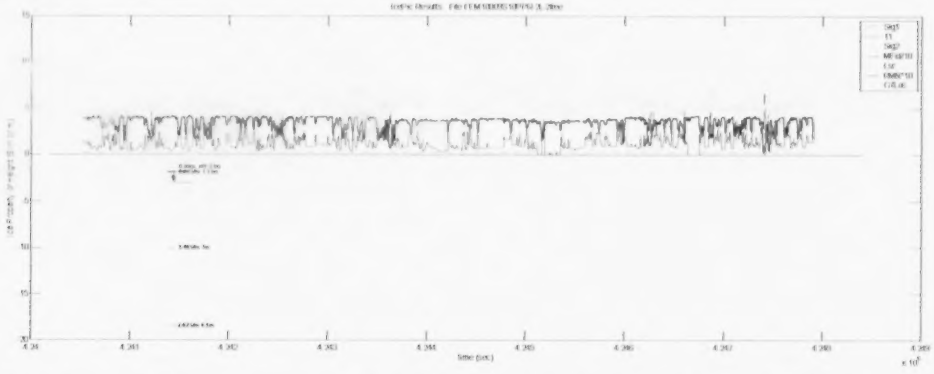

Segment 5, 2 layers, 2 free: the ice thickness is underestimated, and fitting error (black) is high.

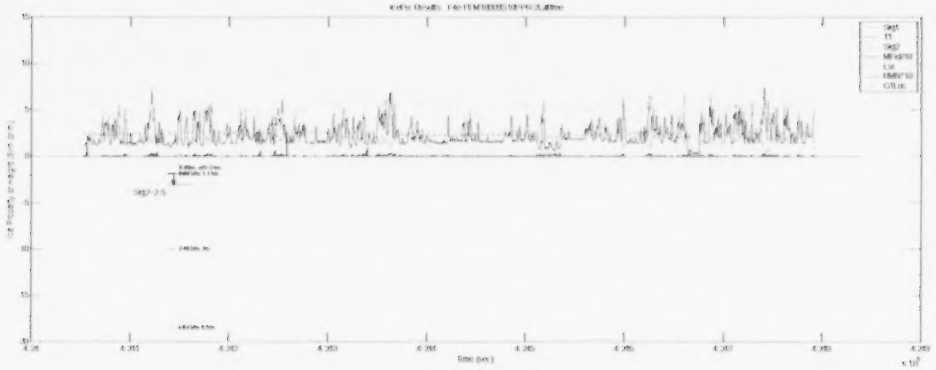

Segment 5, 2 layers, all free: ice thickness is estimated fairly accurately, and Sig2 is matches the CTD sub-ice water conductivity accurately as well. Fitting errors are low.

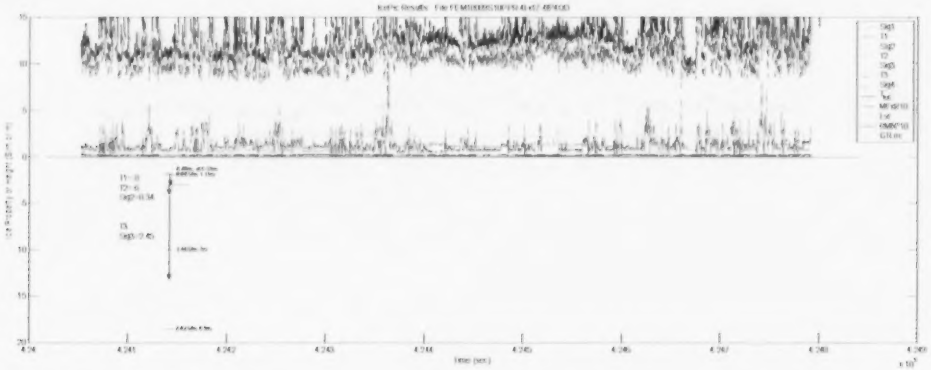

Segment 5 (offshore). Normal seawater close to surface, thin residual sub-ice brackish layer estimated by inversion (not seen by CTD—is it simply not well resolved, sampling artefact, or tidal effect?) The seawater layer thickness is over-estimated. Fitting errors are low to very low.

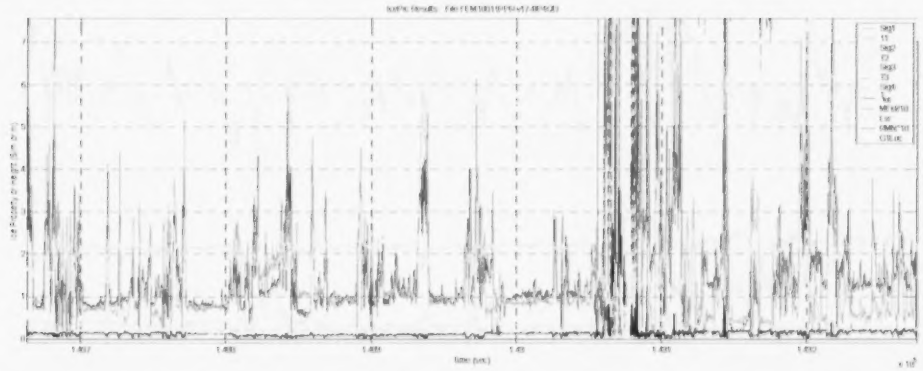

FEM0011 Segment 4 (offshore) estimated Model 17 parameters. This profile intersects the Tarsiut shoal at time ~1.491E5 ms, and passes at approximately right angles through the eastern portion of FEM0009 Segment 5, which passes south of the shoal.

On the shoreward side of the shoal, which acts to anchor the landfast ice in the area, seawater (green) conductivities slowly rise from below 2 S/m to almost 2.3, and the sub-ice brackish layer conductivity's background level remains approximately constant at ~0.3 S/m (cyan), with a typical thickness (magenta) of almost 1m. On the offshore side of the shoal, where at least some of the ice appeared to be younger and more mobile, seawater conductivity was higher (between 2.4 and 2.5 S/m), and sub-ice brackish water was mostly thinner (0.5 to 0.6m) and less conductive at ~0.25 S/m under ice that was mostly more than 1.2m thick. Under thin (<.2m) refrozen leads, the brackish layer was much more conductive (1.2-1.5 S/m) and thinner (0.4m), and fitting errors were slightly higher than on the inshore portion of this segment. The variations in brackish layer properties do not appear to be simple equivalence tradeoffs, as the conductivity-thickness product for the layer also varies strongly between the inshore side of the shoal, the offshore side, and under thin refrozen leads.

Discussion:

While a good fit is not a guarantee of model parameter validity due to uniqueness issues and the impact of noise and systematic error in the input dataset, it is a necessary condition that a model be able to generate a good fit in order to represent the subsurface conductivity conditions. The fact that the model parameters that can be checked against CTD results are in at least reasonable agreement with those ground truth values suggests that the remaining model parameters are probably at least reflective of some aspect of the geological situation in the bottom sediments. These deeper parameters should be of most use in the shallow, freshwater-dominated part of the survey area, since there is less electromagnetic "shielding" of the sediments by conductive seawater and the sediments are closer to the surface.

The relatively poor fits for all models where frozen sediments are apparently present in Segment 1 suggests that these models may need adjustment for such areas. However, remember that the goodness of fit parameter RMN represents the root mean square sum of fitting errors normalized by the corresponding data amplitude at that location. Thus, obtaining equal absolute (in ppm) fitting errors in areas of high and low data amplitude would correspond to higher RMN errors in the area of low data amplitude, because the absolute fitting error is normalized by a smaller number. This normalization method allows inversion of responses of different amplitudes at a given sample point without the optimization process being dominated by the highest-amplitude response.

Fitting five parameters using 8 input data is risky in the sense that conductivity-thickness equivalence can be expected to be significant for the middle layers, but it was necessary to maintain a high degree of parameter freedom in order for this one model to handle the wide range of conditions seen in this survey line. The

effects of equivalence can be seen at various points along the line segments, where oscillation involving parameters that trade off against each other can be seen. While these oscillations make the model plots look "messy", the inverted models are still useful in these zones in the sense that we are usually more interested in combinations of the parameters than in the parameters themselves. For example, while conductivity and thickness can often not be resolved independently, the conductivity-thickness product is usually well-resolved by EM measurements. Similarly, where two thicknesses trade off against each other yielding oscillation in those values, the sum of the two thicknesses is often stable.

For all of the CTD measurement sites where the inversion results can be checked, a combination of model parameters does a reasonably good job of approximating the CTD results. For example, in Segment 2, T1 corresponds to the sum of ice and freshwater thickness above the sediments or deeper, conductive water for CTD sites 43 to 44.

At CTD site 45, which appears in Segments 2 and 3, the different models produce rather different results at CTD site 45, with the 2-layer models both obtaining a thickness intermediate between the ice thickness and the ice+freshwater thickness, while the 4-layer model does an excellent job of matching both ice and sub-ice freshwater thickness as well as approximating its conductivity.

At CTD site 46, a similar situation is seen, with the 2 layer, 2 free parameter T1 value somewhat exceeding the ice thickness, the 2 layer 3 free parameter T1 value somewhat underestimating the combined ice plus freshwater thickness, and Model 17 estimating the ice thickness accurately, somewhat underestimating the subice freshwater thickness, and slightly overestimating the deeper, more saline water thickness. The conductivities of the two water layers were fairly well estimated at 0.26 vs 0.39 S/m from the CTD, and 1.8 vs 1.9 S/m from the CTD.

For CTD site 47, the simple models (especially the 3-free parameter model) estimated ice thickness fairly well. As expected, the model with fixed Sig2 underestimated the ice thickness (by .43m); freeing Sig2 resulted in a slight overestimation (by .14m) of snow+ice thickness. The four-layer model also underestimated the ice thickness (by .32m), but inserted a 0.64m layer of relatively low-conductivity (.3 S/m) water. The estimated underlying seawater conductivity (2.45 S/m) matched the value obtained by the CTD. The thin brackish water layer in the four-layer model was consistently present along the Segment 5 profile, and along the offshore end of Segment 4. While it was not detected in the CTD sounding at site 47, a similar conductivity was obtained by both EM and CTD for the sub-ice water in Segment 4. It seems possible that the sub-ice layer was disturbed during the auger hole clearance process (which involves "pumping" sub-ice water up through the hole to remove ice chips), or that tidal currents might have thinned or shifted this layer during the acquisition of CTD profiles, which occurred at a different date and time from this survey flight.

In an effort to resolve this question, FEM00011, which runs through the same area on a more N-S bearing, was re-inverted with Model 17, again using all EM channels. The results are shown above, along with a brief discussion. It does appear that the brackish layer is a persistent feature, with characteristics that change from inshore to offshore of the Tarsiut shoal: it becomes thinner and less conductive offshore, and below refrozen leads it becomes still thinner but more conductive.

Conclusions:

Two-layer models comprising an upper, resistive layer and a relatively conductive lower layer are useful for quick-look analysis of IcePic data from this survey area in the Mackenzie Delta, but require careful interpretation, as the layer properties correspond to different portions of the ice/water/sediment stack in the inshore, freshwater-dominated area and the offshore, seawater-dominated area. In particular, in the inshore, the upper, resistive layer corresponds to snow+ice+freshwater, while the lower layer corresponds to conductive sediments.

A more complicated 4 layer model was developed in order to improve definition of the ice, water and bottom properties. Some interpretation is still required, but in the offshore area, where substantial thicknesses of saline water are present at shallow depths, it is possible to distinguish the ice itself, a brackish sub-ice layer, saline water and bottom. The transitional zone between these two areas displays a thick, low-salinity layer that thins toward the offshore as the depth to saline water decreases.

Further work will be required to determine whether the thin sub-ice brackish layer in this model that appears to persist beyond the Tarsiut shoal is also present offshore. This layer was not visible in the single CTD measurement closes to Tarsiut, so it is possible that its persistence offshore is an artefact of the model and inversion process.

Appendix 2: Comparison of GPR and EM Data, April 2010

By: Scott Holladay, Geosensors Inc.

Introduction

This section describes the identification of areas of bottom-fast ice, floating ice, and ice resting on the bottom in nearshore Mackenzie Delta region, using EM (electromagnetic) and GPR (ground-penetrating radar) data collected in 2010.

(a) April 1 Observed and Processed Data

The GPR acquisition was carried out along EM profile lines. Most of the profiles of interest for this bottom-fast ice study were acquired on April 1 and 5, 2010, corresponding to EM files FEM10003, FEM10006, FEM10009 and FEM10018. Plots of the lines overlaid on processed polarimetric SAR images place these data in context.

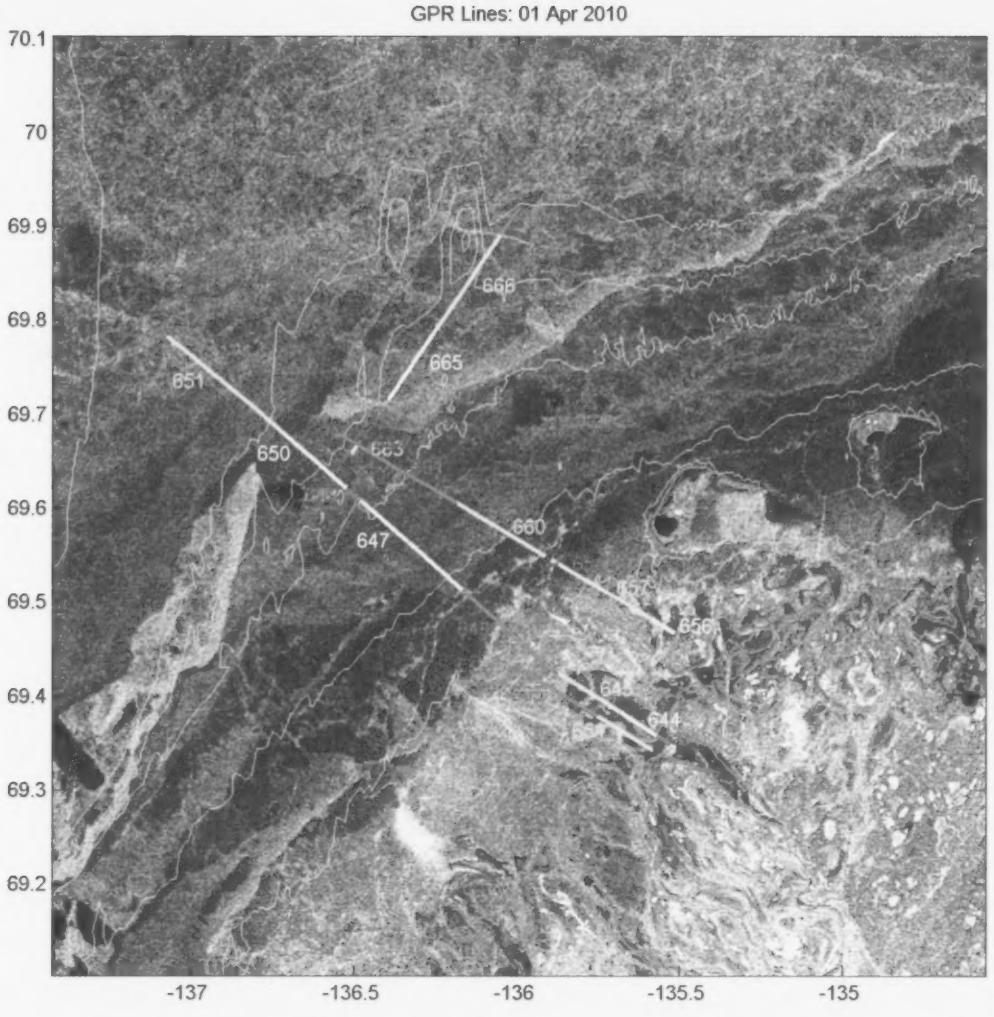

April 1 GPR. The first GPR line of the survey, corresponding to IcePic file FEM10003, started with F643-651 (inshore-offshore) through the main ice-bonded sediment study area south of Garry Island. The second line F654-655, corresponding to FEM10006, ran parallel to the first, and slightly to the SW. The third line F656-667, corresponding to FEM10009, passed close to Garry Island to its north, offshore to the 10m bathymetric contour, then roughly parallel to the 10m contour past the Tarsuit shoal.

1 EM Data, 2-layer EM Inversion Results and GPR Profiles for April 1

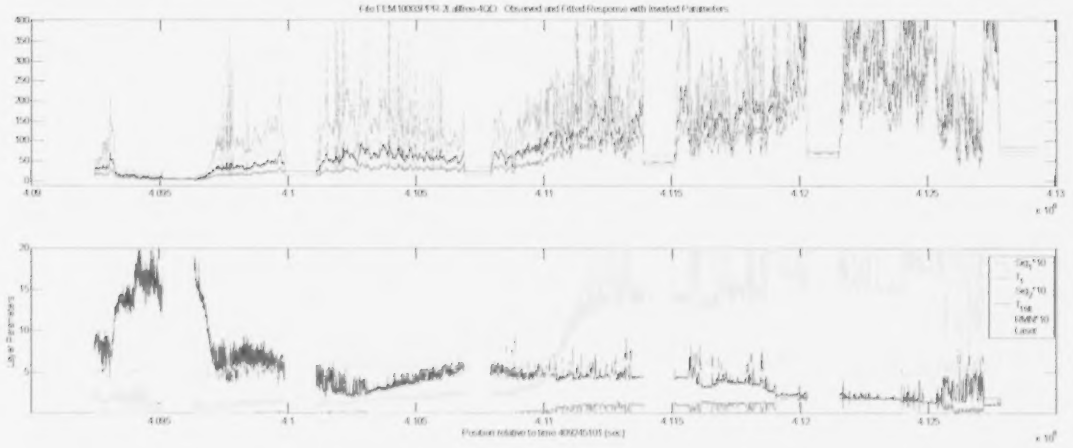

FEM10003, GPR F643 to F651. F649 and higher indicate normal sea ice only

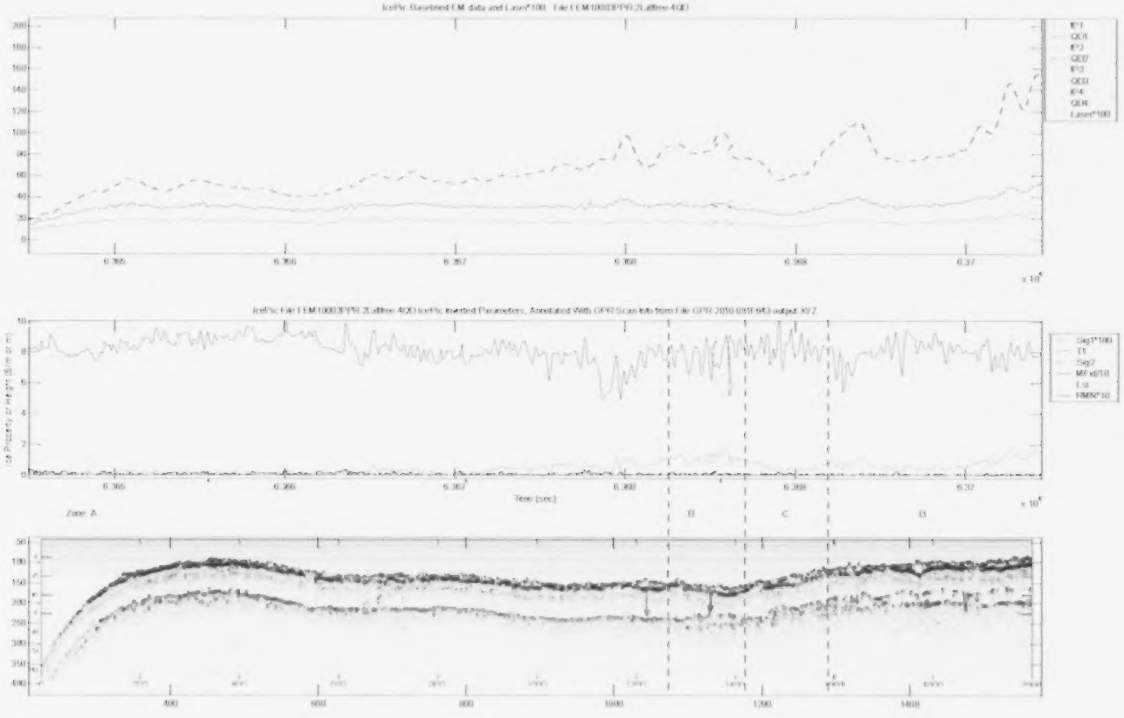

FEM1003, Segment 1a, F643. This segment appears to be completely composed of freshwater ice overlying ice-bonded sediments. Layering within the sediment appears to be visible in all Zones, particularly in B and D. The table below shows ice thickness estimates from GPR at the three arrows marked on the GPR section.

ID	Scan	Upper	Lower	Diff	Thickness	
Red	1277	5.57	7.19	1.62	1.00	
Blue	1362	5.79	6.96	1.17	0.73	Layering appears to be present in seds.
Green	1583	4.82	6.14	1.32	0.82	Layering appears to be present in seds.

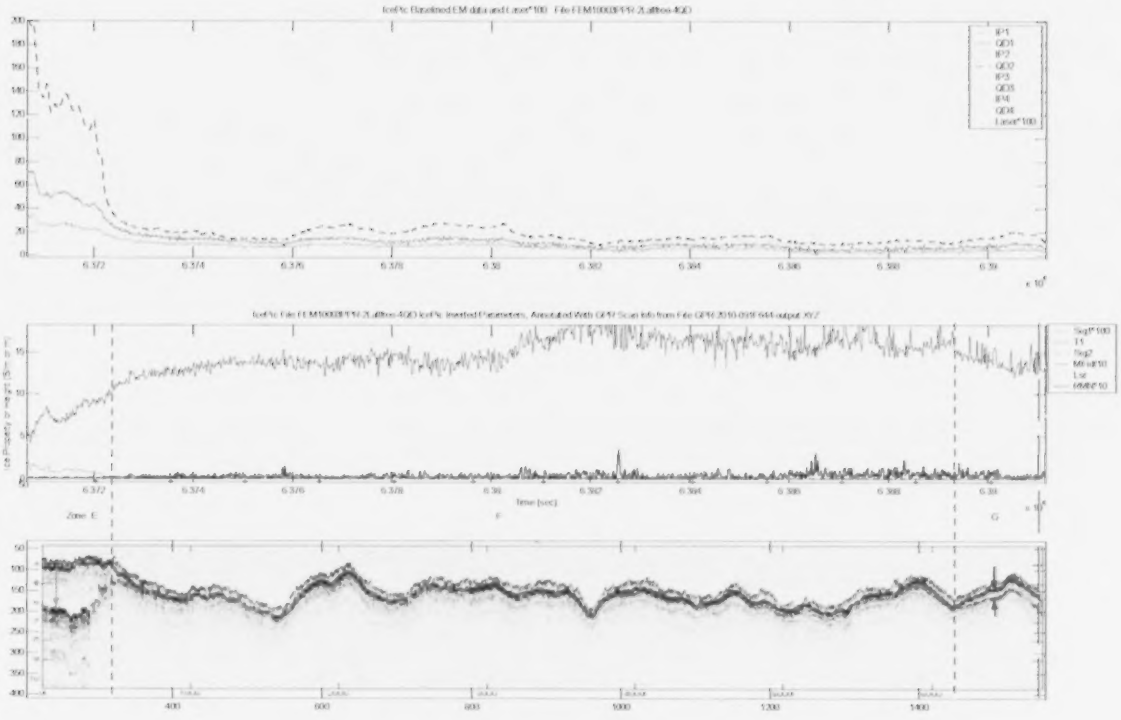

FEM1003, Segment 1b, F644. There is a short section of thick freshwater ice at the inshore end overlying water or unfrozen sediments, followed by what appears very thin ice and frozen sediments, with another thin layer of freshwater ice at the offshore end of the segment. The table below shows ice thickness estimates from GPR at the two arrows marked on the GPR section.

ID	Scan	Upper	Lower	Diff	Thickness	
Red	108	4.07	6.27	2.21	1.37	FW ice, possible deeper echos? Talik?
Blue	6411	5.18	5.67	0.50	0.31	Thin FW ice layer over frozen seds

In this section of the line, there appears to be a fairly thick layer of freshwater ice (Zone E) overlying either water or unfrozen sediments, based on the strength of the ice-bottom echo. From the ice thickness of greater than 2m, it seems likely that unfrozen sediments would be present in this area. This supported by the relatively strong EM response in the area, presumably arising from slightly saline sub-ice water and unfrozen sediments. The estimated T1 value ranges from 5-10m here, and its relatively high conductivity Sig1 is 0.01 to 0.02 S/m. Compare this to the greater T1 of 10-20m and much lower Sig1 for the rest of this Segment (Zones F and G), which appear to correspond to thin ice and snow over deeply

frozen sediments or permafrost. A thickening layer of freshwater ice is visible in Zone G, which coincides with a slow decrease in the inverted T1 value. Low Sig2 values suggest that unfrozen sediments, if present, are relatively thin and deep in this area.

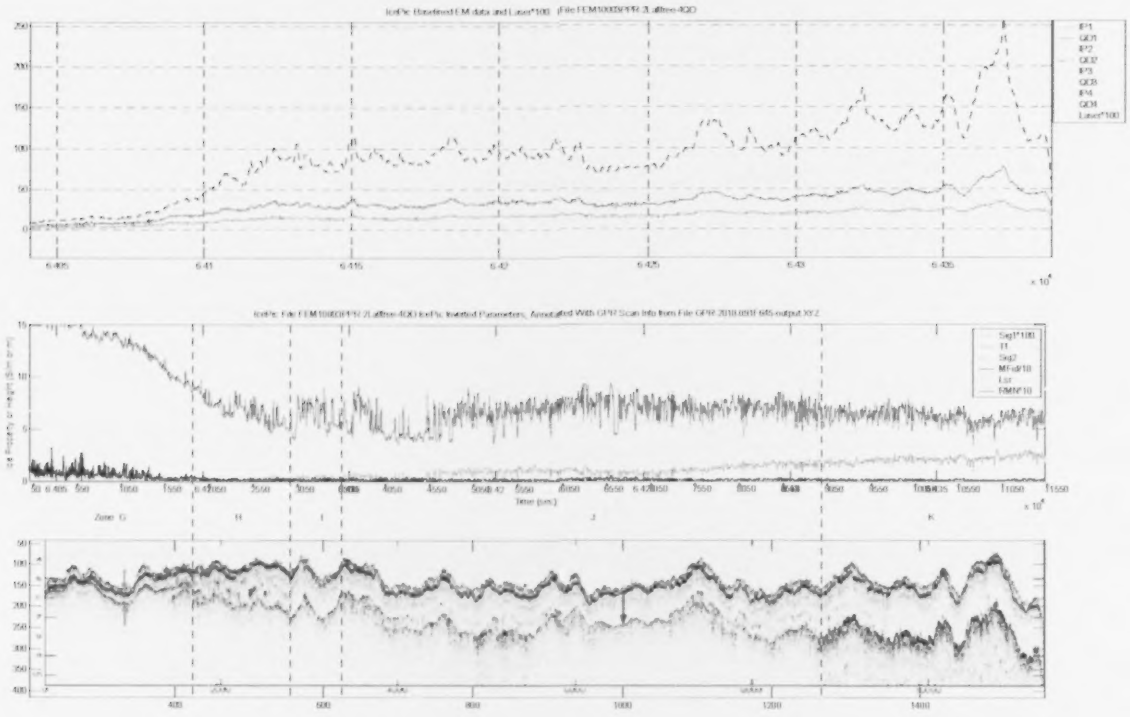

FEM1003, Segment 2, F645. A thin layer of freshwater ice overlying sediments thickens through Zone J. Zone I may represent a channel: the ice-bottom echo is sharper. Zone K marks a transition into freshwater ice overlying water and/or unfrozen sediments, with a possible sediment echo below the ice-bottom echo. The table below shows ice thickness estimates from GPR at the three arrows marked on the GPR section.

ID	Scan	Upper	Lower	Diff	Thickness
Red	921	5.70	6.24	0.54	0.33
Blue	5809	5.48	7.13	1.65	1.02
Green	9513	5.76	8.07	2.31	1.43

Segment 2 displays a transition (Zones G-H) from the thin ice and snow overlying deeply frozen sediments interpreted for most of Segment 1 into an area where relatively thick freshwater ice is bonded to seasonally frozen sediments (Zone J). In Zone K, it appears that the ice layer has become thick enough that any sub-ice sediments are at least partially unfrozen, and water may be present as well. Layering is visible within the ice, especially in Zones J and K, presumably related

to the periodic presence of slightly brackish water during formation. The sharper reflection over Zone I and small coincident dip in the EM, plus the increased T1 estimates in this area, suggests the presence of a layer of liquid water or at least unfrozen sediment below the ice. Low Sig2 values suggest that unfrozen sediments, if present, are relatively thin and deep in this area.

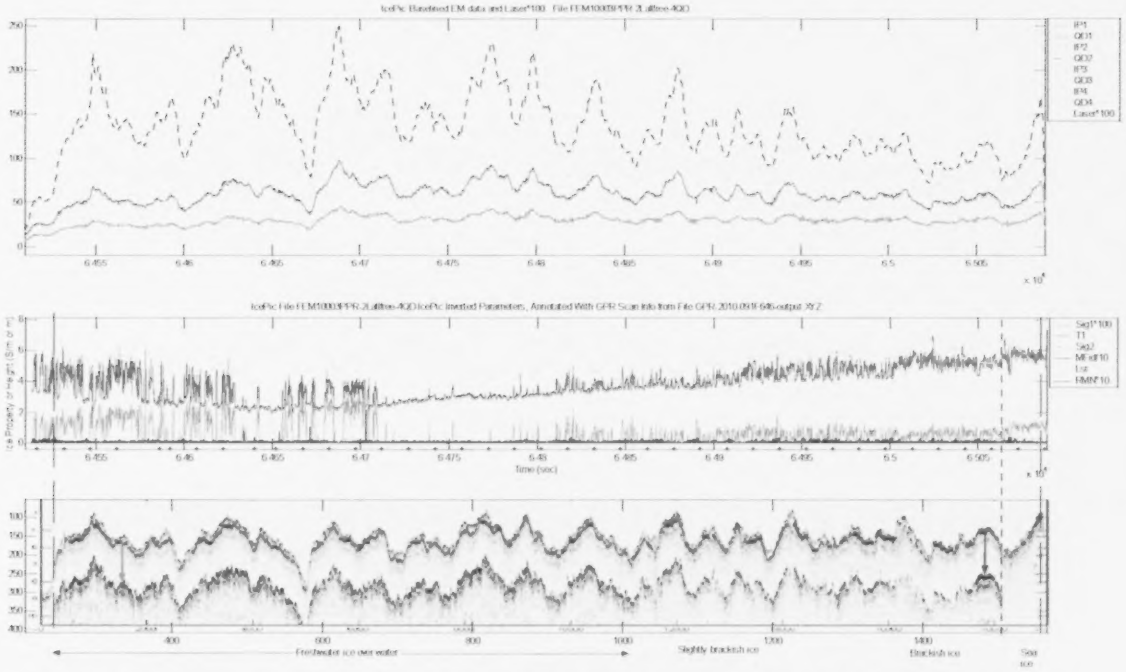

FEM1003, Segment 3, F646. Most of this profile appears to comprise freshwater ice over water and possibly some unfrozen sediments. There are hints of a sediment echo below the ice-bottom echo at the inshore end. Toward the offshore end of the segment, the ice becomes more brackish as noted in the annotations. At the offshore end of the segment, the ice abruptly changes to sea ice. The table below shows ice thickness estimates from GPR at the two arrows marked on the GPR section. A zone of very smooth freshwater ice was present near the blue arrow and may account for the stronger GPR echos in that area.

ID	Scan	Upper	Lower	Diff	Thickness	
Red	1535	5.67	8.06	2.39	1.48	
Blue	17840	4.94	7.58	2.64	1.64	In area of very smooth FW ice near edge of sea ice.

The ice-bottom GPR echo is not as strong as in earlier Segments. This may reflect a slight increase in average ice salinity. The EM responses are relatively strong for the inshore half of the profile, and estimated T1 and Sig1 values are relatively high at the inshore end, decreasing for the first third of the Segment. Sig2 values remain low and nearly constant over the entire Segment. The EM inversion model suggests that unfrozen sediments form the lower layer in this

Segment, and that somewhat saline (~0.02 S/m) sub-ice water is present in decreasing amounts for the first third, at which point the ~2.2m T1 value only slightly exceeds the ~1.5-1.6m ice thickness value. T1 and Sig1 then increase for the last half of the Segment. The increase is likely due to a thickening freshwater wedge beneath the ice, becoming slightly more saline toward the offshore. The transition to sea ice is abrupt, and is accompanied by a small increase in T1. It seems likely that the sea ice has a slightly higher thickness than the freshwater ice in this area. Low Sig2 values suggest that unfrozen sediments, if present, are relatively thin and deep in this area.

One of the zones of very smooth ice noted in the field and technical reports occurs just before the end of this Segment, and is repeated at the start of Segment 4. In Segment 3, it is located between the ~1m dip in T1 left of the blue arrow and the vertical dotted line marking the transition to sea ice.

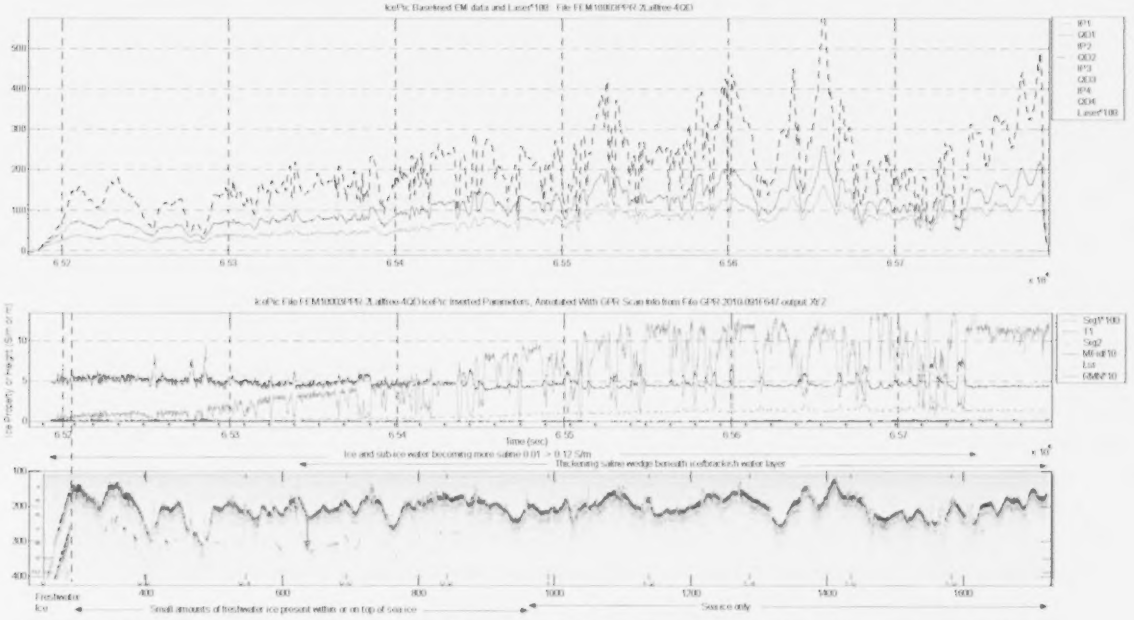

FEM1003, Segment 4, F647. A brief section of freshwater ice is present at the inshore end of this Segment, and there are a few freshwater ice inclusions within the sea ice that is present over the rest of this profile. The table below shows ice thickness estimates from GPR at the arrow marked on the GPR section.

ID	Scan	Upper	Lower	Diff	Thickness	
Red	5240	6.17	8.49	2.33	1.44	Freshwater ice inclusion or layer within sea ice.

One of the zones of very smooth ice noted in the field and technical reports occurs in the freshwater ice portion of this line, and was clearly visible as a series of dips in the laser reflectivity profile. The elevated Sig2 values in this Segment

are probably mainly indicative of the presence of unfrozen sediments and brackish water beneath the ice.

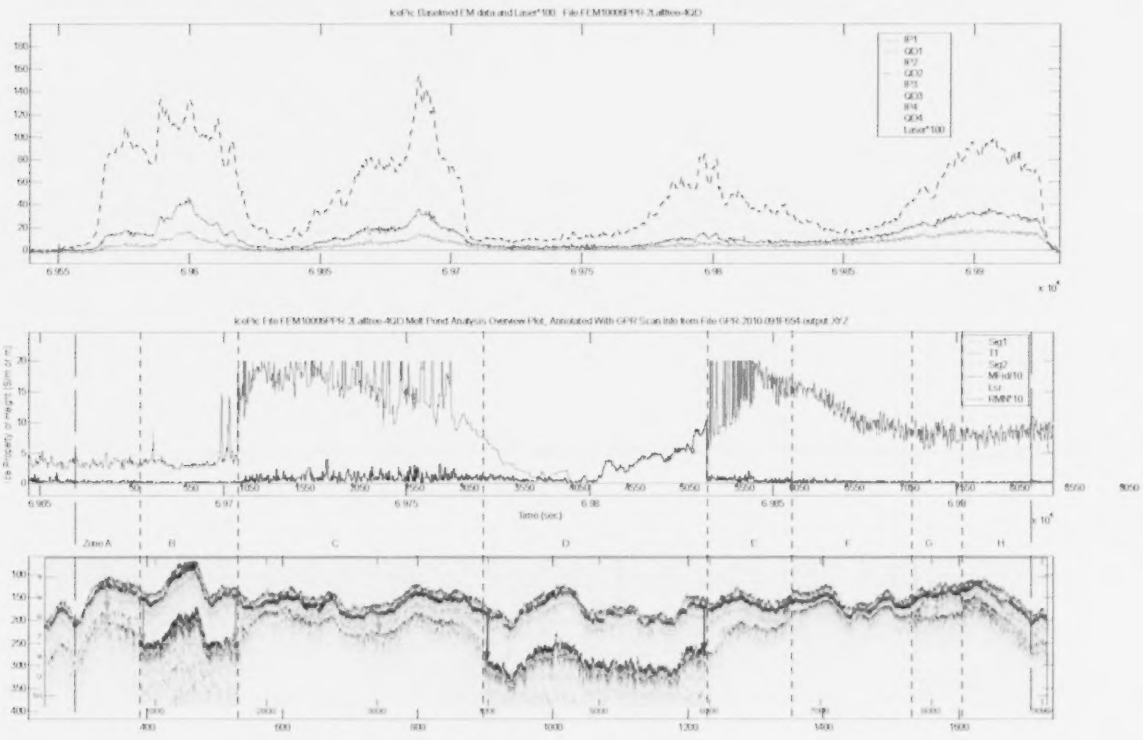

FEM10006, GPR 654. Top panel shows EM quadrature responses, middle shows 2 layer inversion results, bottom shows GPR and annotations. Arrows show ice thicknesses—arrows with same colour are same length. Arrow scan numbers and lengths (corresponding to thicknesses) were picked off the GPR section using GPRViewerNRT and converted to ice thickness using the calibration factor determined empirically above.

ID	Scan	Upper	Lower	Diff	Thickness	Description
A1a	598	4.47	5.69	1.22	0.75	Zone A ice bonded sediment
A1b	598	5.68	6.33	0.65	0.40	Increment to reflection within sediment
B1	873	5.07	7.34	2.27	1.40	Zone B inshore edge ice over water
B2	1730	4.88	7.43	2.55	1.58	Zone B offshore edge ice over water
C1	3034	5.85	6.89	1.04	0.64	Zone C Ice bonded sediment
D1	3981	5.85	8.33	2.48	1.53	Zone D inshore edge ice over water
D2	5995	5.60	7.77	2.18	1.35	Zone D offshore edge ice over water
H1	8105	4.80	5.96	1.16	0.72	Zone G ice bonded sediment

The different Zones in the figure display some similarities in terms of EM response, inverted parameters and GPR results, but also some significant differences. For example:

1. Zones B and D, where ice overlies water (based on the strong ice-bottom reflection), display
   - similar ice thicknesses of about 1.5m and small T1 values in the second panel of the figure above.
   - the EM responses (top panel) for the two zones are quite different, with the inshore Zone B displaying much stronger quadrature values than the more offshore Zone D. While this is due to some extent to lower altitude over Zone B, it may also indicate that the unfrozen sediments underlying the water are thicker in Zone B than in Zone D, or that they are closer to the surface in Zone B.
   - At the EM response peaks, the ratio of high to low frequency quadrature response is 7.5=135/18 for Zone B, and 10.6=85/8 for Zone D, suggesting that integrated sediment conductivities are higher in Zone B. Again, this may imply thicker unfrozen sediments or simply that the shallow unfrozen sediments are more conductive.
   - In the figure below, the model parameters panel has been enlarged to show the upper and lower layer conductivities. The misfit (black dotted line) increases over Zone C and, to a lesser extent, over Zone E. There is a large misfit in the offshore half of Zone D, where the fitting error was very high. These areas of misfit indicate that the model was not able to reproduce the observed responses well in those areas. Further inversion studies may be indicated for those areas.
   - Spikes in Sig1 in Zone 1 correspond to local peaks in the EM response. Sig2 increases at the offshore edge of the junctions of Zones B-C and Zones D-E. Sig1 increases substantially toward the offshore end of Zone E-H, consistent with slowly increasing salinity in the ice+freshwater layer in this area.
2. Zones C and E-H, where thin (about 0.7m) ice overlies sediment, display similar T1 values in the second panel, their GPR responses are comparable, and the EM amplitudes display the same general increasing trend. However, the ice thickness is greater on average for C than for E-H, and E-H displays quite a bit of heterogeneity in the GPR.
3. Zone A displays similar EM amplitudes to Zone C, but the interpreted T1 is quite different. The GPR in A is more similar to E or H than to C. The GPR-estimated ice thickness is greater in A than in most of C or E-H.

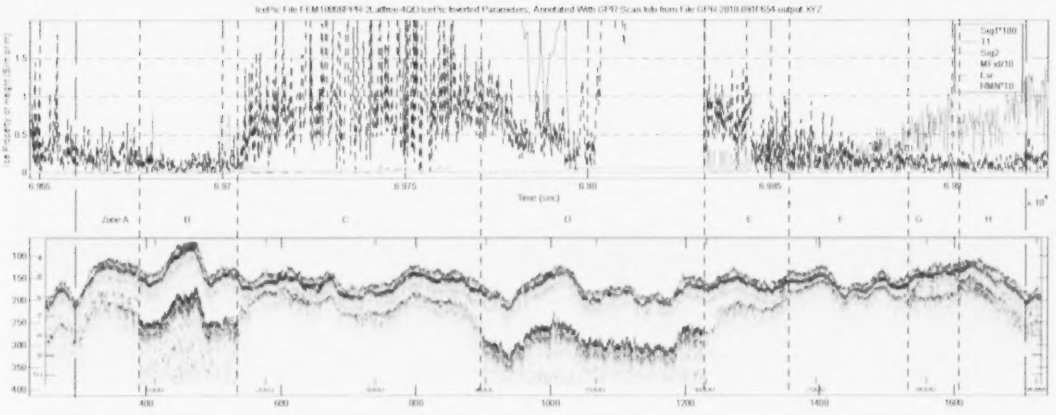

Third and fourth panels from previous figure, with model parameter scale enlarged. Sig2 is shown in green and Sig1*100 in red. Elevated values of Sig2 in a few locations suggest the presence of unfrozen sediments below seasonally frozen sediments and above permafrost.

Examining the image extract from the combined SAR+2-layer parameters introduced earlier, the two T1 peaks (Zone C and Zone E-H) seen in the previous figures coincide with the profile tracking over dark areas in the processed SAR that are associated with bottomfast ice (Solomon and Manson, 2005). The light-grey areas should correspond to floating ice overlying deeper water. These results are consistent with the GPR and EM interpretations described above.

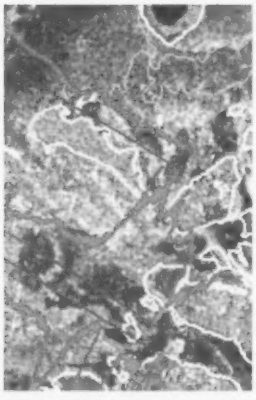

Segment 2 of FEM10006

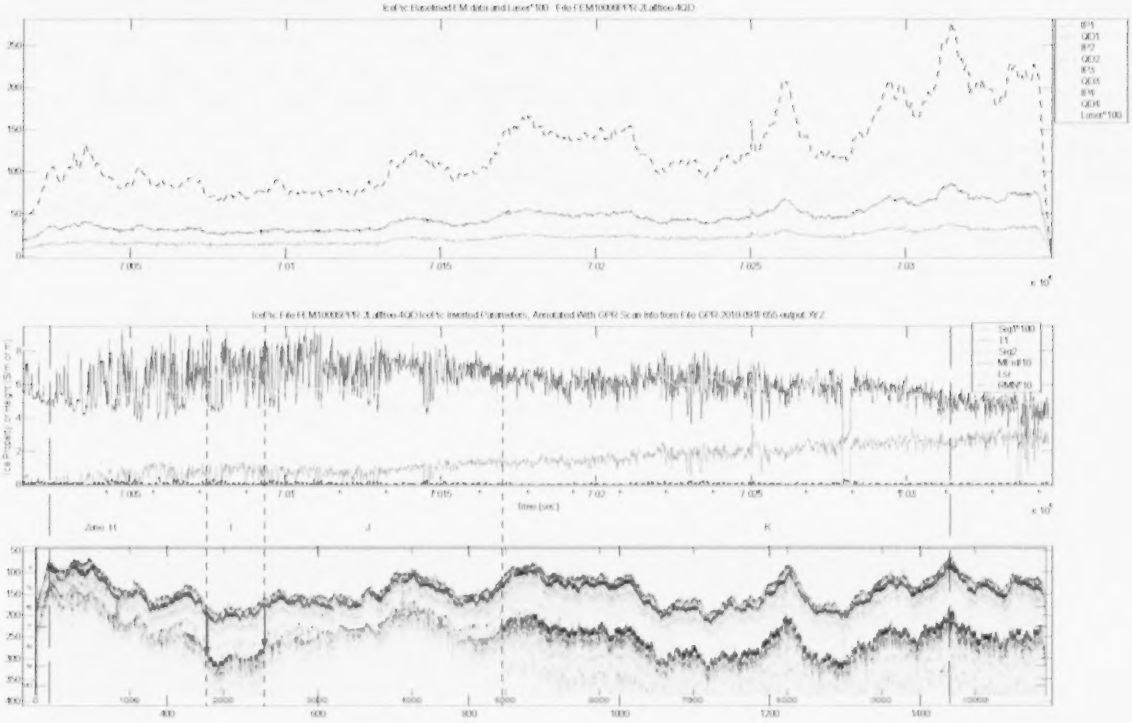

In the Segment 2 of FEM10006, the ice layer thickness as indicated by the GPR file F655 is mostly greater than seen in the Segment 1, especially in Zone K. At the inshore end of this portion of Zone H, there are hints of sediment structure underlying the ice/sediment interface. It appears that water or unfrozen sediments underlie the ice in Zone I, before a return to ice-bonded sediments in Zone J. The presence of echoes within the ice suggest a higher degree of brackishness in this ice compared to Segment 1.

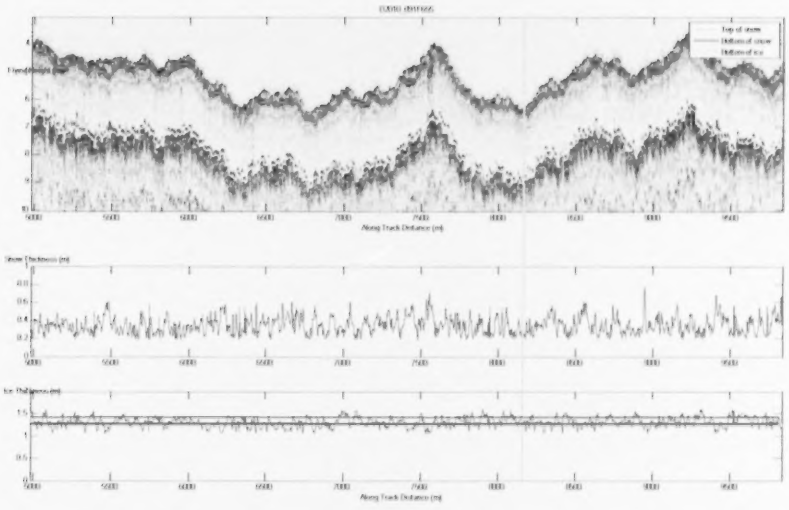

Inverted (by Louis Lalumiere) freshwater snow and ice thickness results, shown above, for a portion of the F655 GPR line that includes the second picked ice thickness (green arrow) in Zone K. This figure was included in Appendix B of Lalumiere's 2010 GPR report. The vertical green line added to Lalumiere's figure corresponds to the picked green arrow (identified as K2 in the table below) in the figure above, while the horizontal black lines in the lowest panel of the figure show the range of ice thicknesses estimated by inversion in the vicinity of the pick. This range is approximately 1.3 to 1.45m, consistent with the value for K2, which was estimated by the direct scaling method used earlier.

ID	Scan	Upper	Lower	Diff	Thickness	
H2	863	5.49	6.59	1.10	0.68	Zone H ice bonded sediment
I1	1867	6.56	8.63	2.07	1.28	Zone I ice over water (inshore)
I2	2445	5.93	8.03	2.10	1.30	Zone I ice over water (offshore)
J1	3930	4.71	5.94	1.23	0.76	Zone J ice bonded sediment
K1	5070	4.43	6.59	2.16	1.34	Zone K ice over water (inshore)
K2	8602	6.50	8.73	2.24	1.39	Zone K ice over water (offshore)

Observations regarding this Segment:

1. Zone H (as in previous segment) exhibits moderate EM response that is anticorrelated to altitude. The GPR suggests that Zones H and J are similar in their degree of ice bonding to the underlying sediments
2. Zone I appears to represent partial ice bonding to the sediments and/or intermittently unfrozen sediments or narrow, thin zones of sub-ice water, as the GPR ice-bottom echo is weaker and more broken up than Zones B,D and K.
3. The ice-bonded sediment areas all exhibit relatively thin ice (.7-.8m), increasing at the edges of ice over water areas), while the apparent ice

over water areas exhibit relatively uniform 1.3-1.4m ice thicknesses with variable amounts of snow cover.

4. A common feature in all inshore-offshore transitions between ice bonded sediment and ice over water is a weak reflection that separates from the ice-sediment echo and appears to thicken toward the offshore.
5. For the inverted model conductivities, Sig2 is relatively uniform at a low value for the entire segment, while Sig1 exhibits a low, broad peak over Zones H-I-J, then increases fairly steadily in the offshore direction.
6. The estimated T1 value initially increases from about 5 to almost 8m for Zones H-J (consistent with the offshore end of Segment 1), then decreases slowly over Zone K to reach 4-5m at the offshore end of the segment.
7. The ice is only 1.3-1.4m thick in this area. Relatively warm Middle Channel water flowing beneath the ice seems likely to be a factor. Comparable ice thicknesses were observed NE of Garry Island in a similar bathymetric setting.

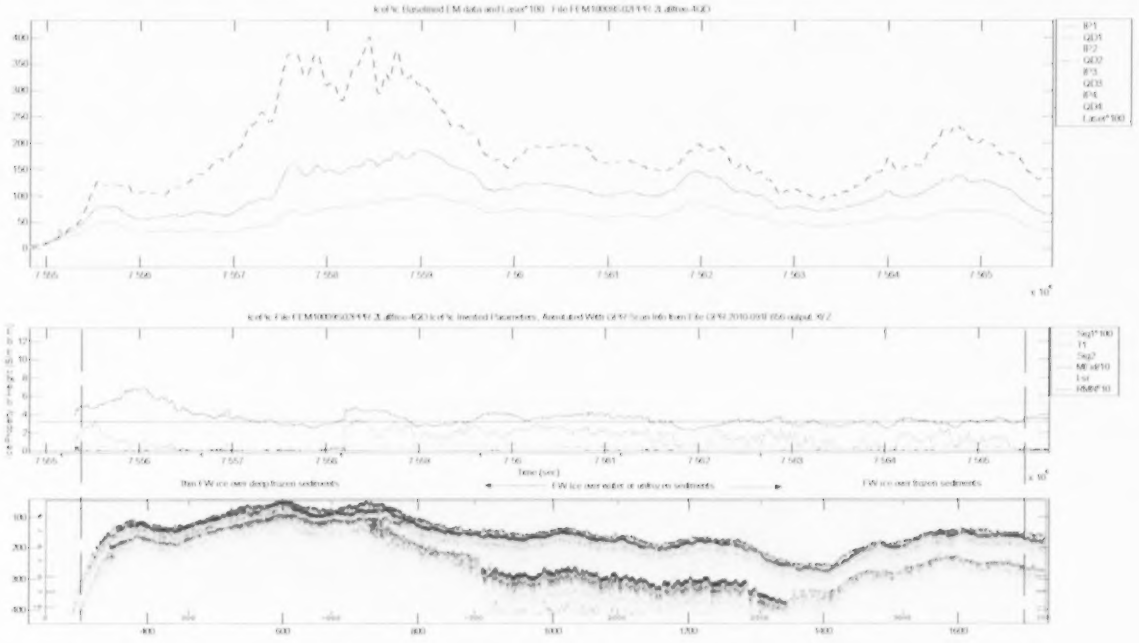

FEM10009 Segment 1a with GPR F656. Note that Sig2 (red dashed) values range up to 0.5 S/m or higher in places, suggesting that deeper sediments may be unfrozen in those areas. Much of the variation in EM response is correlated with altitude, which masks the more subtle deep conductivity effect. A more deeply-frozen area, *i.e.* with lower Sig2 values has been noted at the 1/3 point of this plot.

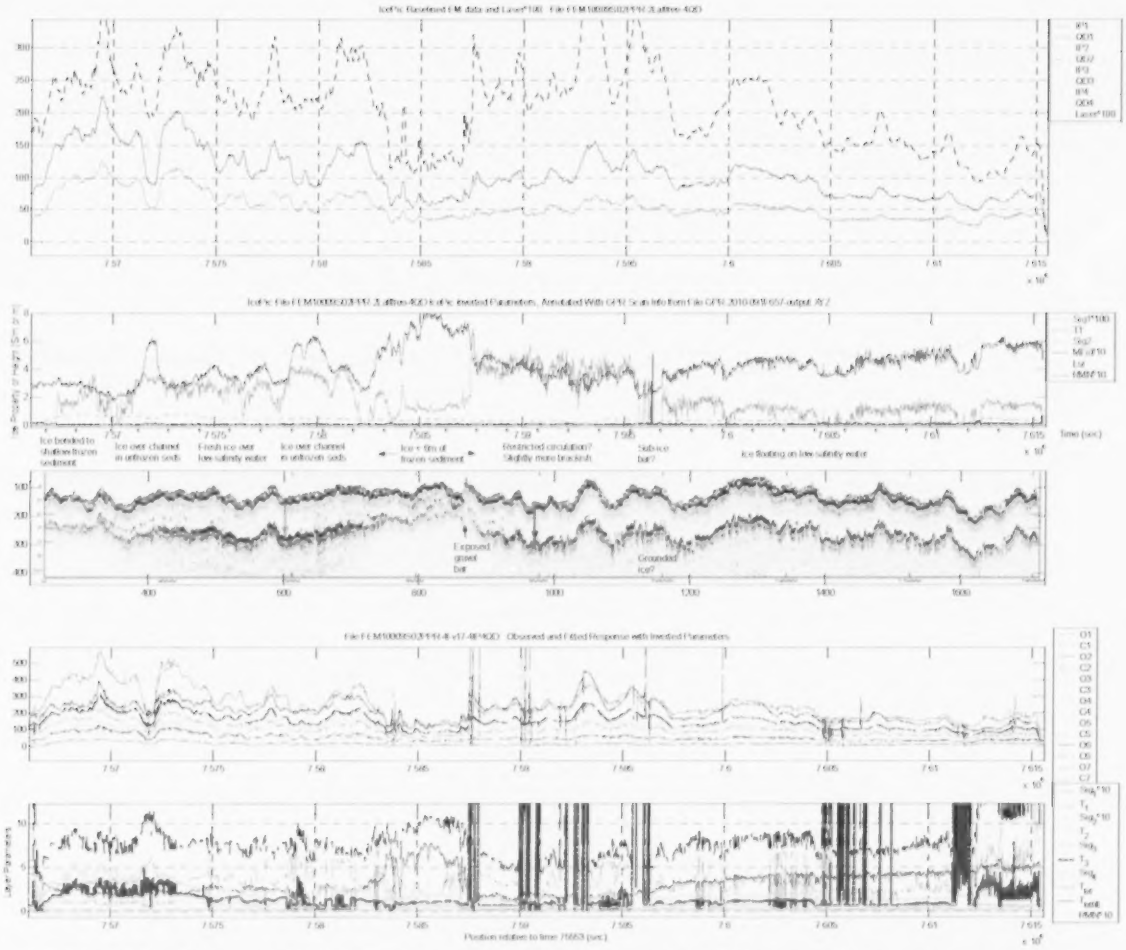

FEM10009 Segment 1b. The upper panels show the 2-layer, all parameters free fit and fitted parameters using the 4 quadrature values as input for the portion of this segment that includes GPR data. The middle panel shows the corresponding GPR F657 data, and the lower panel shows the 4-layer fit and model parameters, obtained by fitting all IP and QD data. The table below shows ice thickness estimates from GPR at the four arrows marked on the GPR section.

ID	Scan	Upper	Lower	Diff	Thickness
Cyan	378	4.88	6.81	1.94	1.20
Red	3866	5.18	7.62	2.45	1.52
Blue	7957	5.40	7.82	2.42	1.50
Green	11510	3.75	6.24	2.49	1.54

As with Segment 1a, the Sig2 values range above 0.5 S/m, suggesting that at least some unfrozen sediments are present below the seasonal frost line.

(b) April 5 Observed and Processed Data

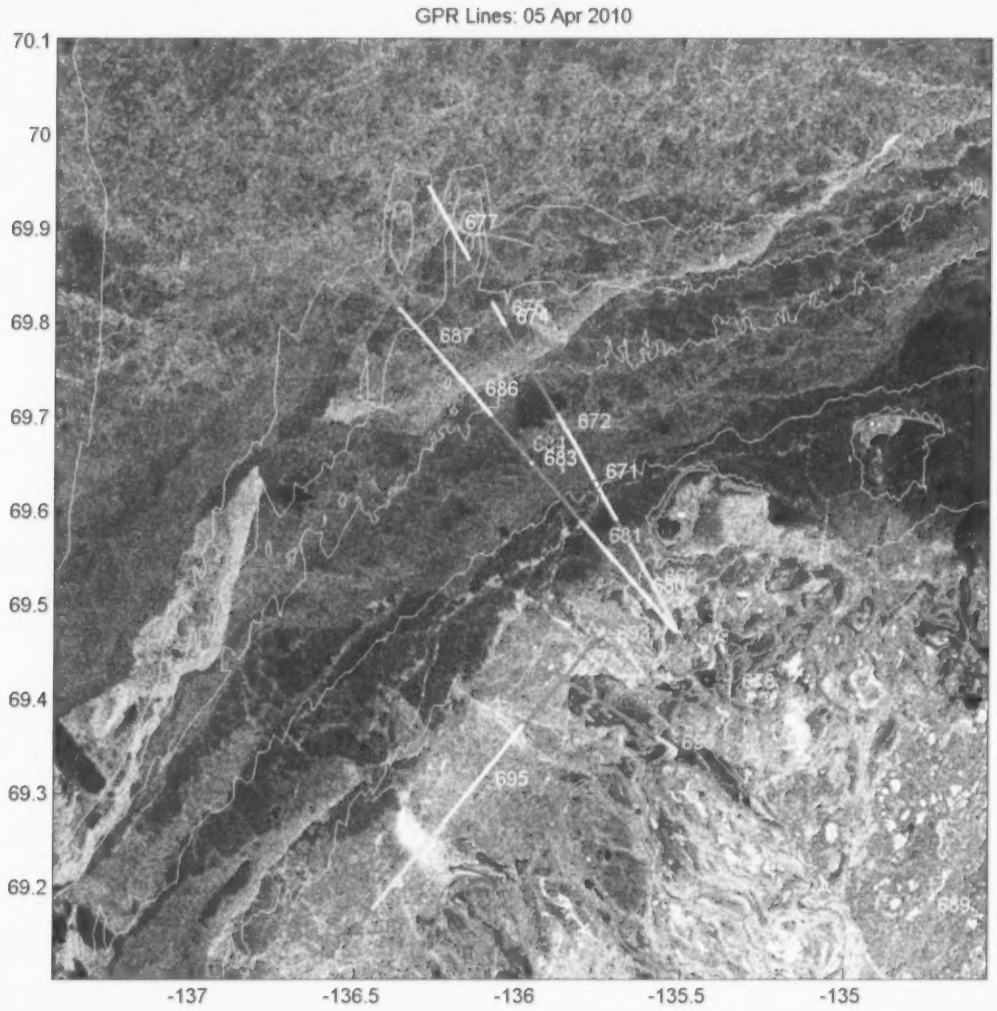

The GPR files of interest for this report on April 5 were F690-91 (92 was aborted) and F693-697. Segments 1a (corresponds to F690), 1b (691) and 2 of the corresponding EM line FEM10018 ran SE-NW, while segments 3a,3b,4,5 and 6 ran NE-SW.

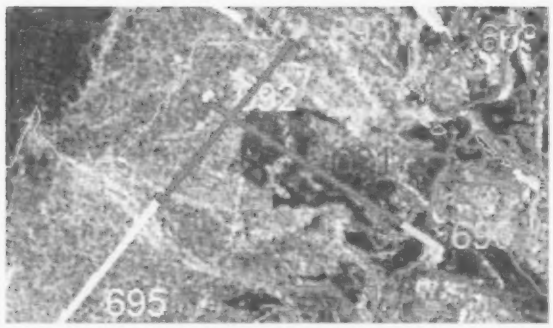

Excerpt from previous, showing first few segments of 5 April survey lines.

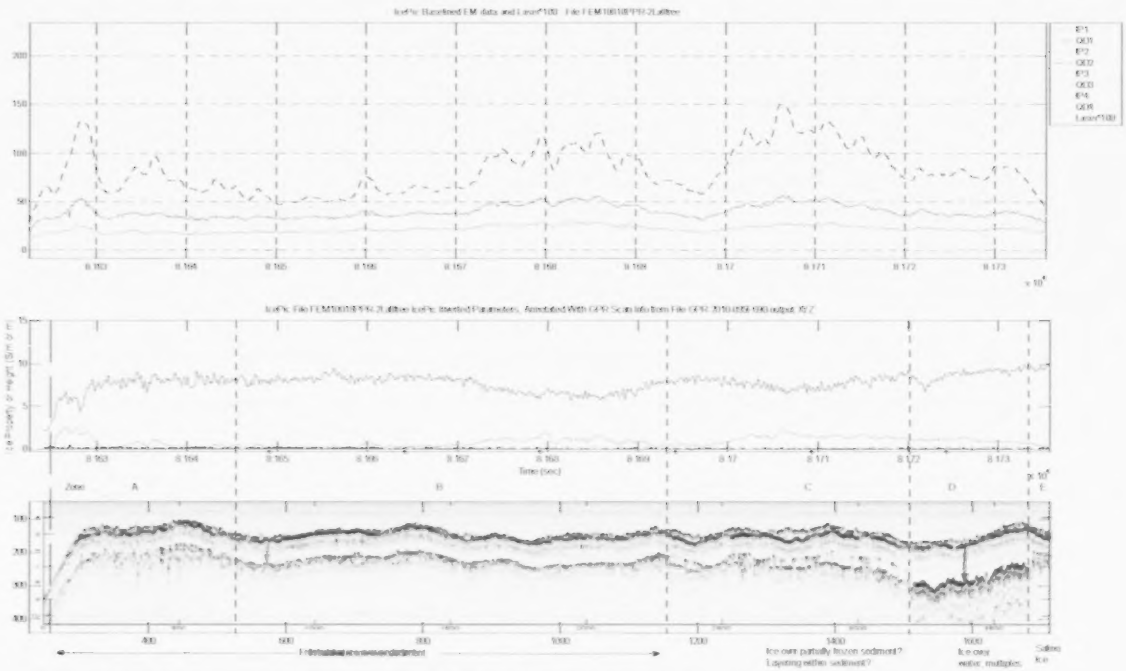

FEM10018 Segment 1a, GPR F690. The table below shows ice thickness estimates from GPR at the two arrows marked on the GPR section.

ID	Scan	Upper	Lower	Diff	Thickness
Red	834	5.28	6.78	1.50	0.93
Blue	3406	5.52	7.85	2.33	1.44

Note the relatively low values for Sig2 for most of this profile. This suggests a reduced thickness (or greater depth) of unfrozen sediments beneath seasonally frozen sediments, compared to some of the previous examples.

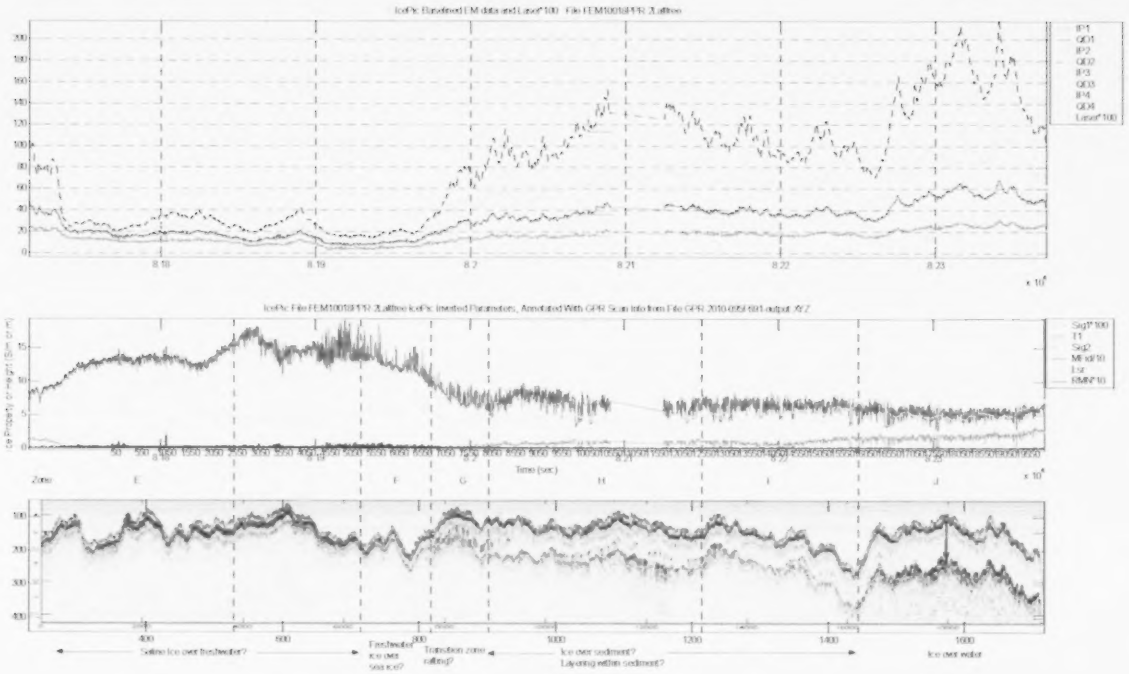

FEM10018 Segment 1b, F691. The table below shows ice thickness estimates from GPR at the arrow marked on the GPR section. The low Sig2 value suggests that unfrozen sediments, if present, are thin and deep.

ID	Scan	Upper	Lower	Diff	Thickness
Blue	18010	4.20	6.69	2.49	1.54

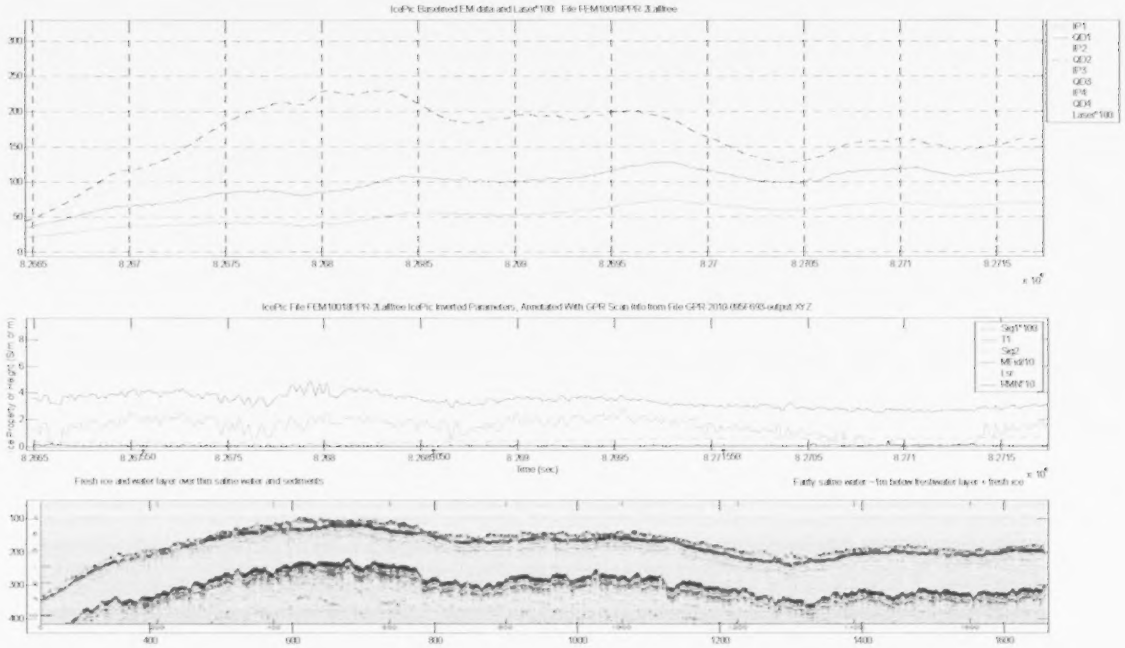

FEM10018 Segment 2. The strong ice-bottom echo indicates floating freshwater ice throughout, while the EM and inverted parameters suggests a layer of slightly brackish water beneath the ice overlying unfrozen sediments.

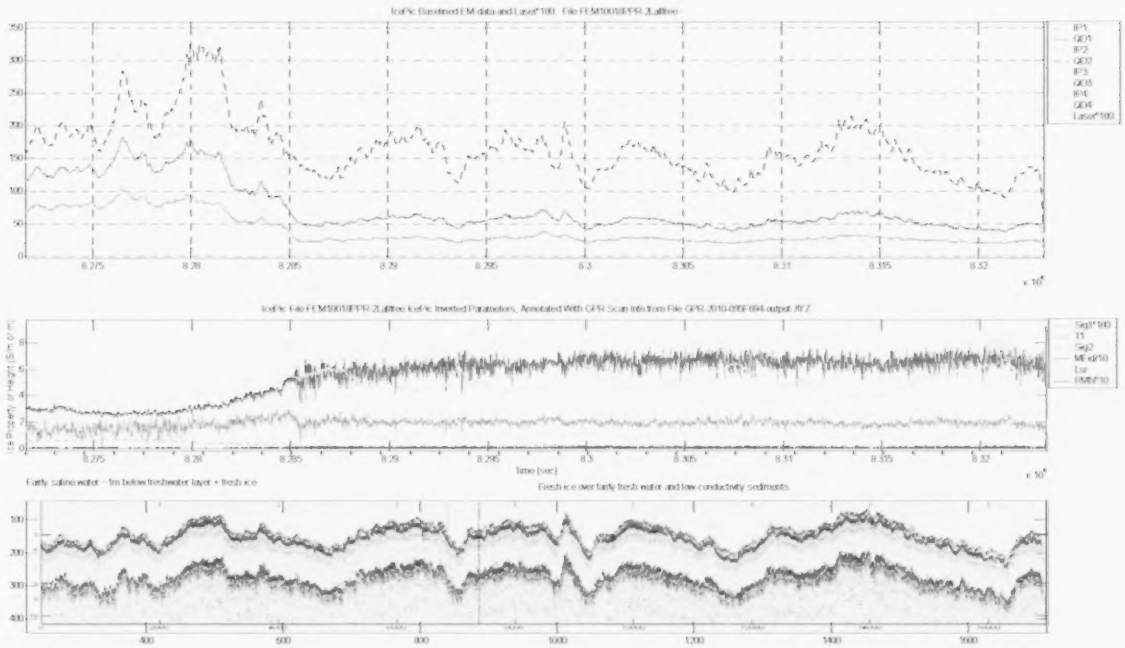

FEM0018 Seg 3. Again, floating freshwater ice is suggested by the GPR, and saline water beneath the ice and a freshwater layer is suggested by the EM at the left (NE) end of this segment. The rest of the segment appears to be relatively uniform, low-salinity water below the ice, overlying low-conductivity sediments. The bathymetry in this area should be less than 2m, although the 2m bathymetric contour does closely approach this line.

As an aside, compare the 2-layer model used here with the 4-layer model that was optimized for FEM10009.

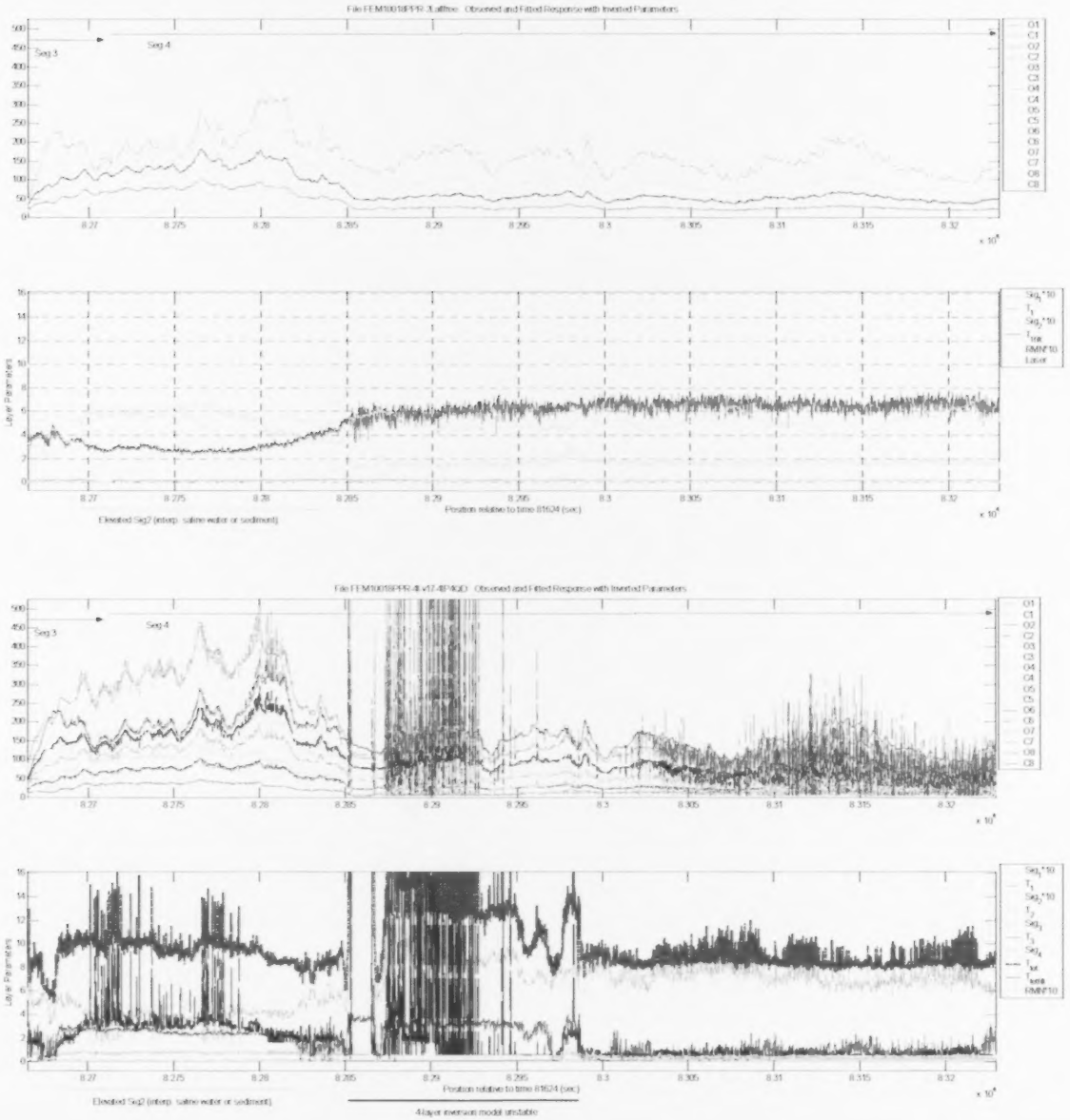

Both models locate the relatively good conductor in the first third of Segment 3. The 4-layer model fits well in this area and distinguishes the freshwater ice and water layer (layer 1) from the more conductive layer beneath it (layer 2).

It would seem natural for this conductive layer to represent brackish water of conductivity 0.4 S/m located in the channel identified by the 2m bathymetric contour, which closely approaches this line. However, the first layer thickness T1 by itself exceeds 2m in this area, and T2 is on the order of 4m in the vicinity of the channel. Even if the channel were deeper than indicated by the bathymetry and a strong tidal effect was present, the combination seems unlikely to account for the entire 4m discrepancy.

Another explanation is that this anomalous layer's properties are only being resolved as a 1.6 S conductivity-thickness product rather than as independent parameters, and that it actually comprises about 0.65m of 2.5 S/m seawater. The sediments in the channel bottom could also be more conductive than surrounding shallower sediments, which would further amplify the EM response of the channel. The four-layer model does provide insights into the conductivity structure, but it should not be taken at face value.

A third explanation is that the portion of the channel that shows as a conductor is almost entirely filled with ice and perhaps a thin layer of freshwater, overlying what may be several metres of unfrozen sediments. The anomalous conductivity that is displayed by the inversion would then be the conductivity of these sediments, which could easily be in the 0.5 S/m range if they are clay rich and/or brine- or seawater-saturated.

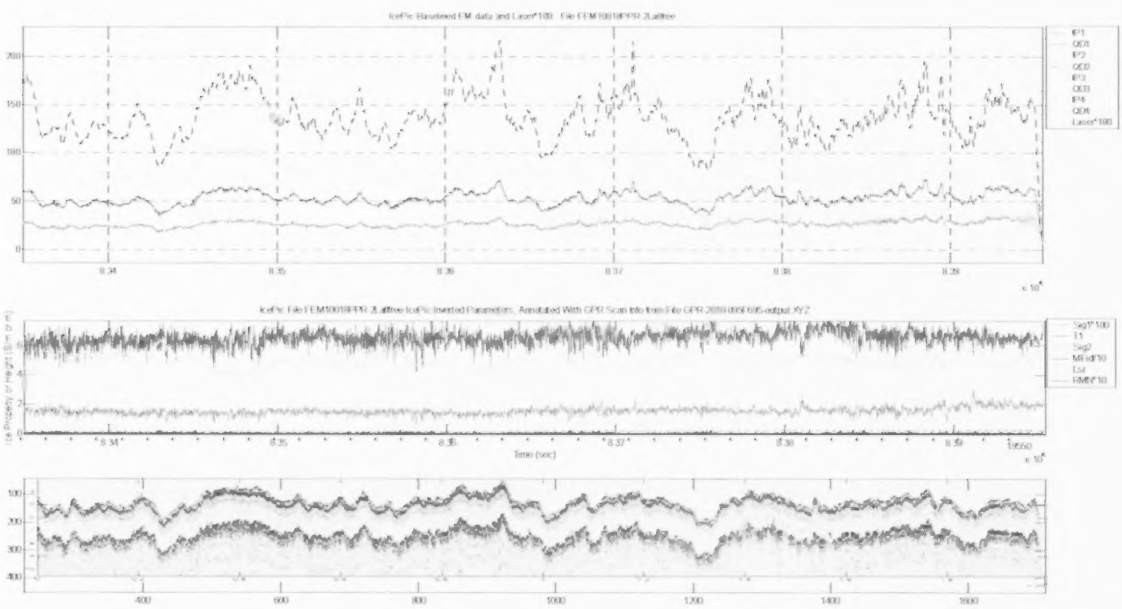

FEM10018 Segment 4. The GPR indicates floating freshwater ice, while the EM suggests that freshwater and relatively thin or resistive unfrozen sediments are present beneath the ice.

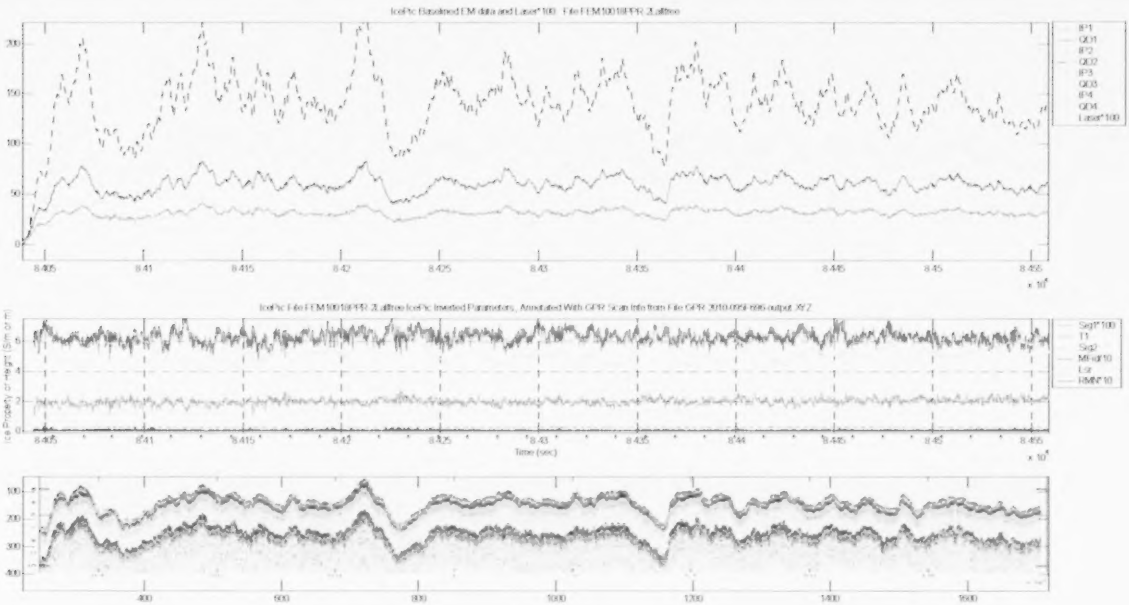

FEM10018 Segment 5. Again, the GPR indicates floating freshwater ice, while the EM suggests that freshwater and relatively resistive or thin unfrozen sediments are present beneath the ice.

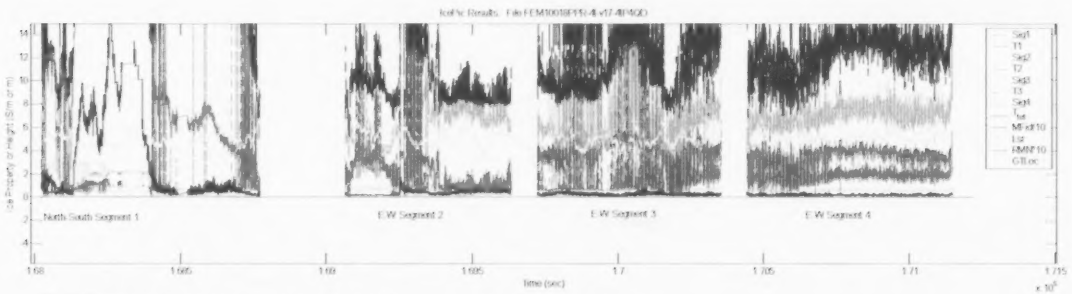

FEM10018, 4 layer Model 17 inversion, zoomed.

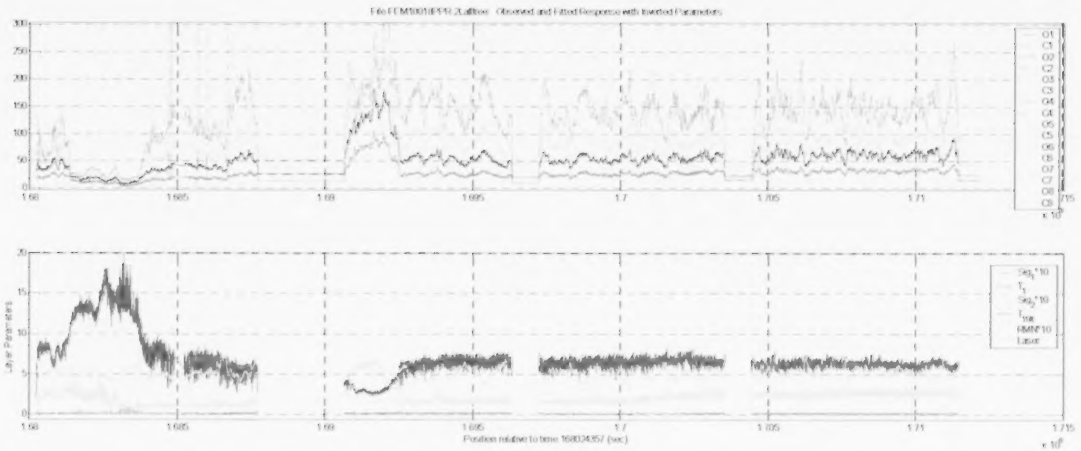

FEM10018, 2 layer inversion with all parameters free.

Interpretation

Interpretation cartoons are presented for FEM10003 and FEM10006 on April 1, and FEM10018 on April 5.

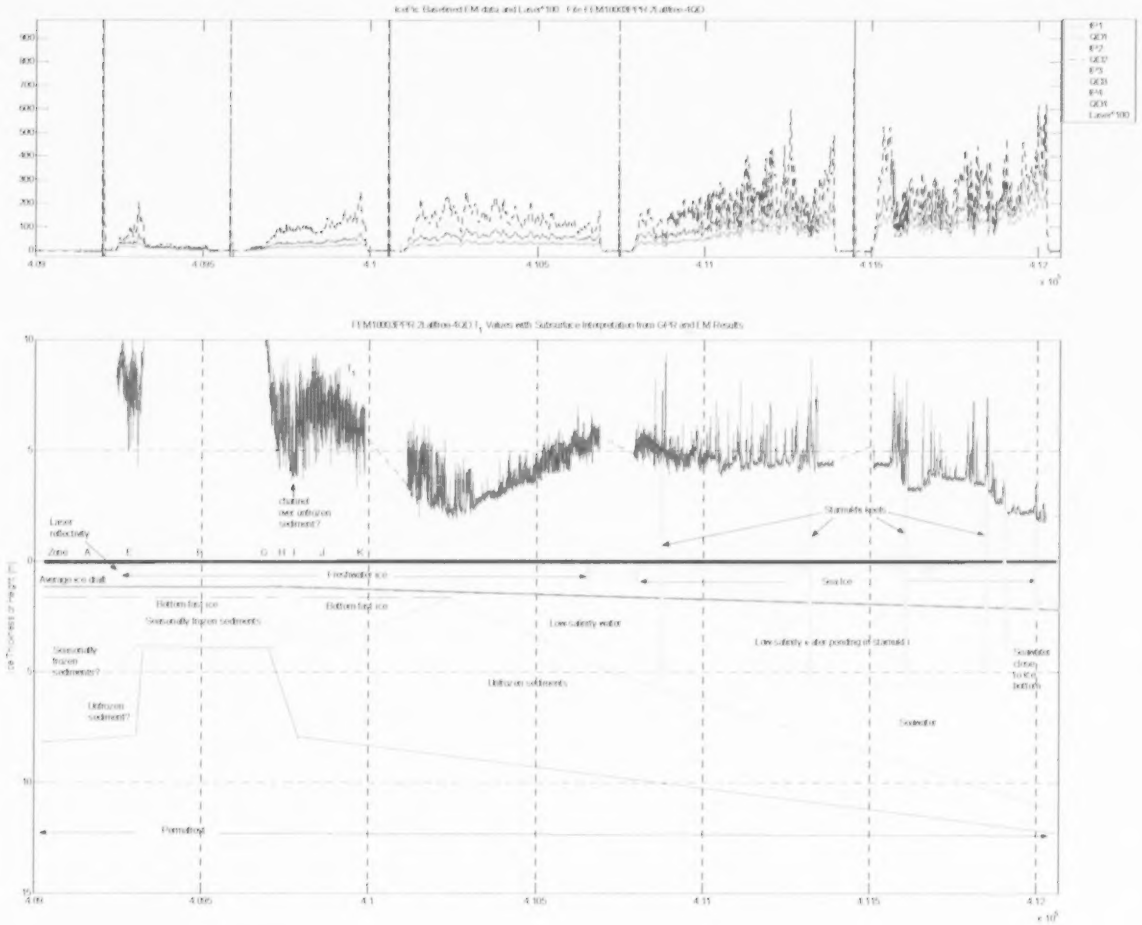

FEM10003 Interpretation cartoon.

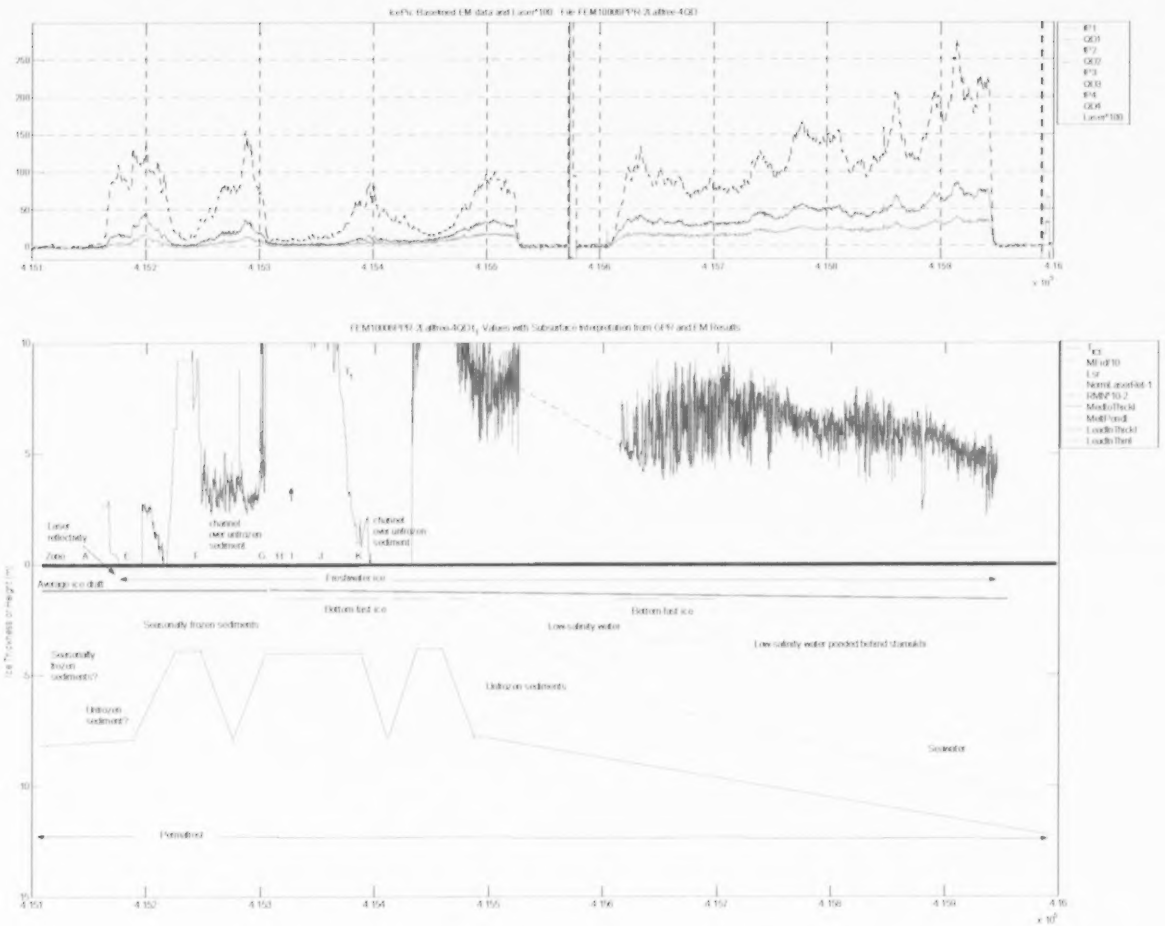

FEM10006 Interpretation cartoon.

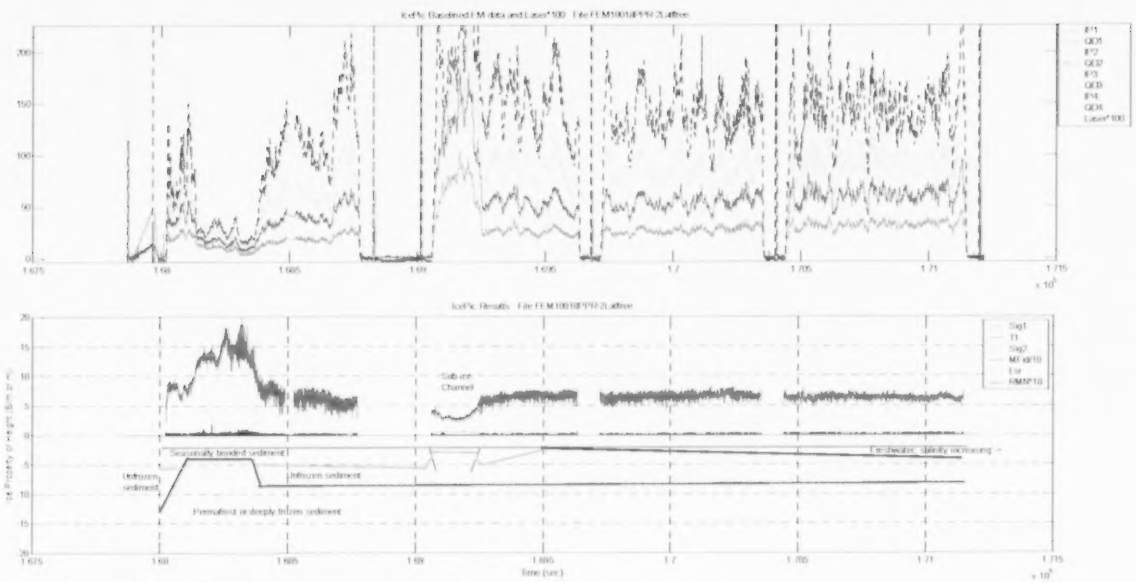

FEM10018 Interpretation cartoon.

Appendix: Calibration of freshwater ice thickness estimates from CTD sites and GPR plots

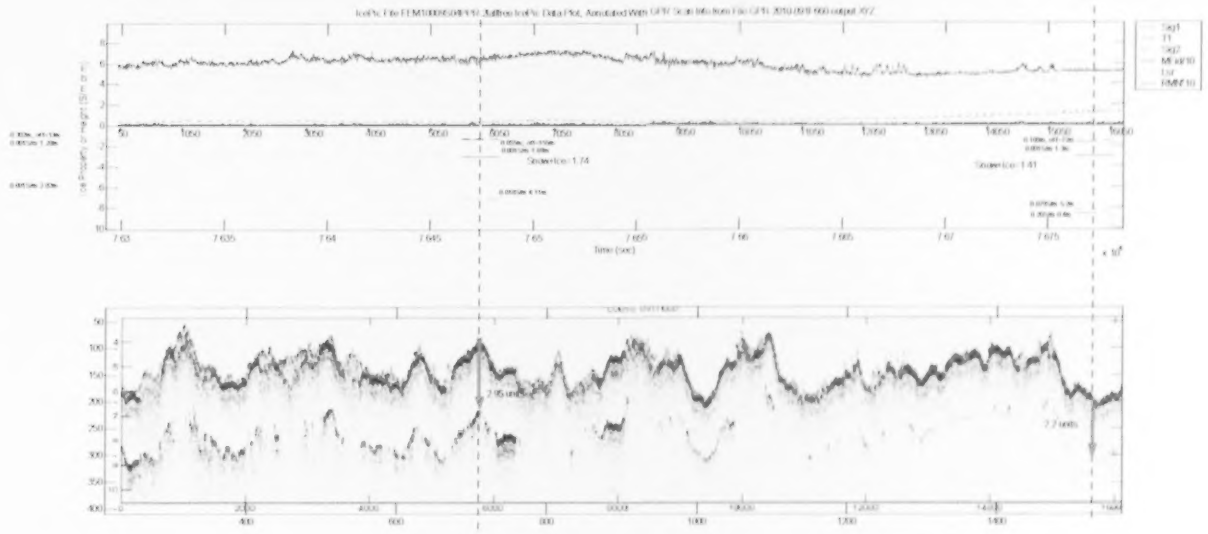

An empirical calibration was performed along Segment 1 of FEM10009, using GPR file F657.
Calibration factor estimates obtained:
Observed/GPR Values
Site 44: C_{44}=1.74m/2.9 units=0.60

Site 45: C_{45}=1.41m/2.2 units =0.64

The calibration sites were 155 and 72m from the survey profile's closest approach. If we conservatively assume +/-5 cm snow/ice depth variability and 0.05 unit reading noise on the GPR results, we get (1.74+/-.05)/(2.9+/- .05), with error
dr=sqrt((.05/1.74)^2+(.05/2.9)^2)*0.60 or 0.020
for the first, and .027 for the second. The individual calibration factors would then be
C_{44}=0.60+/- .020 and
C_{44}=0.64+/-.027

The mean factor and estimated error would then be
C_{mean}=0.62 +/- .017 or 0.62 +/-.02,
or a little over 3%.

Appendix: GPR Interpretation Notes

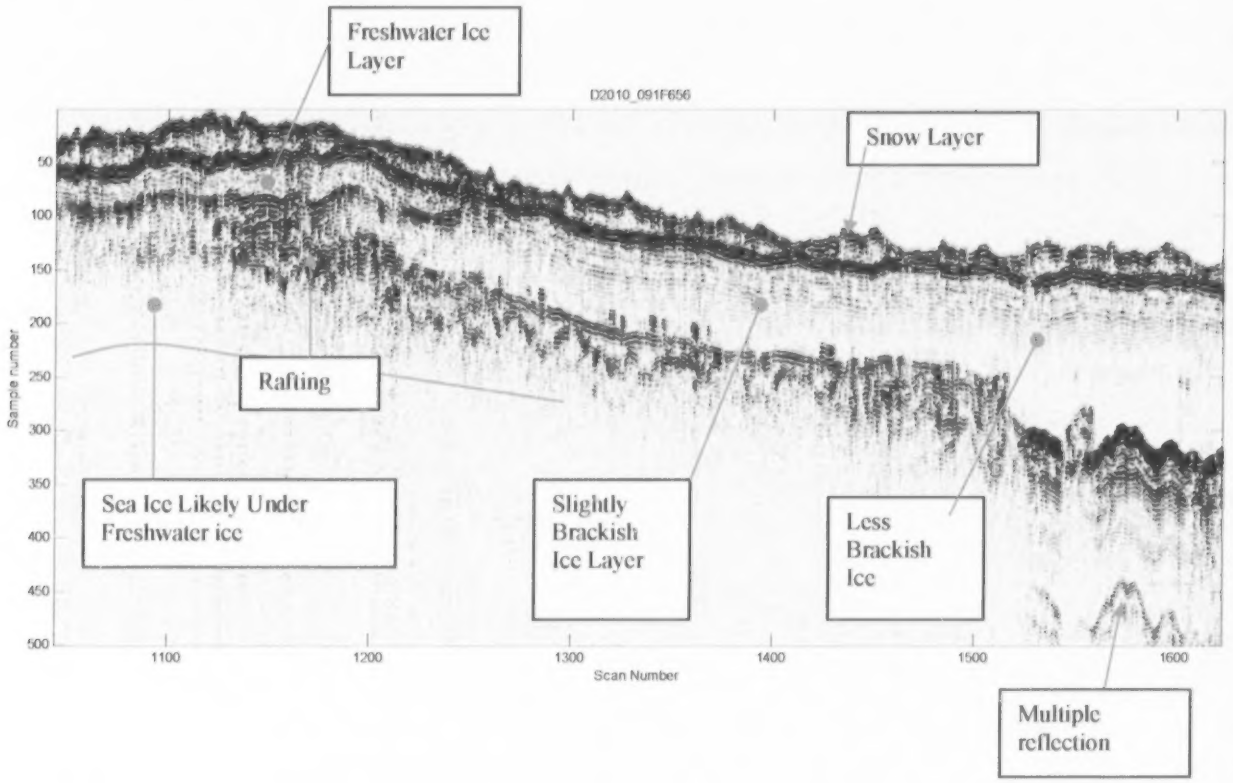

In the figure above, copied from the 2010 GPR report by Louis Lalumiere, some interpretive examples for different ice types is provided for the 1 GHz Noggin GPR used for this field work, in a short excerpt of GPR file D2010_09F656.

At left, a snow layer overlies thin (0.5m) freshwater ice, which appears to overlie saline ice of indeterminate thickness. A zone of interpreted rafting is visible between Scan 1150 and 1200. The region between scan 1200 and 1500 appears to comprise fresh- or slightly brackish water ice of about 1.2m thickness. After 1500, the freshwater ice thickens to about 1.8m.
In addition to Louis' comments, the following interpretations are suggested by the data, location and expected conditions:

1. It seems likely that the (interpreted) saline ice is bonded to frozen sediments in the area before scan 1200—there is a weak reflection near sample 140 that continues into the area of thicker freshwater ice to the right of Scan 1200 that supports this, as does the fact that this short line is located inshore of Garry Island, where the bathymetry is generally less than 2m.
2. It is possible that the emplacement of freshwater ice on top of sea ice seen near Scan 1100 occurred when sea ice bonded to sediments was

flooded with freshwater from a surge arising from the nearby Middle Channel.

3. The features interpreted in the figure as rafting may represent ice structures, including rafting, built up along the shoreline after the (early winter?) event in which some sea ice (after roughly Scan 1150) was removed by flooding, spring tides or storm activity, then replaced by fresh or brackish ice.
4. In the section between 1200 and 1500, the bathymetry is so shallow that it is very likely that the (apparently slightly brackish) ice is bonded to sediments. This seems like a better mechanism than attenuation within this ice for the observed weakening of the ice-bottom echo in this section.
5. Also in this section, there appear to be reflections within the frozen sediments
6. After Scan 1500, the ice appears to overlie water, based on the strong ice-bottom reflection compared to the section before 1500.
7. The presence of water beneath the ice after Scan 1500 is consistent with this survey profile passing into a known channel (the extension of the cyan 2m contour running NE-SW, located southeast of Garry Island—see image below).
8. In this image, the channel runs between two areas of bottom-fast ice, according to the polarimetric SAR image underlying this flight track image, again consistent with the interpreted profile.